DISSERTATION

EVOLUTIONARY UNDERPINNINGS OF MICROGEOGRAPHIC ADAPTATION IN SONG SPARROWS DISTRIBUTED ALONG A STEEP CLIMATE GRADIENT

Submitted by

Maybellene Pascual Gamboa

Graduate Degree Program in Ecology

In partial fulfillment of the requirements

For the Degree of Doctor of Philosophy

Colorado State University

Fort Collins, Colorado

Summer 2021

Doctoral Committee:

Advisor: Cameron K. Ghalambor
Co-advisor: W. Chris Funk

Ruth A. Hufbauer
Scott A. Morrison
T. Scott Sillett
Blair O. Wolf

ABSTRACT

EVOLUTIONARY UNDERPINNINGS OF MICROGEOGRAPHIC ADAPTATION IN SONG SPARROWS DISTRIBUTED ALONG A STEEP CLIMATE GRADIENT

Understanding how evolutionary processes interact to maintain adaptive variation in natural populations has been a fundamental goal of evolutionary biology. Yet, despite adaptation remaining at the forefront of evolutionary theory and empirical studies, there remains a lack of consensus about the evolutionary conditions that enable adaptation to persist in natural populations, especially when considering complex phenotypes in response to multivariate selection regimes. In my dissertation, I disentangle the evolutionary mechanisms that shape adaptive divergence in song sparrows (*Melospiza melodia*) distributed along a climate gradient on the California Channel Islands and nearby coastal California. First, I found evidence that climate, and neither vegetation nor selection for increased foraging efficiency, likely drive adaptive divergence in bill morphology among insular populations. Second, I used an integrated population and landscape genomics approach to infer that bill variation is indicative of microgeographic local adaptation to temperature. Lastly, I tested whether the distinct climate gradient facilitates adaptative divergence in other thermoregulatory traits and found evidence to support environmental temperatures result in fixed population differences in many complementary phenotypes, including plumage color, feather microstructure, and thermal physiology. Collectively, these results find support for microgeographic climate adaptation in a suite of complex phenotypes and demonstrate the utility of integrative approaches to infer local adaptation in natural populations. Finally, by developing a more holistic understanding of

climate adaptation in natural populations, my results inform conservation management of this species of special concern.

ACKNOWLEDGEMENTS

I am immensely grateful for the community of individuals that have supported me throughout my doctoral degree and that continue to provide me with encouragement, mentorship, and resources for the advancement of my personal and career development.

First and foremost, I acknowledge the support and mentorship provided by my co-advisors, Cameron Ghalambor, Chris Funk, and Scott Sillett. Cameron has nurtured my curiosity and encouraged me to think broadly about the natural world. He has provided me with immense guidance in academia and has served as my stronghold when I was struggling in my graduate program. I am grateful for his intellectual insight, compassion, and unyielding support. Chris has helped keep me grounded throughout my dissertation. His patience, practicality, approachability, and willingness to help find solutions to any of the problems I encountered in my research and personal life have been truly appreciated. Scott has provided me with numerous opportunities to advance my career and has consistently given me the resources to bring my ideas to fruition. Together my co-advisors have taught me that my perceived failures are merely learning experiences and have inspired me to practice grace and gratitude in all aspects of my career. Most importantly, I thank my co-advisors for advocating for me when I struggled with my mental health and for believing in me when I felt as if there was no end in sight.

I thank my other committee members, Blair Wolf, Ruth Hufbauer, and Scott Morrison, for helping me navigate through my doctoral degree and for agreeing to support me in my pursuit of an integrative project. Blair enthusiastically provided me with assistance in developing the thermal physiology component of my project. Ruth and Scott provided me with encouragement

and resources to continue my research. I am fortunate to have worked with such a diverse and inspiring committee, and I consider every member integral to my success.

I am grateful to the wonderful mentors outside of my committee, including Jennifer Neuwald, Meena Balgolpal, and Mark Simmons, that have not only positively impacted my development as a researcher, but also greatly shaped my role as an educator. I was fortunate to have worked with Jennifer and Mark for multiple semesters, and I am inspired by their dedication to the development and transformation of their courses. Jennifer has mentored me with compassion, enthusiasm, and grace and has consistently offered support and insight throughout this entire process. Meena has challenged me to think critically about my pedagogy and has taught me that being an educator means being a lifelong learner. Jennifer and Meena are the strong, female voices that helped me advocate for myself and for other marginalized communities in STEM.

I have had the privilege of being a part of the GRHAF (Ghalambor-Ruegg-Hoke-Angeloni-Funk) lab group and Conservation Genomics group in the Department of Biology. I am grateful for the feedback, conversations, and daily interactions with all the members of this lab group. I am especially thankful for the members of the Ghalambor and Funk lab that have provided me with comments on talks and manuscripts, resources and research advice, and humor. In particular, I would like to highlight the wonderful support provided by Alisha Shah, Amanda Cicchino, Brian Gill, Craig Marshall, Dale Broder, Katie Langin, Molly Womack, and Rebecca Cheek.

My field and lab work would not be possible without the contributions of many agencies and individuals. I acknowledge and honor the Chumash Nation, the original stewards of the Channel Islands. I am grateful for the financial support and resources granted by the National

Science Foundation, The Nature Conservancy, Smithsonian Migratory Bird Center, Channel Islands National Park, UC Santa Barbara Santa Cruz Island Field Station, and CSUCI Santa Rosa Island Research Station and for the many positive interactions I had with the faculty and staff from each of these agencies and institutions. I thank my many field technicians and mentees for their help in data collection and light-hearted conversations in the field.

Lastly, I thank my family, friends outside of academia, and husband for their unwavering belief in my abilities. Thank you for providing me with love, unwavering support and encouragement, and laughter throughout this process.

DEDICATION

For Adam, my anchor

TABLE OF CONTENTS

1. INTRODUCTION

"'Things cannot be other than they are…Everything is made for the best purpose. Our noses were made to carry spectacles, so we have spectacles. Legs were clearly intended for breeches, and we wear them.'"[1]

– Dr. Pangloss in Candide, or Optimism, by Voltaire

Background

Understanding how evolutionary processes interact to maintain adaptive variation in natural populations has been a fundamental goal of evolutionary biology. Variation may arise as a product of multiple interacting evolutionary and environmental factors, but, far too often, researchers adopt a Dr. Panglossian perspective *(see above*) and assume that observed diversity in natural populations is representative of adaptation to local conditions. Gould and Lewontin's seminal work, *The spandrels of San Marco and the Panglossian paradigm: a critique of the adaptationist programme*, brought attention to the common false assumption of adaptation among evolutionary biologists, thereby resulting in a critical re-examination of how researchers approach the study of phenotypic variation across heterogeneous landscapes (Pigliucci & Kaplan, 2000). Since the initial publication of Gould and Lewontin's work in 1979, several genomic and molecular techniques have increased our ability to infer adaptation in natural populations (Hoban et al., 2016; Savolainen, Lascoux, & Merilä, 2013; Stapley et al., 2010; Tiffin & Ross-Ibarra, 2014). Despite modern advances in evolutionary and molecular biology to improve inferences of adaptation, the conditions that enable adaptive variation to persist remain inconsistent among populations.

[1]Voltaire, & Butt, J. (1947). *Candide: Or, Optimism*. London, United Kingdom: Penguin Books.

Theory suggests divergent selection across heterogeneous landscapes generates quantifiable patterns of adaptive phenotypic divergence (Fisher, 1930; Lenormand, 2002; Slatkin, 1987), resulting in observable, fixed allelic differences at loci linked to genomic regions that determine phenotype (e..g, Abzhanov et al., 2004; Linnen et al., 2009). However, in practice numerous complicating factors may prevent such relationships from being observed. For example, adaptive phenotypic divergence may result from plasticity (e.g., Losos et al., 2000; Relyea, 2001), epigenetic interactions (Weaver et al., 2004), and a range of other processes that breakdown the relationship between phenotypes and sequence variation. Additionally, divergent selection may be countered by the homogenizing effect of gene flow, thereby preventing local adaptation from arising (Lenormand, 2002; Slatkin, 1987). Alternatively, phenotypic variation may be a product of neutral evolutionary processes (i.e., genetic drift) and may be misconstrued as adaptive based on correlations between phenotypes and the environment (Gould & Lewontin, 1979; Kawecki & Ebert, 2004). Nevertheless, many studies have succeeded in isolating particular genes or regions of the genome that contribute to adaptive phenotypes in natural populations (Barrett et al., 2008; Hoekstra, Hirschmann, Bundey, Insel, & Crossland, 2006; Jones et al., 2012; Lamichhaney et al., 2016), including studies that identify adaptation from divergent selection even in the face of gene flow (e.g., Andrew et al., 2012; Fitzpatrick et al., 2015; Sambatti & Rice, 2006) or within the dispersal capacity of the organism (microgeographic adaptation) (e.g., Anderson et al., 2015; Mikles et al., 2020; Zellmer, 2018). However, many of these studies often rely on a reference genome or build upon well-studied systems and, thus, may not be easily applied to natural populations with less developed resources.

The advent of modern genomic and molecular techniques has given rise to multiple avenues of evolutionary inference as it pertains to the study of adaptation in natural populations

(Hoban et al., 2016; Savolainen et al., 2013; Stapley et al., 2010; Tiffin & Ross-Ibarra, 2014). Traditionally, many researchers applied direct methods to test for local adaptation, including common garden and reciprocal transplant experiments, but such experiments are difficult to conduct *in situ* for protected, rare, or secretive species (Kawecki & Ebert, 2004). As an alternative, many researchers capitalize on modern molecular tools to strengthen inferences of adaptation, but extreme caution should be taken to avoid "molecular spandrels," or just-so stories of adaptation as told with genomic correlations (Barrett & Hoekstra, 2011).

To draw robust conclusions of local adaptation using indirect evidence, links must be established between the phenotype, genotype, and environment (Fig. 1.1) (Barrett & Hoekstra, 2011; Byers et al., 2017; Sork et al., 2013). First, individual phenotypes presumed to be targets of selection are expected to covary with the hypothesized environmental agents of divergent selection (Fisher, 1930). Second, individual phenotypes must be related to genotypic variation in genes likely to modify the phenotype to reject the hypothesis that plasticity drives phenotypic divergence (Barrett & Hoekstra, 2011; Sork et al., 2013). Lastly, environmental variation should be correlated with genotypic variation in genes associated with the phenotype to reject the hypothesis that neutral processes (i.e., genetic drift) alone drive adaptive phenotypic divergence (Barrett & Hoekstra, 2011; Sork et al., 2013). When similar genes or pathways are simultaneously associated with the environment and individual phenotypes, researchers may infer local adaptation (Barrett & Hoekstra, 2011; Sork et al., 2013). Although there is acknowledged utility in this combined population and landscape genomics approach, there are few systems that apply this framework, particularly as it relates to the study of complex phenotypes.

Using an integrative framework to identify and describe local adaptation in response to climate-based selection can uncover adaptive responses in suites of correlated traits that may go unnoticed with univariate, trait-based approaches. Climate-based selection may generate adaptive population differences in behavior, morphology, and/or physiology (Angilletta, 2009; Parmesan, 2006), yet many studies of climate adaptation have centered on analyzing macroevolutionary patterns of thermal physiology (e.g., Buckley & Huey, 2016; Fristoe et al., 2015; Sunday et al., 2014). While thermal physiology is directly correlated with climate and performance in ectotherms, the relationship between physiology and environmental temperatures is less predictable in endotherms (Angilletta, 2009; Angilletta, Cooper, Schuler, & Boyles, 2010). Endotherms actively thermoregulate to maintain high, stable body temperatures when environmental temperatures fluctuate (McNab, 2002). Furthermore, endotherm physiology may be buffered from climate-based selection if populations exhibit adaptive changes in morphology (e.g., changes in avian plumage in response to cold) (Scholander et al., 1950; Tattersall et al., 2012). Relating environmental and genotypic variation (i.e., genotype-environment association analyses) can generate unbiased hypotheses about how climate-based selection results in adaptive divergence in multiple, correlated phenotypes (Rellstab, Gugerli, Eckert, Hancock, & Holderegger, 2015). By describing phenotypes controlled by genes correlated with the environment, evolutionary biologists can provide examples of climate adaptation in natural populations, develop our understanding of how climate affects evolutionary change, and potentially guide management of vulnerable populations in the face of climate change.

Study system

Song sparrows (*Melospiza melodia*) are well-suited for studies aimed at partitioning the evolutionary drivers of local adaptation in response to environmental heterogeneity. Song sparrows are generalist passerines, widely distributed across North America and inhabit diverse ecological niches (Arcese, Sogge, Marra, & Patten, 2002). Across their range, they exhibit extensive phenotypic variation (Arcese et al., 2002; Patten & Pruett, 2009; Smith, 1998) and observed variation is hypothesized to be related to local environmental conditions including temperature (Aldrich, 1984), humidity (Burtt & Ichida, 2004), and salinity (Luttrell, Gonzalez, Lohr, & Greenberg, 2015; Mikles et al., 2020). Additionally, phenotypic differences have been shown to track regional temperatures over time based on analyses of historic data and museum specimens (Greenberg & Danner, 2012; Torti & Dunn, 2005). Thus, climate likely contributes to adaptive variation in song sparrows, and investigating the evolutionary drivers of phenotypic variation along an environmental gradient provides insight into the conditions that result in climate adaptation.

Song sparrows distributed across the California Channel Islands archipelago occupy a remarkable climate gradient and represent an ideal system to examine the evolutionary mechanisms contributing to climate adaptation. Song sparrows are a common and abundant avian species on the four, linearly arrayed northernmost islands (from West to East: San Miguel, Santa Rosa, Santa Cruz, and Anacapa Islands). Birds on San Miguel Island experience cold, mesic, very windy conditions, while birds on Santa Cruz and Anacapa Islands experience hot, xeric, and less windy conditions, comparatively (Schoennerr, Feldmeth, & Emerson, 2003). This distinct gradient within a small spatial extent (<100 km) is uncommon across the entire species complex and offers a rare opportunity to study how selection due to drastic climate differences

correlates with microgeographic adaptive variation. Furthermore, song sparrows are residents on the islands with relatively short dispersal distances, and previous work suggests some low levels of contemporary gene flow among islands (Wilson, Chan, Taylor, & Arcese, 2015). Low estimated contemporary migration rates correspond with high rates of genetic divergence among islands, low levels of allelic richness, and, hence, presumed stronger effects of genetic drift (Wilson et al., 2015; Wilson, 2008). Therefore, song sparrows on the California Channel Islands allow us to infer the relative role of selection, gene flow, and genetic drift in generating and maintaining climate adaptation in natural populations.

Dissertation objectives

The collective aims of my dissertation are to identify environmental correlates of phenotypic divergence in Channel Island song sparrows and to infer the evolutionary processes that facilitate adaptive variation in island populations. I interpret my research within an evolutionary and conservation perspective and provide recommendations for population management in the face of future climate change.

In my first study (Ch. 2), I expanded on a previous study using museum specimens by Greenberg and Danner (2012) that found evidence for bill divergence correlated with temperature by quantifying and testing alternative hypotheses underlying bill variation in contemporary populations. Namely, I assessed whether bill variation is a product of selection for thermoregulatory versus foraging efficiency by relating bill differences with environmental variables and foraging performance. I confirmed that islands differ in mean bill surface area, climate, and vegetative habitat. As expected under the thermoregulatory efficiency hypothesis, birds on hotter islands had larger bills. Congruent with work by Greenberg and Danner (2012), I

found maximum temperature, not vegetation predicted bill differences. Lastly, I found bill differences did not correlate with functional traits linked with foraging efficiency. These results combined provide evidence against the foraging efficiency hypothesis for bill variation and warrant further investigation into the relationship between temperature and bill morphology.

In my second study (Ch. 3), I examined genomic data in a population and landscape genomic framework to determine whether bill variation is genetically based and evidence of local adaptation or a by-product of neutral evolutionary processes. Based on analyses of neutral genetic variation, I found little evidence to suggest genetic drift plays a large role in maintaining bill divergence. Instead, I found that the combined effects of restricted gene flow and selection due to climate likely drive patterns of bill variation. Putatively adaptive loci identified via a combination of differentiation-based and genotype-environment association analyses were found in or near genes involved in bill development pathways. Genome-wide association analyses provided additional support for a genetic basis to variation with candidate loci found in similar bill development pathways, suggesting bill divergence represents local adaptation in island populations. Moreover, I found maximum temperature was also associated with fixed population differences at loci in or near genes associated with plumage color, feather development, and thermal stress responses.

In my final study (Ch. 4), I further investigated climate adaptation by building upon findings in the previous chapter which showed fixed population differences associated with climate in or near genes regulating thermal physiology, plumage color, and feather structure. As expected, maximum temperature was a significant predictor of traits linked with physiological responses to thermal stress and with morphological traits that may improve insulative capacity. Birds sampled from colder regions had elevated basal metabolic rates, lower temperatures that

induce a heat stress response, and reduced abilities to effectively evaporatively cool. Similarly, we found a significant relationship between temperature and feather microstructure with birds in colder environments having more developed contour feathers. This likely aids in water repellence and wind resistance to improve heat retention in cold, wet, and windy conditions (Rijke & Jesser, 2011; Stettenheim, 2000). As with bill variation, we confirmed with genome-wide association analyses to determine whether morphological variation had at least a partial genetic basis and, thus, represents local adaptation.

Conclusions and significance

These dissertation results collectively demonstrate that climate drives adaptive divergence among insular populations at remarkably small spatial scales. I highlighted the importance of applying strong inference to determine agents of selection when considering complex phenotypes and the utility of merged population and landscape genomic approaches to infer adaptation. This highly integrative approach enabled me to disentangle the evolutionary mechanisms that contribute to climate adaptation. Specifically, I found the combined effects of reduced gene flow and strong climate-based selection correlate with phenotypic variation in multiple complementary traits that affect thermoregulatory ability. Most strikingly, this study is an important example of how climate-based selection is sufficient to generate variation in thermal physiology as well as morphology among endotherm populations. Similar patterns of microgeographic adaptation in morphological characters have been observed in other song sparrow populations in response to environmental variation (Mikles et al., 2020). However, my results emphasize that selection operates on the whole organism, and there are multiple avenues in which populations may respond adaptively to environmental heterogeneity.

Conservation and reintroduction implications

Understanding patterns of climate adaptation and genetic diversity in Channel Island song sparrows may inform management decisions for this species of special concern. Song sparrows on San Miguel and Santa Rosa Islands are formally classified as the island endemic subspecies (*Melospiza melodia graminea*) and federally-recognized as a species of conservation concern (Patten & Pruett, 2009; Shuford & Gardali, 2008). Our population genomic analyses suggest all island individuals are more closely-related to each other than they are to mainland individuals (Chapter 3), but subspecies designations are complicated (Coyne & Orr, 2004), particularly in this species complex (Patten & Pruett, 2009). Irrespective of the taxonomic classifications of song sparrows on Santa Cruz and Anacapa Islands, our results uphold previous subspecies delineations between mainland and island conspecifics by confirming San Miguel and Santa Rosa Island populations are genetically and, in part, phenotypically distinct from the mainland subspecies (*Melospiza melodia heermanni*) (Patten & Pruett, 2009). Additionally, evidence of limited gene flow to San Miguel and Santa Rosa Islands (Chapter 3) suggest these island endemic populations are isolated and especially vulnerable to extinction in the absence of proactive conservation management.

As evidenced by a disproportionately higher number of avian extinctions having occurred on islands (Blackburn, Cassey, Duncan, Evans, & Gaston, 2004; Johnson & Stattersfield, 1990; Whittaker, Triantis, & Ladle, 2008), insular populations are highly susceptible to extinction (Frankham, 1997; Frankham, 1998). Indeed, the island endemic song sparrow subspecies currently restricted to San Miguel and Santa Rosa Islands was formerly abundant on Santa Barbara and San Clemente Islands as well (Fig. 1.2; Shuford & Gardali, 2008). The combined effects of human-induced habitat degradation and naturally occurring fires resulted in the

extirpation of these island populations in the 1960s and 1970s, respectively (Shuford & Gardali, 2008). To buffer island taxa from extinction and restore extirpated populations, managers are increasingly considering reintroductions, or the intentional movement of individuals from one region to a historically-occupied site to re-establish viable populations (IUCN/SSC, 2013; Seddon, Armstrong, & Maloney, 2007). The reintroduction of song sparrows to Santa Barbara Island, a Channel Islands National Park owned and managed property, requires the identification of an appropriate population(s) from which to source individuals for translocation (Morrison, Parker, Collins, Funk, & Sillett, 2014). While population genetic and ecological data is often used to select a source population (Armstrong & Seddon, 2008), there is no consensus as to what strategy for source population selection is ideal for all reintroduction efforts.

Traditionally, genetic data were used to inform reintroduction strategies by identifying populations with shared ancestry, as inferred by neutral genetic markers (Cassey, Blackburn, Sol, Duncan, & Lockwood, 2004; Crandall, Bininda-Emonds, Mace, & Wayne, 2000; Ewen, Armstrong, Parker, & Seddon, 2012). This genetic exchangeability strategy (Crandall et al., 2000) assumes individuals that are more genetically similar to the extirpated population are also able to survive and reproduce in the reintroduction environment. Santa Barbara Island song sparrows are most closely-related to both mainland and San Miguel Island song sparrows based on analyses of mitochondrial DNA extracted from museum specimens (Wilson et al., 2015). Measurements of museum specimen bill dimensions also confirm that both San Miguel and Santa Barbara Island song sparrows have small bills when correcting for body size (Greenberg & Danner, 2012), which may be a by-product of gene flow between these regions and further support for genetic exchangeability. Thus, under the genetic exchangeability strategy, evidence of shared mitochondrial haplotypes and historic gene flow is sufficient to justify sourcing

individuals from either San Miguel Island or mainland California for reintroduction to Santa Barbara Island. However, mitochondrial DNA represents only a subset of total genomic variation, and exclusively using mitochondrial markers provides little insight into how locally adapted a population is, or how it will respond to future selection pressures.

An alternative recommendation to incorporate knowledge of local adaptation argues that individuals should be chosen from populations that have environments analogous to the extirpated population, because they will likely exhibit similar adaptations and/or adaptive genetic variation (Houde, Garner, & Neff, 2015). This pre-existing adaptation strategy assumes past selection and local adaptation are more important in predicting reintroduction success than neutral processes alone; directly matching adaptive phenotypes or genotypes increases the likelihood of adaptation to the target environment (Frankham et al., 2011; Houde et al., 2015; McKay, Christian, Harrison, & Rice, 2005). The target environment on Santa Barbara Island is characterized by windy, hot, and arid conditions (Schoennerr et al., 2003). Presumably, individuals would be better able to cope with current and future climate conditions on Santa Barbara Island if those individuals exhibited genotypes locally adapted to hotter climates. The identification of adaptive genomic variation associated with higher temperatures (Chapter 3) suggests it may be beneficial to source individuals from eastern islands (i.e., Santa Cruz or Anacapa Islands) under the pre-existing adaptation strategy. Yet, only selecting individuals with locally adapted genotypes reduces overall genetic diversity in the founding population and renders the population ill-equipped to respond to novel selection pressures (Kardos & Shafer, 2018).

Given the difficulty in predicting future environmental change and fluctuating selection regimes, it is beneficial to consider the amount of both neutral and adaptive genetic variation

when selecting individuals for reintroduction. The adaptive potential strategy proposes using a source population that harbors the greatest amount of genetic variation to maximize evolutionary potential (Houde et al., 2015). Specifically, a population is more likely to persist in response to a complex or novel selection regime by increasing the amount of genetic variation, as achieved by selecting highly admixed or outbred individuals (e.g., Hufbauer, Rutschmann, Serrate, Vermeil de Conchard, & Facon, 2013; Reed, Lowe, Briscoe, & Frankham, 2003; Szűcs, Melbourne, Tuff, & Hufbauer, 2014; Vahsen, Shea, Hovis, Teller, & Hufbauer, 2018) or by sourcing individuals from multiple regions to promote admixture (e.g., Pickup, Field, Rowell, & Young, 2013; Rick et al., 2019). In addition to reintroductions, actively promoting admixture among individuals from genetically-distinct populations through assisted migration efforts may introduce genetic diversity to genetically-depauperate and isolated populations (e.g., San Miguel Island) and reduce extinction risks (Weeks, Stoklosa, & Hoffmann, 2016). On the other hand, our results show that the complex adaptive landscape in response to climate and thermal stress is partially genetically-based, and sourcing individuals from multiple populations may increase the risk of outbreeding depression (Frankham et al., 2011; McKay et al., 2005; Reid et al., 2021; Whitlock et al., 2013). Regardless, there is theoretical and empirical justification for the use one highly admixed population or multiple divergent populations, and the resulting decision will depend on financial and logistical constraints.

The ideal source population(s) for reintroduction represent a compromise of alternative strategies based on knowledge of neutral and adaptive genetic variation, but few reintroduction attempts aim to integrate these strategies. The collective results from this dissertation will aid in the decision to reintroduce song sparrows to an island where they have been extirpated. Consequently, this work represents an important first step in the proactive management of a

species of special concern through collaboration between academics and conservation practitioners. Regardless of the source population selected, subsequent reintroduction efforts provide a unique and exciting opportunity to monitor demographic and evolutionary changes in the founding populations given known phenotypes and genotypes. Thus, this work provides the basis for a potential long-term study of the integration of evolutionary biology and applied conservation.

Figures

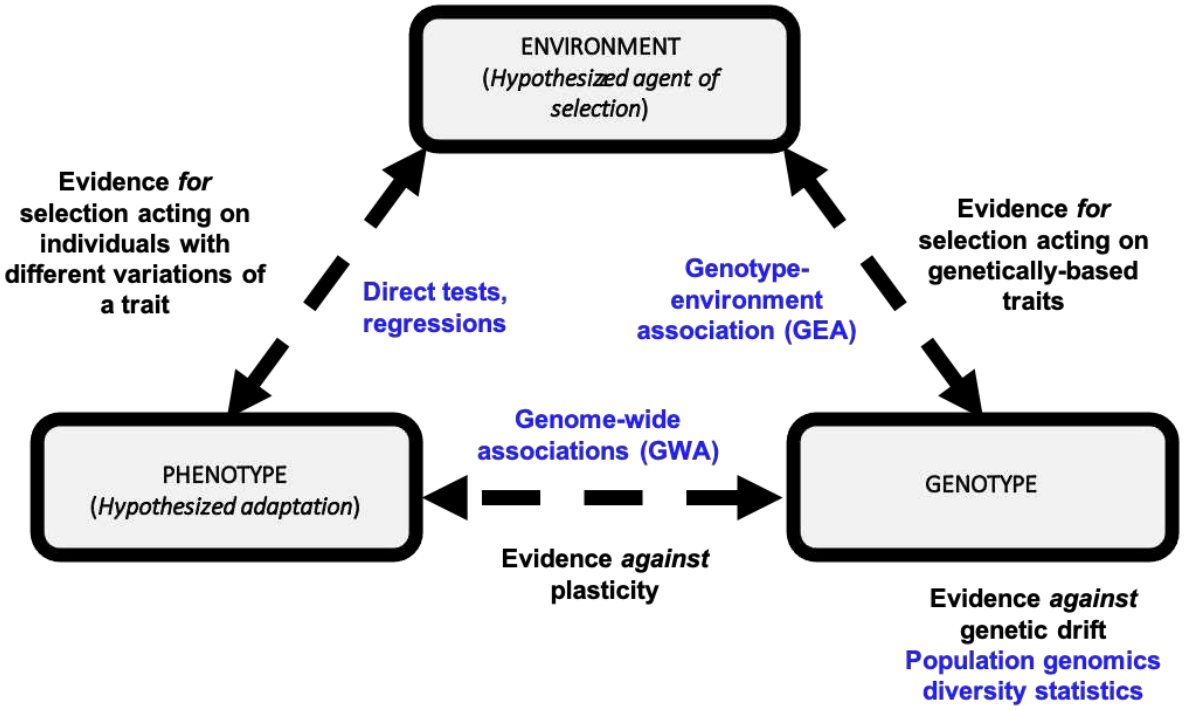

Figure 1.1 Conceptual diagram of an integrative framework to infer local adaptation in natural populations adapted from Barrett and Hoekstra (2011) and Sork *et al.* (2013). Proposed methods (blue) are shown to establish each research objective (black, unboxed).

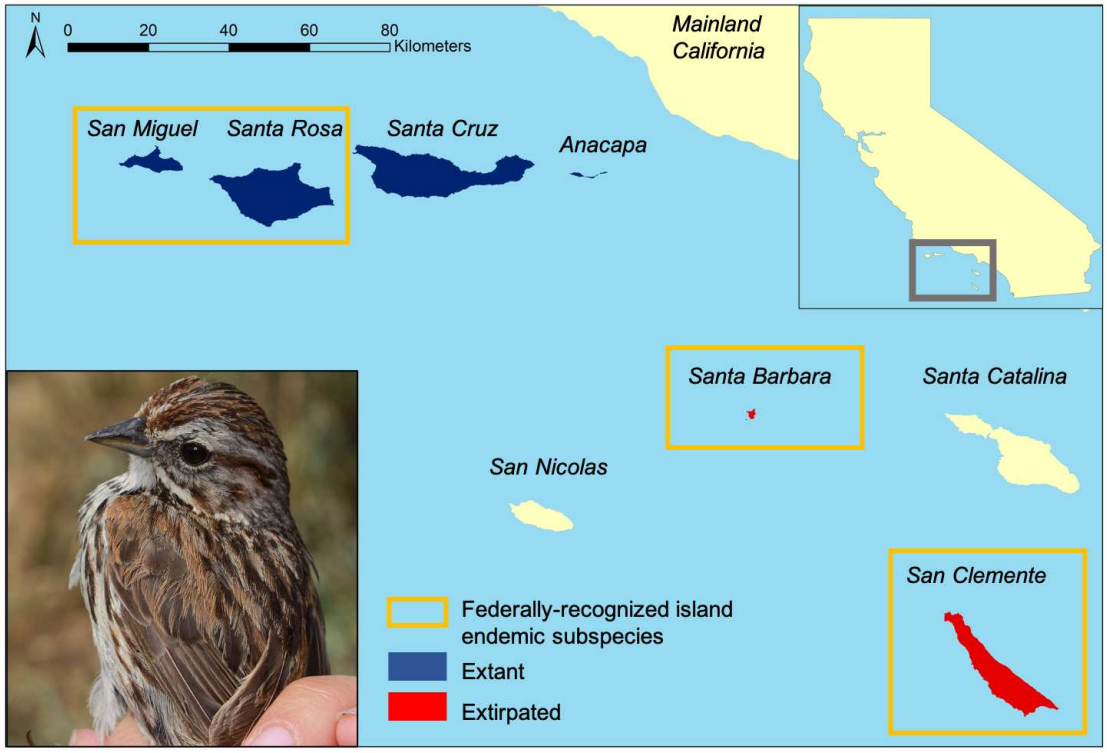

Figure 1.2 Extant (blue) and extirpated (red) song sparrow populations on the California Channel Islands. Island populations that are classified as the island endemic subspecies (*Melospiza melodia graminea*) and considered species of species concern are highlighted with an orange box. Inset shows the location of the archipelago with respect to California.

LITERATURE CITED

Abzhanov, A., Protas, M., Grant, B. R., Grant, P. R., & Tabin, C. J. (2004). Bmp4 and morphological variation of beaks in Darwin's finches. *Science*, *305*(5689), 1462–1465.

Aldrich, J. W. (1984). Ecogeographical variation in size and proportions of song sparrows (Melospiza melodia). *Ornithological Monographs*, (35), iii–134.

Anderson, J. T., Perera, N., Chowdhury, B., & Mitchell-Olds, T. (2015). Microgeographic patterns of genetic divergence and adaptation across environmental gradients in Boechera stricta (Brassicaceae). *American Naturalist*, *186*(S1), S60–S73.

Andrew, R. L., Ostevik, K. L., Ebert, D. P., & Rieseberg, L. H. (2012). Adaptation with gene flow across the landscape in a dune sunflower. *Molecular Ecology*, *21*(9), 2078–2091.

Angilletta Jr, M. J. (2009). *Thermal Adaptation*. Oxford, United Kingdom: Oxford University Press.

Angilletta Jr, M. J., Cooper, B. S., Schuler, M. S., & Boyles, J. G. (2010). The evolution of thermal physiology in endotherms. *Frontiers in Bioscience*, *E2*, 861–881.

Arcese, P., Sogge, M. K., Marra, A. B., & Patten, M. A. (2002). Song Sparrow (Melospiza melodia). In *The Birds of North America Onlins (A. Poole, Ed.)*. Retrieved from http://bna.birds.cornell.edu.bnaproxy.birds.cornell.edu/bna/species/704

Armstrong, D. P., & Seddon, P. J. (2008). Directions in reintroduction biology. *Trends in Ecology & Evolution*, *23*(1), 20–25.

Barrett, R. D. H., & Hoekstra, H. E. (2011). Molecular spandrels: tests of adaptation at the genetic level. *Nature Review Genetics*, *12*(11), 767–780.

Barrett, R. D. H., Rogers, S. M., & Schluter, D. (2008). Natural selection on a major armor gene in threespine stickleback. *Science*, *322*(5899), 255–257.

Blackburn, T. M., Cassey, P., Duncan, R. P., Evans, K. L., & Gaston, K. J. (2004). Avian extinction and mammalian introductions on oceanic islands. *Science*, *305*(5692), 1955–1958.

Buckley, L. B., & Huey, R. B. (2016). Temperature extremes: geographic patterns, recent changes, and implications for organismal vulnerabilities. *Global Change Biology*, *22*(12), 3829–3842.

Burtt, E. H., & Ichida, J. M. (2004). Gloger's Rule, feather-degrading bacteria, and color variation among song sparrows. *The Condor*, *106*(3), 681–686.

Byers, K. J. R. P., Xu, S., & Schlüter, P. M. (2017). Molecular mechanisms of adaptation and speciation: why do we need an integrative approach? *Molecular Ecology*, *26*(1), 277-290.

Cassey, P., Blackburn, T. M., Sol, D., Duncan, R. P., & Lockwood, J. L. (2004). Global patterns of introduction effort and establishment success in birds. *Proceedings of the Royal Society B: Biological Sciences*, *271*(Suppl_6), S405–S408.

Coyne, J. A., & Orr, H. A. (2004). *Speciation* (Vol. 37). Sunderland, Massachussetts: Sinauer Associates.

Crandall, K. A., Bininda-Emonds, O. R. P., Mace, G. M., & Wayne, R. K. (2000). Considering evolutionary processes in conservation biology. *Trends in Ecology & Evolution*, *15*(7), 290–295.

Ewen, J. G., Armstrong, D. P., Parker, K. A., & Seddon, P. J. (Eds.) (2012). *Reintroduction biology: integrating science and management*. West Sussex, United Kingdom: John Wiley & Sons.

Fisher, R. A. (1930). *The genetical theory of natural selection*. Oxford, United Kingdom: The Clarendon Press.

Fitzpatrick, S. W., Gerberich, J. C., Kronenberger, J. A., Angeloni, L. M., & Funk, W. C. (2015). Locally adapted traits maintained in the face of high gene flow. *Ecology Letters*, *18*(1), 37–47.

Frankham, R. (1997). Do island populations have less genetic variation than mainland populations?. *Heredity*, *78*(3), 311–327.

Frankham, R. (1998). Inbreeding and Extinction: Island Populations. *Conservation Biology*, *12*(3), 665–675.

Frankham, R., Ballou, J. D., Eldridge, M. D. B., Robert, C., Ralls, K., Dudash, M. R., & Fenster, C. B. (2011). Predicting the probability of outbreeding depression. *Conservation Biology*, *25*(3), 465–475.

Fristoe, T. S., Burger, J. R., Balk, M. A., Khaliq, I., Hof, C., & Brown, J. H. (2015). Metabolic heat production and thermal conductance are mass-independent adaptations to thermal environment in birds and mammals. *Proceedings of the National Academy of Sciences*, *112*(52), 15934-15939.

Gould, S. J., & Lewontin, R. C. (1979). The spandrels of San Marco and the Panglossian paradigm: a critique of the adaptationist programme. *Proceedings of the Royal Society B: Biological Sciences*, *205*(1161), 581–598.

Greenberg, R., & Danner, R. M. (2012). The influence of the California marine layer on bill size in a generalist songbird. *Evolution*, *66*(12), 3825–3835.

Hoban, S., Kelley, J. L., Lotterhos, K. E., Antolin, M. F., Bradburd, G., Lowry, D. B., … Whitlock, M. C. (2016). Finding the genomic basis of local adaptation: pitfalls, practical solutions, and future directions. *American Naturalist*, *188*(4), 379-397.

Hoekstra, H. E., Hirschmann, R. J., Bundey, R. A., Insel, P. A., & Crossland, J. P. (2006). A single amino acid mutation contributes to adaptive beach mouse color pattern. *Science*, *313*(5783), 101–104.

Houde, A. L. S., Garner, S. R., & Neff, B. D. (2015). Restoring species through reintroductions: strategies for source population selection. *Restoration Ecology*, *23*(6), 746-753.

Hufbauer, R. A., Rutschmann, A., Serrate, B., Vermeil de Conchard, H., & Facon, B. (2013). Role of propagule pressure in colonization success: disentangling the relative importance of demographic, genetic and habitat effects. *Journal of Evolutionary Biology*, *26*(8), 1691–1699.

IUCN/SSC. (2013). *Guidelines for Reintroductions and Other Conservation Translocations*.

Johnson, T. H., & Stattersfield, J. (1990). A global review of island endemic birds. *Ibis*, *132*(2), 167–180.

Jones, F. C., Grabherr, M. G., Chan, Y. F., Russell, P., Mauceli, E., Johnson, J., … Chris. (2012). The genomic basis of adaptive evolution in threespine sticklebacks. *Nature*, *484*(7392), 55–61.

Kardos, M., & Shafer, A. B. A. (2018). The peril of gene-targeted conservation. *Trends in Ecology & Evolution*, *33*(11), 827–839.

Kawecki, T. J., & Ebert, D. (2004). Conceptual issues in local adaptation. *Ecology Letters*, *7*(12), 1225–1241.

Lamichhaney, S., Han, F., Berglund, J., Wang, C., Almen, M. S., Webster, M. T., … Andersson, L. (2016). A beak size locus in Darwin's finches facilitated character displacement during a drought. *Science*, *352*(6284), 470–473.

Lenormand, T. (2002). Gene flow and the limits to natural selection. *Trends in Ecology & Evolution*, *17*(4), 183–189.

Linnen, C. R., Kingsley, E. P., Jensen, J. D., Hoekstra, H. E., Linnen, C. R., Kingsley, E. P., … Hoekstra, H. E. (2009). On the origin and spread of an adaptive allele in deer mice. *Science*, *325*(5944), 1095–1098.

Losos, J. B., Creer, D. A., Glossip, D., Goellner, R., Roberts, G., Haskell, N., … Ettling, J. (2000). Evolutionary implications of phenotypic plasticity in the hindlimb of the lizard Anolis sagrei. *Evolution*, *54*(1), 301–305.

Luttrell, S. A. M., Gonzalez, S. T., Lohr, B., & Greenberg, R. (2015). Digital photography quantifies plumage variation and salt marsh melanism among Song Sparrow (Melospiza melodia) subspecies of the San Francisco Bay. *Auk*, *132*(1), 277–287.

McKay, J. K., Christian, C. E., Harrison, S., & Rice, K. J. (2005). '"How local is local ?"' — a review of practical and conceptual issues in the genetics of restoration. *Restoration Ecology*, *13*(3), 432–440.

McNab, B. K. (2002). *The Physiological Ecology of Vertebrates*. Ithaca, New York: Cornell Universty Press.

Mikles, C. S., Aguillon, S. M., Chan, Y. L., Arcese, P., Benham, P. M., Lovette, I. J., & Walsh, J. (2020). Genomic differentiation and local adaptation on a microgeographic scale in a resident songbird. *Molecular Ecology*, *29*(22), 4295–4307.

Morrison, S. A., Parker, K. A., Collins, P. W., Funk, W. C., & Sillett, T. S. (2014). Reintroduction of historically extirpated taxa on the California Channel Islands. *Monographs of the Western North American Naturalist*, *7*(1), 531–542.

Parmesan, C. (2006). Ecological and evolutionary responses to recent climate change. *Annual Review of Ecology, Evolution, and Systematics*, *37*, 637–669.

Patten, M. A., & Pruett, C. L. (2009). The song sparrow, Melospiza melodia, as a ring species: patterns of geographic variation, a revision of subspecies, and implications for speciation. *Systematics and Biodiversity*, *7*(1), 33–62.

Pickup, M., Field, D. L., Rowell, D. M., & Young, A. G. (2013). Source population characteristics affect heterosis following genetic rescue of fragmented plant populations. *Proceedings of the Royal Society B: Biological Sciences*, *280*(1750), 20122058.

Pigliucci, M., & Kaplan, J. (2000). The fall and rise of Dr Pangloss: Adaptationism and the Spandrels paper 20 years later. *Trends in Ecology & Evolution*, *15*(2), 66–70.

Reed, D. H., Lowe, E. H., Briscoe, D. A., & Frankham, R. (2003). Fitness and adaptation in a novel environment: effect of inbreeding, prior environment, and lineage. *Conservation Biology*, *17*(1), 230–237.

Reid, J. M., Arcese, P., Nietlisbach, P., Wolak, M. E., Muff, S., Dickel, L., & Keller, L. F. (2021). Immigration counter-acts local micro-evolution of a major fitness component: Migration-selection balance in free-living song sparrows. *Evolution Letters*, *5*(1), 48–60.

Rellstab, C., Gugerli, F., Eckert, A. J., Hancock, A. M., & Holderegger, R. (2015). A practical guide to environmental association analysis in landscape genomics. *Molecular Ecology*, *24*(17), 4348–4370.

Relyea, R. A. (2001). Morphological and Behavioral Plasticity of Larval Anurans in Response to Different Predators. *Ecology*, *82*(2), 523–540.

Rick, K., Ottewell, K., Lohr, C., Thavornkanlapachai, R., Byrne, M., & Kennington, W. J. (2019). Population genomics of Bettongia lesueur: admixing increases genetic diversity with no evidence of outbreeding depression. *Genes*, *10*(11).

Rijke, A. M., & Jesser, W. A. (2011). The water penetration and repellency of feathers revisited. *Condor*, *113*(2), 245–254.

Sambatti, J. B. M., & Rice, K. J. (2006). Local adaptation, patterns of selection, and gene flow in the Californian serpentine sunflower (Helianthus exilis). *Evolution, 60*(4), 696–710.

Savolainen, O., Lascoux, M., & Merilä, J. (2013). Ecological genomics of local adaptation. *Nature*, *14*(11), 807–820.

Schoennerr, A. A., Feldmeth, C. R., & Emerson, M. J. (2003). *The Natural History of the Islands of California*. Berkeley, California: University of California Press.

Scholander, P. F., Hock, R., Walters, V., & Irving, L. (1950). Adaptation to cold in Arctic and tropical mammals and birds in relation to body temperature, insulation, and basal metabolic rate. *Biological Bulletin*, *99*(2), 259–271.

Seddon, P. J., Armstrong, D. P., & Maloney, R. F. (2007). Developing the science of reintroduction biology. *Conservation Biology*, *21*(2), 303–312.

Shuford, W. D., & Gardali, T. (Eds.). (2008). Channel Island song sparrow. In *California bird species of special concern: A ranked assessment of species, subspecies, and distinct populations of birds of immediate conservation concern in California. Studies of Western Birds 1.* Camarillo, CA: Western Field Ornithologists and California Department of Fish and Game.

Slatkin, M. (1987). Gene flow and the geographic structure of natural populations. *Science*, *236*(4803), 787–792.

Smith, J. I. (1998). Allometric influence on phenotypic variation in the Song Sparrow (Melospiza melodia). *Zoological Journal of Linnean Society*, *122*(3), 427–454.

Sork, V. L., Aitken, S. N., Dyer, R. J., Eckert, A. J., Legendre, P., & Neale, D. B. (2013). Putting the landscape into the genomics of trees: Approaches for understanding local adaptation and population responses to changing climate. *Tree Genetics and Genomes*, *9*(4), 901–911.

Stapley, J., Reger, J., Feulner, P. G. D., Smadja, C., Galindo, J., Ekblom, R., … Slate, J. (2010). Adaptation genomics: the next generation. *Trends in Ecology & Evolution*, *25*(12), 705–712.

Stettenheim, P. R. (2000). The Integumentary Morphology of modern birds—an overview. *American Zoologist*, *40*(4), 461–477.

Sunday, J. M., Bates, A. E., Kearney, M. R., Colwell, R. K., Dulvy, N. K., Longino, J. T., & Huey, R. B. (2014). Thermal-safety margins and the necessity of thermoregulatory behavior across latitude and elevation. *Proceedings of the National Academy of Sciences of the United States of America*, *111*(15), 5610–5615.

Szűcs, M., Melbourne, B. A., Tuff, T., & Hufbauer, R. A. (2014). The roles of demography and genetics in the early stages of colonization. *Proceedings of the Royal Society B: Biological Sciences*, *281*(1792), 20141073.

Tattersall, G. J., Sinclair, B. J., Withers, P. C., Fields, P. A., & Seebacher, F. (2012). Coping with thermal challenges: physiological adaptations to environmental temperatures. *Comprehensive Physiology*, *2*(3), 2151–2202.

Tiffin, P., & Ross-Ibarra, J. (2014). Advances and limits of using population genetics to understand local adaptation. *Trends in Ecology & Evolution*, *29*(12), 673–680.

Torti, V. M., & Dunn, P. O. (2005). Variable effects of climate change on six species of North American birds. *Oecologia*, *145*(3), 486–495.

Vahsen, M. L., Shea, K., Hovis, C. L., Teller, B. J., & Hufbauer, R. A. (2018). Prior adaptation, diversity, and introduction frequency mediate the positive relationship between propagule pressure and the initial success of founding populations. *Biological Invasions*, *20*(9), 2451–2459.

Weaver, I. C. G., Cervoni, N., Champagne, F. A., Alessio, A. C. D., Sharma, S., Seckl, J. R., … Meaney, M. J. (2004). Epigenetic programming by maternal behavior. *Nature Neuroscience*, *7*(8), 847–854.

Weeks, A. R., Stoklosa, J., & Hoffmann, A. A. (2016). Conservation of genetic uniqueness of populations may increase extinction likelihood of endangered species: The case of Australian mammals. *Frontiers in Zoology*, *13*(1), 1–9.

Whitlock, R., Stewart, G. B., Goodman, S. J., Piertney, S. B., Butlin, R. K., Pullin, A. S., & Burke, T. (2013). A systematic review of phenotypic responses to between-population outbreeding. *Environmental Evidence*, *2*(1), 1–21.

Whittaker, R. J., Triantis, K. A., & Ladle, R. J. (2008). A general dynamic theory of oceanic island biogeography. *Journal of Biogeography*, *35*(6), 977–994.

Wilson, A. (2008). *The role of insularity in promoting intraspecific differentiation in song sparrows* (Doctoral dissertation, University of British Columbia).

Wilson, A. G., Chan, Y., Taylor, S. S., & Arcese, P. (2015). Genetic divergence of an avian endemic on the Californian Channel Islands. *Plos One*, *10*(8), e0134471.

Zellmer, A. J. (2018). Microgeographic morphological variation across larval wood frog populations associated with environment despite gene flow. *Ecology and Evolution*, *8*(5), 2504–2517.

2. ENVIRONMENTAL CORRELATES AND FUNCTIONAL CONSEQUENCES OF BILL DIVERGENCE IN ISLAND SONG SPARROWS

Summary

Inferring the environmental selection pressures responsible for phenotypic variation is a challenge in adaptation studies as traits often have multiple functions and are shaped by complex selection regimes. We provide experimental evidence that morphology of the multifunctional avian bill is related to climate, not foraging efficiency, in song sparrows (*Melospiza melodia*) on the California Channel Islands. Our research builds on a study in song sparrow museum specimens that demonstrated a positive correlation between bill surface area and maximum temperature, suggesting a greater demand for dry heat dissipation in hotter, xeric environments. We sampled contemporary sparrow populations across three climatically distinct islands to test the alternate hypotheses that song sparrow bill morphology is either a product of vegetative differences with functional consequences for foraging efficiency or related to maximum temperature and, consequently, important for thermoregulation. Measurements of >500 live individuals indicated a significant, positive relationship between maximum temperature and bill surface area when correcting for body size. In contrast, maximum bite force, seed extraction time, and vegetation on breeding territories (a proxy for food resources) were not significantly associated with bill dimensions. While we cannot exclude the influence of foraging ability and diet on bill morphology, our results are consistent with the hypothesis that variation in song sparrows' need for thermoregulatory capacity across the northern Channel Islands selects for divergence in bill surface area.

Introduction

Determining the environmental factors that drive adaptation in traits is a central goal in evolutionary biology, but this is often challenging in natural populations (Kawecki & Ebert, 2004; MacColl, 2011; Reznick & Travis, 1996). Such challenges arise because traits may serve different functions such that the observed phenotypic variation is a product of multifarious selection pressures (e.g., Egea-Serrano et al., 2014; Pfrender, 2012; Shultz and Burns, 2017; Templeton and Shriner, 2004; Wilkins et al., 2013). Multiple selection pressures can act either synergistically, shifting the population phenotypic mean towards a predictable adaptive optimum, or act antagonistically such that the observed phenotypic means represents a compromise, or trade-off between different functions (Svensson & Calsbeek, 2012). This concept of adaptation as a compromise between different functions is reinforced by empirical studies of natural populations (e.g., Egea-Serrano et al., 2014; Ghalambor et al., 2003; Kim et al., 2011; Robinson et al., 2006). Thus, testing which aspects of the environment act as important selection pressures requires consideration of the different functions of a given trait and the functional consequences associated with shifting trait means (Ghalambor et al., 2003; Jones, Leith, & Rawlings, 1977).

The avian bill is one of the most studied multifunctional, morphological traits. The bill is involved in many fitness-related behaviors including ectoparasite removal (Clayton et al., 2005), communication (Ballentine, 2006; Podos, 2001), tool creation and use (Fayet, Hansen, & Biro, 2020; Rutz et al., 2016; Troscianko, Von Bayern, Chappell, Rutz, & Martin, 2012), thermoregulation (Greenberg, Cadena, Danner, & Tattersall, 2012; Ryeland, Weston, & Symonds, 2017; Symonds & Tattersall, 2010), and, most notably, food acquisition (Barbosa & Moreno, 1999; Benkman, 1993; Temeles & Kress, 2003). Consequently, predicting local optima

for bill sizes is difficult given the potentially conflicting functional demands. For example, an increase in bill morphology in the Darwin's finches is associated with improved foraging efficiency on hard seeds, yet it is also predicted to cause correlated changes in syllable rate and frequency bandwidth of vocal signals, which alters song production (Podos & Nowicki, 2004). Furthermore, finches with increased bill surface area have greater heat dissipation, which is hypothesized to improve thermoregulatory function (Tattersall, Chaves, & Danner, 2018). Similar interspecific patterns of bill divergence correlated with multiple environmental drivers and resulting in functional consequences have been documented in other passerines as well (Friedman et al., 2019). Bill morphology in any bird species is, therefore, a product of trade-offs among multiple selection pressures including, but not limited to, climate, food resources, and vocal signaling. Bill dimensions also have a strong genetic component, indicating that this important trait can readily evolve in response to selection (Åkesson, Bensch, Hasselquist, Tarka, & Hansson, 2008; Boag, 1983; Grant, 1983; Jensen et al., 2003; Keller, Grant, Rosemary Grant, & Petren, 2001). Given that the strength of selection may shift over time and space (Siepielski, DiBattista, & Carlson, 2009; Siepielski et al., 2013), investigating avian bill morphology differences among environments and populations can provide insight into how multiple selection pressures act to generate and maintain variation.

The relationship between bill morphology and foraging ability has received extensive attention, with numerous empirical studies finding correlations between bill size and characteristics of available food resources or foraging ability (e.g., Langin et al., 2015; Nebel et al., 2005; Temeles et al., 1993). For instance, bill depth in the medium ground finch (Geospiza fortis) is positively correlated with the abundance of large, hard seeds, and evolution in response to fluctuations in seed availability across years results in rapid adaptation (Grant & Grant, 2006).

Relatively small modifications in bill morphology among Darwin's finches result in functional differences in bite force (Herrel et al., 2010). This strong selection pressure on bill morphology for improved foraging ability has resulted in diversification and adaptive radiation in several avian families (Benkman, 2003; Burns, Hackett, & Klein, 2003; Grant & Grant, 2002; Lamichhaney et al., 2015; Lerner, Meyer, James, Hofreiter, & Fleischer, 2011; Parchman, Benkman, & Britch, 2006). These striking results coupled with other empirical studies suggest bill morphology should be strongly associated with foraging and dietary resources. Yet, selection for foraging efficiency may not operate in isolation from other environmental and ecological drivers.

The avian bill has also been studied in the context of thermoregulation and, specifically, heat dissipation (Tattersall, Arnaout, & Symonds, 2016). The bird bill is an exposed, vascularized network that exchanges heat directly with the environment, thereby acting as a 'thermal window' between internal temperature and external, ambient temperature (Hagan & Heath, 1980; Symonds & Tattersall, 2010; Tattersall, Andrade, & Abe, 2009). Increased blood flow to the vascularized region of the bill results in increased heat dissipation (Tattersall et al., 2016). By dissipating dry heat through radiation rather than panting, birds in arid, xeric environments may reduce evaporative water loss while maintaining body temperature equilibrium (Dawson, 1981; Tattersall et al., 2016). However, selection for large bills to increase thermoregulatory capacity could also impact diet depending on the availability of food resources and on how strongly bill dimensions affect functionality, namely in bite force and seed extraction (Herrel et al., 2010; Soons et al., 2015; van der Meij & Bout, 2004). Thus, testing the relative importance of food resources and climate on bill variation and evaluating the functional

consequences of population shifts in bill morphology allows for inferring how selection operates on integrated traits.

Here, we investigate the relationship between variation in bill surface area, feeding performance, and climate in song sparrows (*Melospiza melodia*) breeding on the California Channel Islands. These island populations provide an ideal system for investigating how environmental factors influence adaptation in bill morphology. Song sparrows are continuously distributed along a climatic gradient ranging from cold, wet, and very windy on San Miguel and Santa Rosa Islands to hot, arid, and less windy on Santa Cruz and Anacapa Islands (Schoennerr Feldmeth, & Emerson, 2003; Fig. 2.1). In this system, maximum island temperature has been shown to be positively correlated with bill surface area of song sparrow museum specimens and implicated in aiding in thermoregulation (Greenberg & Danner, 2012). Yet, the islands' west-to-east climate gradient is also associated with vegetation differences (Junak et al., 2007) that could affect song sparrow habitat composition and food availability. We sampled contemporary sparrow populations across three climatically distinct islands (San Miguel, Santa Rosa, and Santa Cruz Islands) to test two hypothesized functional adaptations in song sparrow bills: thermoregulation and foraging efficiency. If bill morphology is acting as a thermoregulatory trait, we predicted that variation among song sparrow populations would be correlated with climatic differences across islands. If foraging efficiency explained variation in bill morphology, we predicted that bite force or seed extraction time would change as a function of bill dimensions, given that song sparrows primarily consume seeds during the non-breeding season (Arcese, Sogge, Marra, & Patten, 2002). We additionally assessed plant composition in song sparrow habitats (a proxy for food resources) across the three islands. Our combined assessments

of the environmental correlates and functional consequences of bill variation allowed us to infer how complex selection regimes shape individual morphology and feeding performance.

Methods

Animal capture and morphological measurements

We captured and measured song sparrows on San Miguel, Santa Rosa, and Santa Cruz Islands during three breeding seasons (February-June) from 2014-2016 (Fig. 2.1A). All birds were target-captured using mist-nets and song playback in the morning (thirty minutes before sunrise to four hours after sunrise) when territory defense and foraging activities are high. We measured bill dimensions (depth, width, and length) from the anterior edge of the nares (Fig. 2.1B-C), tarsometatarsus length, wing length (0.01 mm precision), and mass. Estimates of bill depth, width, and length were used to generate total bill surface area, following Greenberg and Danner (2012). When comparing bill surface area among populations, we used the residual of a linear regression model with bill surface area as the response and the first principal component of an analysis of tarsometatarsus length and wing length as the predictor (Greenberg & Danner, 2012). Tarsometatarsus and wing lengths are indicators of structural body size in birds, and this approach allows us to control for allometry (Rising & Somers, 1989). Negative values for residual bill surface area are indicative of smaller bill sizes than predicted by body sizes alone and, conversely, positive values suggest larger bill sizes than predicted by body sizes alone.

We applied nonparametric tests in R (R Core Team 2020) to determine whether raw (uncorrected for body size) and residual (corrected for body size) bill surface area differed by island. We used Kruskal-Wallis tests (*kruskal.test*) to assess whether island raw and residual bill surface area mean ranks differed, while accounting for unequal variances. We did not include sex

in our models, because body size corrections account for allometric differences between males and females. To further investigate island differences, we performed post-hoc, pairwise comparisons of island mean ranks and output 95% confidence intervals around estimated differences using Mann-Whitney U tests (*wilcox.test*) with Bonferroni corrections for multiple-testing.

Testing if song sparrows experience different thermal environments and habitats

We extracted climate data at 1 km^2 (30s) spatial resolution from WorldClim v. 1.4 (Hijmans, Cameron, Parra, Jones, & Jarvis, 2005) for all sampling locations using ArcGIS v. 10.4 (ESRI 2011) to test if birds on different islands experience different temperatures. Minimum, maximum, and mean monthly temperatures were highly correlated ($r^2 > 0.7$). Based on previous work showing a significant, positive correlation between residual bill surface area and maximum temperature (Greenberg & Danner, 2012), we limited our analyses to maximum temperature and extracted monthly temperatures in July, the hottest month of the year on average for the northern Channel Islands. Extracted maximum temperature values served as a proxy for climate in individual song sparrow territories. As with analyses of bill dimensions, we performed a nonparametric Kruskal-Wallis test to compare island mean ranks and quantified pairwise differences in island mean ranks and 95% confidence intervals using post-hoc Mann-Whitney U tests.

Song sparrows generally occupy low shrubland and, occasionally, riparian and coastal sage scrub habitat across the Channel Islands (Shuford & Gardali, 2008). To infer if sparrows use different habitats with different plant species (a proxy for dietary resources), we conducted vegetation surveys within a 25-meter radius of each mist-net location for sampled birds. Because sampling occurred during the breeding season, these measurements were taken within the

approximated territories of sampled birds and, thus, reflect the plant species available. We recorded dominant woody vegetation type to the species level, when possible, for all plants that comprised >50% of the total area. Additionally, we identified commonly occurring vegetation types and categorized the relative abundance of these vegetation types at all sparrow sampling sites. Presence and coverage of vegetation types within the sampling area was recorded using a ranked scale including absent (0%; 1), trace (<10%; 2), some (10-25%; 3), prominent (25-50%; 4), and dominant (>50%; 5). To infer island-level vegetative differences among song sparrow territories, we used Fisher's exact test in R (*fisher.test*) to test for an association between ranked abundance of vegetation types and island. We modeled the null distribution of the test statistic using 10,000 Monte Carlo simulations, allowing us to estimate the p-value under the null hypothesis that the abundance of different vegetation types is independent of the island sampled.

We modeled vegetation for individual sampling locations by transforming ordinal vegetation data to quantitative dimensions using nonlinear principal components analysis (NLPCA) implemented in the R package *Gifi* (Mair & de Leeuw, 2019). This multivariate method reduced the complexity of correlated vegetation variables to two principal components in ordination space while accounting for ranked abundance of each vegetation type. We visually inspected NLPCA results and assessed loadings of categorical values on dimensional space to infer what factors drive variation in the first two axes of variation ($PC1_{veg}$ and $PC2_{veg}$) among song sparrow territories. We plotted individual sampling locations in vegetation space along $PC1_{veg}$ and $PC2_{veg}$ axes and constructed 95% kernel density contours to visually assess overlap among islands in vegetation space. To statistically compare these reduced vegetation descriptors ($PC1_{veg}$ and $PC2_{veg}$) among islands, we again applied a nonparametric Kruskal-Wallis test to account for unequal variances. We performed post-hoc Mann-Whitney U tests with Bonferroni

corrections and extracted estimated island means and 95% confidence intervals around these differences. NLPCA dimensions ($PC1_{veg}$ and $PC2_{veg}$) were used for subsequent tests relating habitat and residual bill surface area.

We performed linear regression to determine whether vegetation and climate were significant predictors of residual bill surface area. We used the R function *lm* to model residual bill surface area as predicted by maximum temperature and two vegetation dimensions ($PC1_{veg}$ and $PC2_{veg}$) resulting from NLPCA of all vegetation sampling sites. We generated 95% confidence intervals around unstandardized beta estimates using the function *confint* in the base *stats* package in R and extracted standardized beta coefficients for all predictors using the R package *lm.beta* (Behrendt, 2014). Unstandardized and standardized beta coefficients allowed us to evaluate the relative importance of climate versus vegetation (a proxy for diet) for predicting variation in song sparrow bill surface area.

Measuring maximum bite force to infer the functional consequences of bill variation

To determine whether divergence in bill morphology results in functional consequences for food acquisition, we compared bill functional morphology between Santa Cruz and San Miguel Island song sparrows. We expected functional differences to be largest between these populations based on pronounced climate differences between islands and on phenotypes observed in museum specimens by Greenberg and Danner (2012). All sampling and estimates of bite force were performed in early spring 2014, when birds are primarily foraging on seeds. We measured maximum bite force in the field using a custom-manufactured force meter (Herrel et al., 2005; van der Meij & Bout, 2004). Briefly, we used a piezoelectric isometric force transducer (type 9203, Kistler, Switzerland) fitted to custom-built stainless-steel bite plates (specifications in Herrel et al., 1999) and connected to a charge amplifier (type 5995, Kistler, Switzerland). A

micrometer head allowed adjustment of the spacing between bite plates. For each measurement, we held the bird upright and positioned the bite force meter between the mandible and maxilla. We positioned the ends of the plates two-thirds of the distance from the bill tip to commissure, the location where song sparrows crush seeds (Danner, *pers. obs.*). The meter had a precision of 0.1 Newtons. We recorded the maximum bite force over a period of 15 seconds. Birds were gently coaxed to open the bill by tapping on the tomia with a thin, metal spade. Preliminary analyses on song sparrows indicated that bite force did not decline across observations when measurements were interspersed with 15-second rest intervals (Danner, *pers. obs*). Thus, we recorded three measurements per bird with one-minute rest intervals to ensure recovery and used the maximum bite force for all further analyses. All morphological measurements were taken shortly before releasing the birds to minimize the effect of handling stress on bite force and seed extraction trials. We maintained the same force meter settings for all individuals.

To assess the relationship between bill dimensions and bite force, we performed multiple regression analysis. We included bill depth and body size as predictors, because these traits have been found to strongly predict bite force in other passerines (Herrel et al., 2005; Soons et al., 2015; van der Meij & Bout, 2008). We generated a composite score of body size ($PC1_{bod}$) using PCA of tarsometatarsus and wing lengths for individuals used in bite force analyses. We applied linear regression in R using the function *lm* with bill depth and $PC1_{bod}$ as our predictors for maximum bite force. We did not include island sampled in our analyses as this was not independent of bill dimensions. We extracted standardized beta coefficients and 95% confidence intervals around unstandardized beta coefficients to compare the effects of both predictors on maximum bite force.

Quantifying seed extraction time to infer the functional consequences of bill variation

We held a subset of captured males in 2014 for caged field trials to quantify foraging efficiency. Females were excluded from trials to prevent interruption of incubating or laying behaviors. Following capture, we immediately placed birds in covered trial cages for acclimation to experimental conditions (Appendix 1 Fig. S1.1). All subjects were provided with water throughout the duration of the trial. We provided a two-hour acclimation and fasting period prior to the initiation of each trial. During the acclimation period, we monitored activity continuously via video cameras. Following acclimation, we initiated recording and slowly poured 10 grams of sterilized nyjer seed (*Guizotia abyssinica*) through a funnel in a brown plastic tube, which dispersed seeds across the floor of the cage. Sterilized nyjer seed is commonly used as bird feed for small passerines, and sterilization ensures the subsequent germination does not occur. Although *G. abyssinica* is not found on the Channel Islands and may not represent typical seed resources, song sparrows are generalist, ground-foragers. Thus, we assumed that our experimental food provisioning method facilitated normal foraging behavior. Trials lasted 45-120 minutes depending on latency to eat. We recorded behavioral notes during both acclimation and trial periods.

We reviewed foraging trial videos to quantify seed extraction time across multiple seeds. We counted the number of frames between when a bird's bill tip lifted from the floor of the cage with a seed, to when the husk fell from the tomium (van der Meij & Bout, 2006). We divided the number of frames by the camera's frame capture rate (29.97 frames/second) to calculate seed extraction time. The high temporal resolution of the cameras provided a precision of 0.033 seconds. We included only feeding events in which seed manipulation was observed throughout the entire seed extraction process.

Seed extraction is a complex task that requires manipulation of the bill along multiple axes. Consequently, we performed a PCA of bill depth, width, and length and used the first axis of variation ($PC1_{bill}$) to test whether differences in bill morphology is result in differences in seed extraction time. We included $PC1_{bill}$ of bill dimensions as a fixed effect in a linear mixed model predicting seed extraction time using the function *lmer* in the package *lme4* (Bates, Mächler, Bolker, & Walker, 2015). We accounted for repeated observations of the same bird by including individual as a random effect. We extracted 95% confidence intervals around the estimated coefficient for $PC1_{bill}$ using the function *confint* to infer the strength of $PC1_{bill}$ in modifying seed extraction time.

Results

Patterns of bill variation in contemporary populations

From 2014-2016, we measured 542 adult song sparrows (San Miguel Island, n = 104; Santa Rosa Island, n = 194; Santa Cruz Island, n = 244) sampled from 432 unique net locations (San Miguel Island, n = 68; Santa Rosa Island, n = 141; Santa Cruz Island, n = 223; Fig. 2.1). Patterns of bill variation in contemporary populations aligned with our expectations based on previous research using museum specimens (Greenberg & Danner, 2012). Islands differed significantly in mean ranks for both raw bill surface area ($H_{df=2}$ = 138.30, $P < 0.001$) and residual bill surface area ($H_{df=2}$ = 143.96, $P < 0.001$) using Kruskal-Wallis tests. We found all Mann-Whitney U pairwise comparisons of raw and residual bill surface areas between islands were significant (Table 2.1). We confirmed larger bills were found on Santa Cruz Island, medium bills were found on Santa Rosa Island, and the smallest bills were found among San Miguel Island birds based on Hodges–Lehmann estimates of medians (Table 2.1).

Maximum temperature and vegetation within breeding territories across islands

Environmental conditions within song sparrow breeding territories differed among the 432 unique sampling locations across islands (San Miguel Island, $n = 68$; Santa Rosa Island, $n = 141$; Santa Cruz Island, $n = 223$; Fig. 2.1). We found mean ranks in island maximum temperatures were significantly different ($H_2 = 282.63$, $P < 0.001$). Post-hoc pairwise comparisons of maximum temperature were significantly different between island pairs as expected, such that Santa Cruz Island had a higher and San Miguel has lower median estimates of maximum temperature in territories (Table 2.1). Additionally, we found ranked abundances in broad vegetation types were significantly associated with island sampled using 10,000 Monte Carlo simulations in Fisher's exact test ($P < 0.001$). Common dominant vegetation included coyote brush (*Baccharis pilularis*), toyon (*Heteromeles arbutifolia*), silver bush lupine (*Lupinus albifrons*), introduced sweet fennel (*Foeniculum vulgare*), and a mix of annual and perennial grasses (Appendix 1 Table S1.1).

Using NLPCA, we reduced the complexity in correlated ranked abundance of vegetation types among sampling locations. The first two principal components explained a total of 52.7% of the variation in vegetation. The first axis ($PC1_{veg}$) explained 30.5% of the variation in vegetation, and the abundance of grasses and the joint effects of the abundance of lupine, miscellaneous forbs, and other substrates (i.e., bare ground or rock, water) loaded in opposing directions (Fig. 2.2A). This suggests that positive values along $PC1_{veg}$ are indicative of territories with more lupine, forbs, and other substrates and less grass, and negative values represent the inverse of this relationship (Fig. 2.2A). The second axis of variation ($PC2_{veg}$) explained 22.2% of variation in vegetation and reflects a trade-off in fennel and coyote brush (Fig. 2.2A). Positive

values indicate more fennel and less coyote brush, and negative values represent less fennel and more coyote brush (Fig. 2.2A).

We found islands overlapped in vegetation space based on 95% kernel density contours (Fig. 2.2B). We assessed these relationships statistically using nonparametric tests and found significant differences among island mean ranks in both vegetation dimensions ($PC1_{veg}$, H_2 = 31.73, $P < 0.001$; $PC2_{veg}$, $H_2 = 241.85$, $P < 0.001$; Table 2.1). Using post-hoc Mann-Whitney U tests, we found $PC1_{veg}$ scores for Santa Rosa Island territories were more negative, such that territories on Santa Rosa Island had more grass and less miscellaneous forbs, bare ground and rock, open water, and lupine compared to Santa Cruz and San Miguel Islands (Fig. 2.2B). In contrast, we found $PC2_{veg}$ scores for Santa Cruz Island territories were significantly greater, with Santa Cruz territories encompassing more fennel and less coyote brush compared to Santa Rosa and San Miguel Islands (Fig. 2.2B).

Multiple regression analysis was used to assess the relative importance of vegetation ($PC1_{veg}$ and $PC2_{veg}$) and maximum temperature in driving bill differences in adult song sparrows (Santa Cruz, $n = 218$ birds, Santa Rosa, $n = 146$ birds, San Miguel, $n = 81$ birds). These variables together explained a significant proportion of variation in residual bill surface area ($F_{3,442}$ = 55.25, $P < 0.001$, adjusted $R^2 = 0.27$; Fig. 2.3). We found residual bill surface area was significantly predicted by maximum island temperatures ($\beta_{standardized} = 0.40$, $\beta_{unstandardized} = 3.06$ (2.20 — 3.93), $t = 10.350$, $P < 0.001$). Although we found island differences in vegetation space, neither $PC1_{veg}$ ($\beta_{standardized} = -0.05$, $\beta_{unstandardized} = -0.28$ (-0.77 — 0.20), $t = -1.147$, $P = 0.25$) nor $PC2_{veg}$ ($\beta_{standardized} = 0.04$, $\beta_{unstandardized} = 0.20$ (-0.43 — 0.83), $t = 0.610$, $P = 0.54$) were significant predictors. Vegetation space was used as a proxy for available food resources, and these results suggest climate, not food, is likely driving differences in residual bill surface area.

Functional consequences of bill variation between island populations

Contrary to predictions from the foraging efficiency hypothesis, we did not find evidence that differences in bill morphology result in functional differences in bite force between birds on San Miguel (n = 28) and Santa Cruz Island (n = 28). Body size ($PC1_{bod}$) and bill depth together explained very little of the variation in maximum bite force ($F_{2,53}$ = 1.45, P = 0.24, adjusted R^2 = 0.02; Fig. 2.4A). Although Santa Cruz Island birds tended to have larger structural bodies ($PC_{bod(Cruz)}$, mean±sd = 0.22±1.09; $PC_{bod(Miguel)}$, mean±sd = -0.22±1.02), body size distributions generally overlapped and did not significantly predict maximum bite force ($\beta_{standardized}$ = 0.17, $\beta_{unstandardized}$ = 0.23 (-0.14 — 0.59), t = 1.247, P = 0.22). Island sampling groups differed in bill depth as expected with birds on Santa Cruz Island having deeper bills ($Depth_{(Cruz)}$, mean±sd = 6.15±0.21; $Depth_{(Miguel)}$, mean±sd = 5.54±0.20; Fig. 2.4A). Yet, we found little evidence to suggest that these differences in depth result in synonymous changes in maximum bite force ($\beta_{standardized}$ = 0.17, $\beta_{unstandardized}$ = -0.74 (-1.80 — 0.32), t = -1.394, P = 0.17).

We performed foraging trials in adult, male song sparrows from Santa Cruz Island (n = 23) and San Miguel Island (n = 10), and, again, found little evidence for an effect of bill morphology on seed extraction time. The first principal component ($PC1_{bill}$) in a PCA of bill depth, width, and length explained 58% of the variation in bill dimensions and was largely driven by bill depth and width (Appendix 1 Fig. S1.2). San Miguel Island and Santa Cruz Island birds overlapped along PC1 (Fig. 2.4B), but San Miguel birds loaded more positively (shallower, narrower, slightly longer bills). In contrast, Santa Cruz Island birds loaded more negatively, suggesting birds tended to have deeper, wider, slightly shorter bills. The mean number of observed extracted seeds was 60 seeds per individual (sd = 32, range = 8 – 163), and 13% of variance was explained by individual effects. $PC1_{bill}$ had a very weak to negligible effect on seed

extraction time (β = 0.009 (-0.14 – 0.16), t_{32} = 0.115, P = 0.91). These results combined with bite force analyses suggest that morphological differences in bills do not facilitate differences in foraging efficiency in island song sparrows.

Discussion

Identifying the ecological correlates of phenotypic variation provides insights into the selection pressures that may shape complex traits and their multiple functions. The avian bill is one such complex trait that has primarily been studied in the context of foraging ability despite its critical role in preening, communication, and thermoregulation. Indeed, there has been growing appreciation for the role of climate in shaping variation in bill morphology, as mounting evidence suggests the bill is an important tool for heat dissipation and thermoregulation (e.g., Gardner et al., 2016; Greenberg & Danner, 2013; Ryeland et al., 2017; Symonds & Tattersall, 2010). Here, we tested whether climate and/or vegetation composition within breeding territories significantly predicted bill variation in song sparrows on the California Channel Islands (i.e., San Miguel, Santa Rosa, and Santa Cruz Islands). We confirmed that bill size, maximum temperature, and vegetation composition differed among islands. However, only maximum temperature significantly predicted residual bill surface area in multiple regression analysis including vegetation dimensions as predictors (Fig. 2.3). We did not find a significant relationship between bill morphology and either maximum bite force or seed extraction time. This provides additional evidence against foraging efficiency as a strong selective pressure in this system. Together, these results suggest that climate may be more important than diet and foraging ability in the evolution of a complex phenotype in song sparrows on the California Channel Islands.

Vegetation differences do not directly result in synonymous changes in bill morphology

Analysis of habitat composition with respect to vegetation provides key insights into the potential food resources available for breeding birds. Because song sparrows on the Channel Islands occupy a strong east-west climate gradient, we expected some degree of habitat differences among island breeding sites. Thus, it is not surprising that ranked abundance in our focal vegetation categories were significantly associated with island sampled. For example, Santa Cruz Island is characterized by greater heterogeneity in topography, soil composition, and climate, which is correlated with increases in species richness and diversity of plants compared to Santa Rosa and San Miguel Islands (Schoennerr et al., 2003). Our results demonstrate increased diversity in vegetation space ($PC1_{veg}$ and $PC2_{veg}$) within Santa Cruz Island territories (Fig. 2.2B). Yet, 95% kernel density contours also suggest a large proportion of overlap in vegetation space among islands (Fig. 2.2B), and similar plant taxa identifiable to the genus and species level were present across all islands (Appendix 1 Table S1.1). Future studies that include more extensive vegetation and habitat sampling may allow for the parsing of fine-scale habitat differentiation among islands, but whether any differences in vegetation result in differences in food resources is uncertain. Direct observation of foraging behavior and evaluation of the available dietary resources during the non-breeding season, when song sparrows most heavily rely on seeds, would enable stronger inferences regarding the relationships among foraging ability, diet, and bill morphology. Nevertheless, our analyses support the hypothesis that climate may facilitate vegetative differences among song sparrow territories, but differences in vegetation did not directly predict bill morphology in multiple regression analyses. Hence, vegetation, a proxy for food resources and diet, may not be a strong selective pressure generating

bill variation across islands, and we found further evidence against selection operating on foraging ability in experimental tests of foraging efficiency (Fig. 2.4A-B).

Variation in bill morphology does not result in differences in foraging efficiency

We did not find a relationship between variation in bill morphology and either bite force or seed extraction time (Fig. 2.4A-B), despite evidence that bill dimensions affect feeding performance in other passerines (Anderson, Mcbrayer, & Herrel, 2008; Herrel et al., 2005; Navalón, Bright, Marugán-Lobón, & Rayfield, 2019). Indeed, some of the most well-documented cases of specialization in resource acquisition with respect to bill variation occur in island systems (Burns et al., 2003; Grant & Grant, 2002). Of these cases, Darwin's ground finches (*Geospiza sp.*) are perhaps most notable and ecologically similar to song sparrows in their foraging behavior and diet (De León, Podos, Gardezi, Herrel, & Hendry, 2014). In Darwin's finches, birds exhibit correlations between both bill dimensions and bite force (Herrel et al., 2005; Soons et al., 2015; van der Meij & Bout, 2008) and bill dimensions and seed extraction times (van der Meij & Bout, 2008). The discordance between our results and findings from studies of Darwin's finches may be attributed to multiple factors.

First, sparrows are generalist foragers with a heavy insectivorous diet during the breeding season and a transition to a granivorous diet during the non-breeding season (Arcese et al., 2002), whereas Darwin's ground finches' diets consist primarily of seeds throughout the year (De León et al., 2014). Specialization on seeds and food limitation in ground finches facilitate competitive interactions among species that overlap in their dietary niches (De León et al., 2014), resulting in strong selection on individuals to optimize bill morphology for increased foraging efficiency. On the California Channel Islands, it is unclear whether food resources are limited and whether food limitation imposes a strong selective pressure on song sparrow

populations. Mass comparisons between sparrows from the Channel Islands and nearby mainland California found island sparrows to heavier than mainland sparrows when correcting for structural body size, suggesting island birds are in better condition (Danner, Greenberg, & Sillett, 2014). Increased mass among island sparrows supports the hypotheses that food resources are not limited and reduced interspecific competition for food favors the sparrows' generalist diets (Blondel, 2000; Clegg, 2010; Diamond, 1970; Keast, 1970; Scott, Clegg, Blomberg, Kikkawa, & Owens, 2003). As a result, variation in bill morphology may be decoupled from foraging efficiency traits measured in this study.

Additionally, methodological limitations may have prevented us from quantifying key traits associated with foraging. For example, previous research in Darwin's finches identify a link between muscle mass and maximum bite force (Herrel et al., 2005; Herrel et al., 2010; Soons et al., 2015), and other skeletal features are correlated with bite force and closing velocity (Corbin, Lowenberger, & Gray, 2015). These methods require analysis of euthanized individuals, which we were unable perform. Here, we evaluated bite force differences elicited from the posterior section of the bill, not from the anterior (the tip) where functional differences in grasping and object manipulation occur across avian families (Clayton et al., 2005; Demery, Chappell, & Martin, 2011; Gentle, Hughes, & Hubrecht, 1982; Sustaita, 2007). Skeletal structures associated with foraging traits are highly-correlated (van der Meij & Bout, 2008), and our measures adequately estimate a large proportion of variation in overall bill morphology. Yet, future studies quantifying unmeasured phenotypic traits in this study may better estimate the functional consequences of craniofacial variation. Finally, we were limited to using readily available bird seed for foraging trials to increase our ability to observe detailed manipulation of the food resource. We did not compare nyjer seed characteristics with those used by song

sparrows on the Channel Islands during the winter months. Yet, seed availability during winter months were likely similar given that non-native, seed-producing plant species (e.g., annual grasses) are widespread (Junak et al., 2007) and were present at most sampling locations (Appendix 1 Table S1.1). Sample size does not appear to be an issue, as a power analysis suggests that our sample sizes were sufficient to detect a biologically relevant difference in maximum bite force given our experimental design (Appendix 1 Fig. S1.3). Although we did not find evidence that foraging efficiency is an important driver of variation in bill shape in our study populations, further research is needed to definitively exclude the possibility that differing food resources among islands is a selective force. Our experimental design provides a framework for future studies to test how bill dimensions influence multiple components of foraging efficiency (i.e., both bite force and seed extraction).

Evidence for the bill as a thermoregulatory trait in island sparrows

Our results are consistent with the hypothesis that selection operates on the bill to improve thermoregulatory ability in passerines occupying xeric environments. Increasing empirical evidence demonstrate a relationship between climate and bill morphology that aligns with the thermoregulatory hypothesis (reviewed by Tattersall et al., 2016), and this relationship may be traced over evolutionary time (Campbell-Tennant, Gardner, Kearney, & Symonds, 2015). The ability to radiate heat from unfeathered structures is particularly important for small passerines, including song sparrows, which are more vulnerable to dehydration from evaporative water loss and, thus, more susceptible to adverse effects of thermal stress (Mckechnie & Wolf, 2009; Whitfield, Smit, McKechnie, & Wolf, 2015). Indeed, our results are consistent with previous research that identified a significant, positive correlation between climate and bill morphology in eastern and Atlantic song sparrows (Danner & Greenberg, 2014). A similar

pattern has been described in Darwin's finches (Tattersall et al., 2018) and other similarly-sized passerines (Greenberg & Danner, 2012; LaBarbera, Hayes, Marsh, & Lacey, 2017; Laiolo & Rolando, 2001). The magnitude of the effect of climate in predicting bill morphology may change according to seasonality (Greenberg, Etterson, & Danner, 2013), environmental variation during development (Burness, Huard, Malcolm, & Tattersall, 2013; Labarbera, Marsh, Hayes, & Hammond, 2020), habitat type (Luther & Greenberg, 2014), and sex (Greenberg & Danner, 2013). Importantly, selection may act simultaneously on other traits to facilitate thermoregulation, including internal nasal structures (Danner et al., 2017), plumage (Wolf & Walsberg, 2000), and physiological performance (e.g., Noakes et al., 2016; Tieleman et al., 2003; White et al., 2007; Whitfield et al., 2015). Thus, further research that explores the complex relationship between temperature, humidity, and other morphological and physiological traits is needed to better understand how climate facilitates and maintains phenotypic variation.

Conclusions

Consistent with previous studies using museum specimens, variation in bill morphology among contemporary song sparrow populations on the California Channel Island is correlated with maximum temperature, suggesting an important thermoregulatory function. Differences in the vegetation and habitats used by sparrows on different islands were not strongly predictive of observed bill divergence. Variation in bill morphology was also not correlated with bite force or seed extraction, perhaps because song sparrows are generalist foragers. We hope that our results encourage future research about how different environmental agents of selection simultaneously act on avian bills to optimize the multiple, fitness-related functions of foraging, thermoregulation, preening, and vocalization.

Tables and Figures

Table 2.1 Nonparametric pairwise island comparisons (median±c.i.) for song sparrow raw (uncorrected for body size) and residual (corrected for body size) bill surface areas, maximum environmental temperatures (*T*), and vegetation dimensions (PC1, PC2). Pairwise comparisons were estimated using the Hodges-Lehmann method for bill surface areas in 542 birds (San Miguel Island, *n* = 104; Santa Rosa Island, *n* = 194; Santa Cruz Island, *n* = 244) and for temperature and vegetation characteristics across 432 unique sampling locations (San Miguel Island, *n* = 68; Santa Rosa Island, *n* = 141; Santa Cruz Island, *n* = 223)**.** Vegetation dimensions include PC1 and PC2 from nonlinear PCA (NLPCA) of ranked abundance in vegetation categories within breeding song sparrow territories. All islands had significantly different ($P < 0.05$) mean ranks in all bill and environmental variables based on nonparametric Kruskal-Wallis tests. Post-hoc Mann-Whitney U 95% confidence intervals around differences in mean ranks are shown in parentheses. Bill surface area analyses include only adult, breeding, territorial birds with complete phenotype measurements, and maximum temperature was extracted only for these unique sampling locations. Vegetation sampling occurred at most of these temperature sampling locations and at locations for territorial birds that did not have complete phenotype measurements. Asterisks denote significant differences in population distributions between islands based on Mann-Whitney U tests.

Island Comparison	Bill Surface Area		Maximum Temperature	Vegetation NLPCA Dimensions	
	Raw (mm^2)	Residual	*T* (ºC)	PC1 (30.4%)	PC2 (22.2%)
Santa Cruz – Santa Rosa	2.32*** (1.33 - 3.28)	2.72*** (1.77 - 3.70)	1.00*** (0.80 - 1.10)	0.35*** (0.22 - 0.54)	1.38*** (1.20 - 1.55)
Santa Cruz – San Miguel	7.67*** (6.58 - 8.76)	7.67*** (6.58 - 8.76)	1.80*** (1.70 - 1.90)	-0.34 (-0.67 - 0.00)	1.36*** (1.13 - 1.59)
Santa Rosa – San Miguel	5.49*** (4.35 - 6.58)	5.03*** (3.93 - 6.11)	0.80*** (0.70 - 0.80)	-0.81*** (-1.12 - -0.51)	0.00 (-0.10 - 0.11)

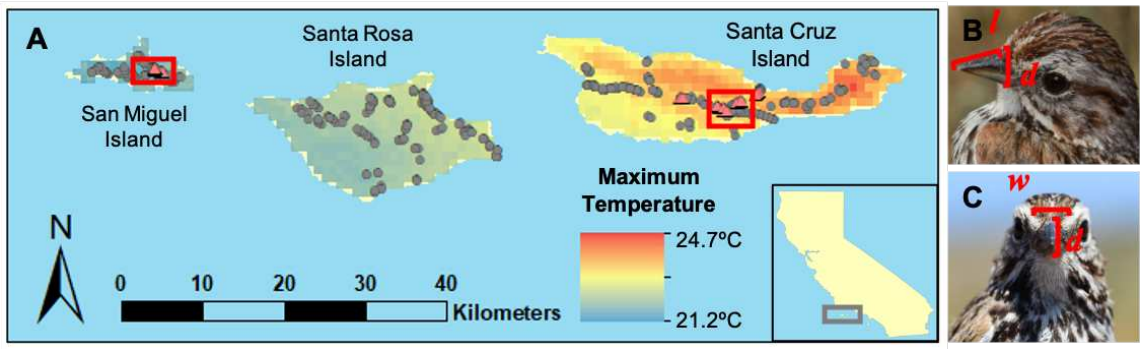

Figure 2.1 Sampling locations for comparison of song sparrow bill morphology (grey circles), seed extraction time (red triangles), and maximum bite force (red boxed regions) across three climatically distinct islands (A) and measurements of bill length, depth (B), and width (C) used for quantifying bill morphology. Bill length (*l*), depth (*d*), and width (*w*) were taken from the anterior edge of the nares and used to calculate residual (body-size corrected) bill surface area following Greenberg and Danner (2012). All sampling was conducted during the breeding season (February-June) from 2014-2016. Inset shows the location of the northern Channel Islands with respect to California.

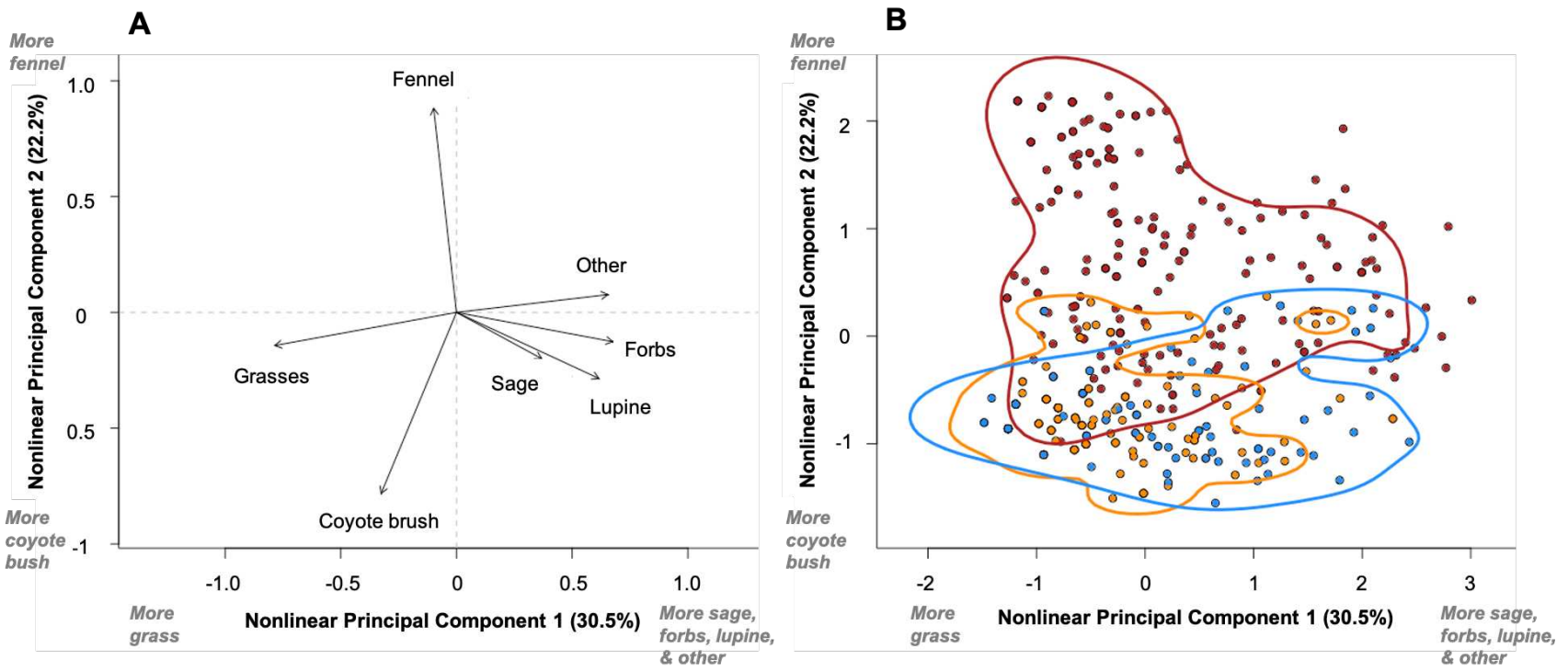

Figure 2.2 Variable loadings (A) and PC1, PC2, and 95% kernel density contours by island (B) from nonlinear PCA of vegetation within song sparrow territories. Sampling of 432 unique sampling locations occurred during the breeding season from 2014-2016 on San Miguel Island (blue; n = 68), Santa Rosa Island (orange; n = 141), and Santa Cruz Island (red; n = 223).

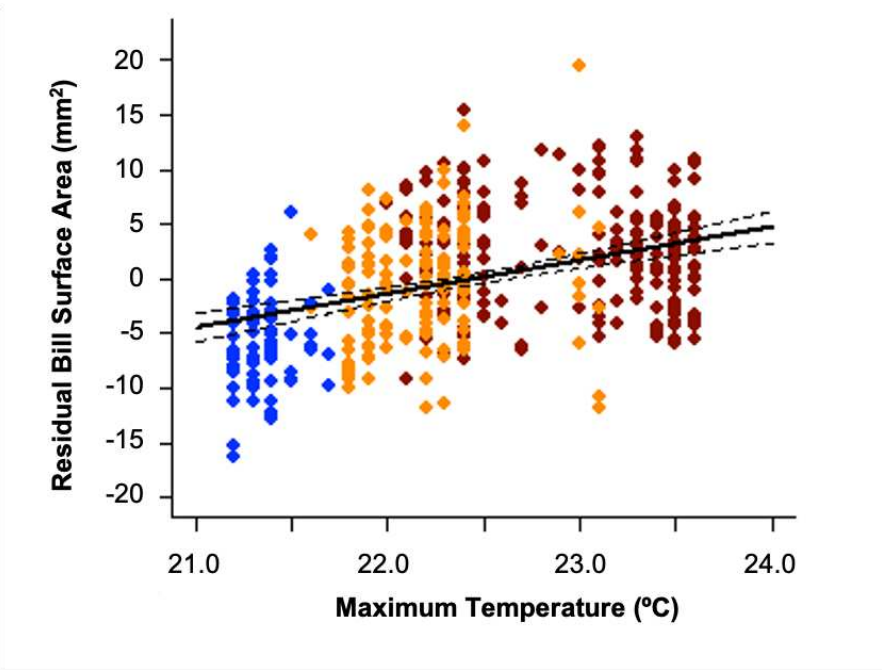

Figure 2.3 Residual bill surface area predicted by maximum temperature in song sparrows (*n* = 446) on the California Channel Islands. Residual bill surface area is total bill surface area corrected for skeletal body size and calculated from measures of bill depth, width, and length, tarsometatarsus length, and wing length in adult song sparrows on San Miguel Island (*n* = 81), Santa Rosa Island (orange, *n* = 147), and Santa Cruz Island (red, *n* = 218). Primary and secondary axes of variation from nonlinear PCA of vegetation (PC1 and PC2) were included in the linear regression analysis and were not significant predictors of residual bill surface area.

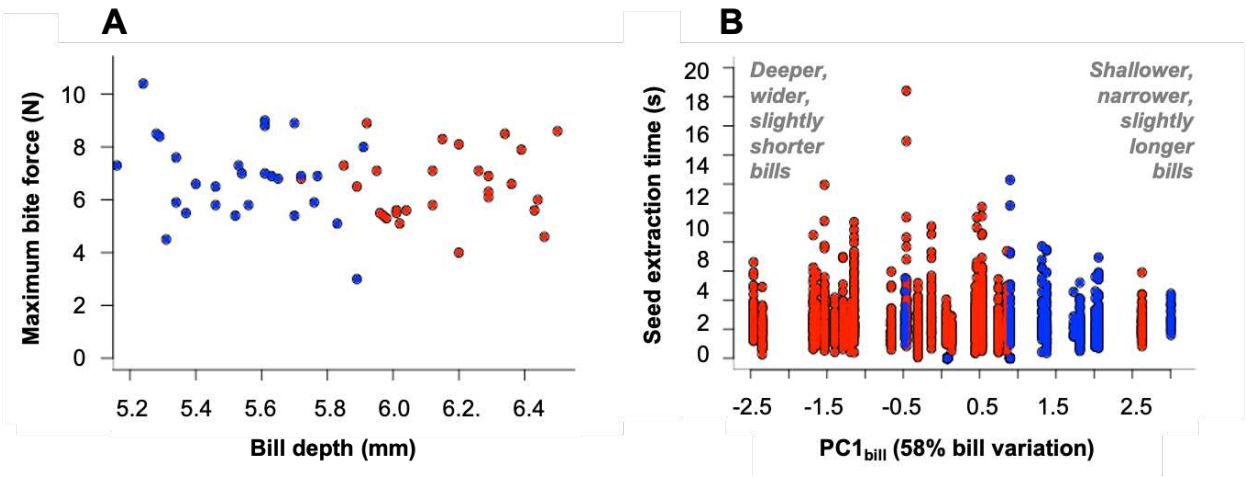

Figure 2.4 Relationship between song sparrow bill dimensions and foraging traits [maximum bite force (A) and seed extraction time (B)] between birds on Santa Cruz Island (red; $n_A = 28$, $n_B = 23$) and San Miguel Island (blue; $n_A = 28$, $n_B = 10$). $PC1_{bill}$ is the first orthogonal axis in a PCA of bill depth, width, and length taken from the anterior edge of the nares.

LITERATURE CITED

Åkesson, M., Bensch, S., Hasselquist, D., Tarka, M., & Hansson, B. (2008). Estimating heritabilities and genetic correlations: comparing the "animal mode" with parent-offspring regression using data from a natural population. *PLoS One*, *3*(3), e1739.

Anderson, R. A., Mcbrayer, L. D., & Herrel, A. (2008). Bite force in vertebrates: opportunities and caveats for use of a nonpareil whole-animal performance measure. *Biological Journal of the Linnean Society*, *93*(4), 709–720.

Arcese, P., Sogge, M. K., Marra, A. B., & Patten, M. A. (2002). Song sparrow (Melospiza melodia). In *The Birds of North America Online* (A. Poole). Retrieved from http://bna.birds.cornell.edu/bna/species/704.

Ballentine, B. (2006). Morphological adaptation influences the evolution of a mating signal. *Evolution, 60*(9), 1936–1944.

Barbosa, A., & Moreno, E. (1999). Evolution of foraging strategies in shorebirds: an ecomorphological approach. *The Auk*, *116*(3), 712–725.

Bates, D., Mächler, M., Bolker, B. M., & Walker, S. C. (2015). Fitting linear mixed-effects models using lme4. *Journal of Statistical Software*, *67*(1).

Behrendt, S. (2014). *lm.beta: Add Standardized Regression Coefficients to lm-Objects*. Retrieved from https://cran.r-project.org/package=lm.beta.

Benkman, C. W. (1993). Adaptation to single resources and the evolution of crossbill (Loxia) diversity. *Ecological Monographs*, *63*(3), 305–325.

Benkman, C. W. (2003). Divergent selection drives the adaptive radiation of crossbills. *Evolution*, *57*(5), 1176–1181.

Blondel, J. (2000). Evolution and ecology of birds on islands: trends and prospects. *Vie et Milieu*, *50*(4), 205–220.

Boag, P. T. (1983). The heritability of external morphology in Darwin's ground finches (Geospiza) on Isla Daphne Major, Galapagos. *Evolution*, *37*(5), 877–894.

Burness, G., Huard, J. R., Malcolm, E., & Tattersall, G. J. (2013). Post-hatch heat warms adult beaks: Irreversible physiological plasticity in Japanese quail. *Proceedings of the Royal Society B: Biological Sciences*, *280*(1767).

Burns, K. J., Hackett, S. J., & Klein, N. K. (2003). Phylogenetic relationships of Neotropical honeycreepers evolution of feeding morphology. *Journal of Avian Biology*, *34*(4), 360–370.

Campbell-Tennant, D. J. E., Gardner, J. L., Kearney, M. R., & Symonds, M. R. E. (2015). Climate-related spatial and temporal variation in bill morphology over the past century in Australian parrots. *Journal of Biogeography*, *42*(6), 1163–1175.

Clayton, D. H., Moyer, B. R., Bush, S. E., Jones, T. G., Gardiner, D. W., Rhodes, B. B., & Goller, F. (2005). Adaptive significance of avian beak morphology for ectoparasite control. *Proceedings of the Royal Society B: Biological Sciences*, *272*(1565), 811–817.

Clegg, S. M. (2010). Evolutionary changes following island colonization in birds: empirical insights into the roles of microevolutionary processes. In J. B. Losos & R. E. Ricklefs (Eds.), *The theory of island biogeography revisited* (pp. 293–325). Princeton, New Jersey: Princeton University Press.

Corbin, C. E., Lowenberger, L. K., & Gray, B. L. (2015). Linkage and trade-off in trophic morphology and behavioural performance of birds. *Functional Ecology*, *29*(6), 808–815.

Danner, R. M., & Greenberg, R. (2014). A critical season approach to Allen's rule: bill size declines with winter temperature in a cold temperate environment. *Journal of Biogeography*, 114–120.

Danner, R. M., Greenberg, R., & Sillett, T. S. (2014). The implications of increased body size in the song sparrows of the California Islands. *Monographs of the Western North American Naturalist*, *7*(1), 348–356.

Danner, R. M., Gulson-Castillo, E. R., James, H. F., Dzielski, S. A., Frank III, D. C., Sibbald, E. T., & Winkler, D. W. (2017). Habitat-specific divergence of air conditioning structures in bird bills. *The Auk*, *134*, 65–75.

Dawson, W. R. (1981). Evaporative losses of water by birds. *Comparative Biochemistry and Physiology Part A: Physiology*, *71*(4), 495–509.

De León, L. F., Podos, J., Gardezi, T., Herrel, A., & Hendry, A. P. (2014). Darwin's finches and their diet niches: the sympatric coexistence of imperfect generalists. *Journal of Evolutionary Biology*, *27*(6), 1093–1104.

Demery, Z. P., Chappell, J., & Martin, G. R. (2011). Vision, touch and object manipulation in senegal parrots Poicephalus senegalus. *Proceedings of the Royal Society B: Biological Sciences*, *278*(1725), 3687–3693.

Diamond, J. M. (1970). Ecological consequences of island colonization by southwest Pacific birds, I. Types of niche shifts. *Proceedings of the National Academy of Sciences*, *67*(2), 529–536.

Egea-Serrano, A., Hangartner, S., Laurila, A., & Räsänen, K. (2014). Multifarious selection through environmental change: acidity and predator-mediated adaptive divergence in the moor frog (Rana arvalis). *Proceedings of the Royal Society B: Biological Sciences*, *281*(1780), 20133266.

Fayet, A. L., Hansen, E. S., & Biro, D. (2020). Evidence of tool use in a seabird. *Proceedings of the National Academy of Sciences*, *117*(3), 1277–1279.

Friedman, N. R., Miller, E. T., Ball, J. R., Kasuga, H., Remeš, V., & Economo, E. P. (2019). Evolution of a multifunctional trait: shared effects of foraging ecology and thermoregulation on beak morphology, with consequences for song evolution. *Proceedings of the Royal Society B: Biological Sciences*, *286*(1917), 20192474.

Gardner, J. L., Symonds, M. R. E., Joseph, L., Ikin, K., Stein, J., & Kruuk, L. E. B. (2016). Spatial variation in avian bill size is associated with humidity in summer among Australian passerines. *Climate Change Responses*, *3*(1), 1–11.

Gentle, M. J., Hughes, B. O., & Hubrecht, R. C. (1982). The effect of beak trimming on food intake, feeding behaviour and body weight in adult hens. *Applied Animal Ethology*, *8*(1–2), 147–159.

Ghalambor, C. K., Walker, J. A., & Reznick, D. N. (2003). Multi-trait selection, adaptation, and constraints on the evolution of burst swimming performance. *Integrative and Comparative Biology*, *438*(43), 431–438.

Grant, P. R. (1983). Inheritance of size and shape in a population of Darwin's finches, Geospiza conirostris. *Proceedings of the Royal Society B: Biological Sciences*, *220*(1219), 219–236.

Grant, P. R., & Grant, B. R. (2002). Adaptive radiation of Darwin's finches. *American Scientist*, *90*(2), 130–139. doi: 10.1511/2002.2.130

Grant, P. R., & Grant, B. R. (2006). Evolution of character displacement in Darwin's finches. *Science*, *313*(5784), 224–226.

Greenberg, R., Cadena, V., Danner, R. M., & Tattersall, G. J. (2012). Heat loss may explain bill size differences between birds occupying different habitats. *PloS One*, *7*(7), e40933.

Greenberg, R., & Danner, R. M. (2012). The influence of the California marine layer on bill size in a generalist songbird. *Evolution*, *66*(12), 3825–3835.

Greenberg, R., & Danner, R. M. (2013). Climate, ecological release and bill dimorphism in an island songbird. *Biology Letters*, *9*(3), 20130118.

Greenberg, R., Etterson, M., & Danner, R. M. (2013). Seasonal dimorphism in the horny bills of sparrows. *Ecology and Evolution*, *3*(2), 389–398.

Hagan, A., & Heath, J. E. (1980). Regulation of heat loss in the duck by vasomotion in the bill. *Journal of Thermal Biology*, *5*, 95–101.

Herrel, A., Podos, J., Huber, S. K., & Hendry, A. P. (2005). Evolution of bite force in Darwin's finches: a key role for head width. *Journal of Evolutionary Biology*, *18*(3), 669–675.x

Herrel, A., Spithoven, L., Van Damme, R., & De Vree, F. (1999). Sexual dimorphism of head size in Gallotia galloti: testing the niche divergence hypothesis by functional analyses. *Functional Ecology*, *13*(3), 289–297.

Herrel, A., Soons, J., Aerts, P., Dirckx, J., Boone, M., Jacobs, P., … Podos, J. (2010). Adaptation and function of the bills of Darwins finches: divergence by feeding type and sex. *Emu*, *110*(1), 39–47.

Hijmans, R. J., Cameron, S. E., Parra, J. L., Jones, P. G., & Jarvis, A. (2005). Very high resolution interpolated climate surfaces for global land areas. *International Journal of Climatology*, *25*(15), 1965–1978.

Jensen, H., Saether, B.-E., Ringsby, T. H., Tufto, J., Griffith, S. C., & Ellegren, H. (2003). Sexual variation in heritability and genetic correlations of morphological traits in house sparrow (Passer domesticus). *Journal of Evolutionary Biology*, *16*(6), 1296–1307.

Jones, J. S., Leith, B. H., & Rawlings, P. (1977). Polymorphism in cepaea: a problem with too many solutions? *Annual Review of Ecology and Systematics*, *8*(1), 109–143.

Junak, S., Knapp, D. A., Haller, J. R., Philbrick, R., Schoenherr, A., & Keeler-Wolf, T. (2007). The California Channel Islands. In *Terrestrial Vegetation of California* (3rd Edition). Berkeley, California: University of California Press.

Kawecki, T. J., & Ebert, D. (2004). Conceptual issues in local adaptation. *Ecology Letters*, *7*(12), 1225–1241.

Keast, A. (1970). Adaptive evolution and shifts in niche occupation in island birds. *The Association for Tropical Biology and Conservation*, *2*(2), 61–75.

Keller, L. F., Grant, P. R., Rosemary Grant, B., & Petren, K. (2001). Heritability of morphological traits in Darwin's finches: misidentified paternity and maternal effects. *Heredity*, *87*(3), 325–336.

Kim, S. Y., Noguera, J. C., Morales, J., & Velando, A. (2011). Quantitative genetic evidence for trade-off between growth and resistance to oxidative stress in a wild bird. *Evolutionary Ecology*, *25*(2), 461–472.

LaBarbera, K., Hayes, K. R., Marsh, K. J., & Lacey, E. A. (2017). Complex relationships among environmental conditions and bill morphology in a generalist songbird. *Evolutionary Ecology*, *31*(5), 707–724.

Labarbera, K., Marsh, K. J., Hayes, K. R. R., & Hammond, T. T. (2020). Context-dependent effects of relative temperature extremes on bill morphology in a songbird. *Royal Society Open Science, 7*(4), 192203.

Laiolo, P., & Rolando, A. (2001). Ecogeographic correlates of morphometric variation in the red-billed Chough Pyrrhocorax pyrrhocorax and the Alpine Chough Pyrrhocorax graculus. *Ibis*, *143*(3), 602–616.

Lamichhaney, S., Berglund, J., Almén, M. S., Maqbool, K., Grabherr, M., Martinez-Barrio, A., … Andersson, L. (2015). Evolution of Darwin's finches and their beaks revealed by genome sequencing. *Nature*, *518*(7539), 371–375.

Langin, K. M., Sillett, T. S., Funk, W. C., Morrison, S. A., Desrosiers, M. A., & Ghalambor, C. K. (2015). Islands within an island: repeated adaptive divergence in a single population. *Evolution*, *69*(3), 653–665.

Lerner, H. R. L., Meyer, M., James, H. F., Hofreiter, M., & Fleischer, R. C. (2011). Multilocus resolution of phylogeny and timescale in the extant adaptive radiation of Hawaiian honeycreepers. *Current Biology*, *21*(21), 1838–1844.

Luther, D., & Greenberg, R. (2014). Habitat type and ambient temperature contribute to bill morphology. *Ecology and Evolution*, *4*(6), 699–705.

MacColl, A. D. C. (2011). The ecological causes of evolution. *Trends in Ecology & Evolution*, *26*(10), 514–522.

Mair, P., & de Leeuw, J. (2019). *Gifi: Multivariate Analysis with Optimal Scaling*. Retrieved from https://cran.r-project.org/package=Gifi.

McKechnie, A. E., & Wolf, B. O. (2009). Climate change increases the likelihood of catastrophic avian mortality events during extreme heat waves. *Biology Letters*, *6*(2), 253–256.

Navalón, G., Bright, J. A., Marugán-Lobón, J., & Rayfield, E. J. (2019). The evolutionary relationship among beak shape, mechanical advantage, and feeding ecology in modern birds. *Evolution*, *73*(3), 422–435.

Nebel, S., Jackson, D. L., & Elner, R. W. (2005). Functional association of bill morphology and foraging behaviour in calidrid sandpipers. *Animal Biology*, *55*(3), 235–243.

Noakes, M., Wolf, B., & McKechnie, A. (2016). Seasonal and geographical variation in heat tolerance and evaporative cooling capacity in a passerine bird. *Journal of Experimental Biology*, *219*(6), 859–869.

Parchman, T. L., Benkman, C. W., & Britch, S. C. (2006). Patterns of genetic variation in the adaptive radiation of New World crossbills (Aves: Loxia). *Molecular Ecology*, *15*(7), 1873–1887.

Pfrender, M. E. (2012). Triangulating the genetic basis of adaptation to multifarious selection. *Molecular Ecology*, *21*(9), 2051–2053.

Podos, J. (2001). Correlated evolution of morphology and vocal signal structure in Darwin's finches. *Nature*, *409*(6817), 185–188.

Podos, J., & Nowicki, S. (2004). Beaks, adaptation, and vocal evolution in Darwin's finches. *Bioscience*, *54*(6), 501-510.

Reznick, D. N., & Travis, J. (1996). The empirical study of adaptations in natural populations. In M. R. Rose & G. V. Lauder (Eds.), *Adaptations* (pp. 243–290). San Diego, California: Academic Press.

Rising, J. D., & Somers, K. M. (1989). The measurement of overall body size in birds. *The Auk*, *106*(4), 666–674.

Robinson, M. R., Pilkington, J. G., Clutton-Brock, T. H., Pemberton, J. M., & Kruuk, L. E. B. (2006). Live fast, die young: trade-offs between fitness components and sexually antagonistic selection on weaponry in soay sheep. *Evolution*, *60*(10), 2168-2181.

Rutz, C., Klump, B. C., Komarczyk, L., Leighton, R., Kramer, J., Wischnewski, S., … Masuda, B. M. (2016). Discovery of species-wide tool use in the Hawaiian crow. *Nature*, *537*(7620), 403–407.

Ryeland, J., Weston, M. A., & Symonds, M. R. E. (2017). Bill size mediates behavioural thermoregulation in birds. *Functional Ecology*, *31*(4), 885–893.

Schoennerr, A. A., Feldmeth, C. R., & Emerson, M. J. (2003). *The Natural History of the Islands of California*. Berkeley, California: University of California Press.

Scott, S. N., Clegg, S. M., Blomberg, S. P., Kikkawa, J., & Owens, I. P. F. (2003). Morphological shifts in island-dwelling birds: the roles of generalist foraging and niche expansion. *Evolution*, *57*(9), 2147–2156.

Shuford, W. D., & Gardali, T. (Eds.). (2008). Channel Island song sparrow. In *California bird species of special concern: A ranked assessment of species, subspecies, and distinct populations of birds of immediate conservation concern in California. Studies of Western Birds 1.* Camarillo, CA: Western Field Ornithologists and California Department of Fish and Game.

Shultz, A. J., & Burns, K. J. (2017). The role of sexual and natural selection in shaping patterns of sexual dichromatism in the largest family of songbirds (Aves: Thraupidae). *Evolution*, *71*(4), 1061–1074.

Siepielski, A. M., DiBattista, J. D., & Carlson, S. M. (2009). It's about time: the temporal dynamics of phenotypic selection in the wild. *Ecology Letters*, *12*(11), 1261–1276.

Siepielski, A. M., Gotanda, K. M., Morrissey, M. B., Diamond, S. E., DiBattista, J. D., & Carlson, S. M. (2013). The spatial patterns of directional phenotypic selection. *Ecology Letters*, *16*(11), 1382–1392.

Soons, J., Genbrugge, A., Podos, J., Adriaens, D., Aerts, P., Dirckx, J., & Herrel, A. (2015). Is beak morphology in Darwin's finches tuned to loading demands?. *PLoS One*, *10*(6), e0129479.

Sustaita, D. (2007). Musculoskeletal underpinnings to differences in killing behavior between North American accipiters (Falconiformes: Accipitridae) and falcons (Falconidae). *Journal of Morphology*, *269*(3), 283–301.

Svensson, E. I., & Calsbeek, R. (Eds.). (2012). *The adaptive landscape in evolutionary biology*. Oxford, United Kingdom: Oxford University Press.

Symonds, M. R. E., & Tattersall, G. J. (2010). Geographical variation in bill size across bird species provides evidence for Allen's rule. *The American Naturalist*, *176*(2), 188–197.

Tattersall, G. J., Andrade, D. V, & Abe, A. S. (2009). Heat exchange from the toucan bill reveals a controllable vascular thermal radiator. *Science*, *325*(5939), 468–470.

Tattersall, G. J., Arnaout, B., & Symonds, M. R. E. (2016). The evolution of the avian bill as a thermoregulatory organ. *Biological Reviews*, *92*(3), 1630-1656.

Tattersall, G. J., Chaves, J. A., & Danner, R. M. (2018). Thermoregulatory windows in Darwin's finches. *Functional Ecology*, *32*(2), 358–368.

Temeles, E. J., & Kress, W. J. (2003). Adaptation in a plant-hummingbird association. *Science*, *300*(5619), 630–633.

Temeles, E. J., Roberts, W. M., Url, S., & Mark, W. (1993). Dimorphism in bill length on foraging behavior: an experimental analysis of hummingbirds. *Oecologia*, *94*(1), 87–94.

Templeton, C. N., & Shriner, W. M. (2004). Multiple selection pressures influence Trinidadian guppy (Poecilia reticulata) antipredator behavior. *Behavioral Ecology*, *15*(4), 673–678.

Tieleman, B. I., Williams, J. B., Buschur, M. E., & Brown, C. R. (2003). Phenotypic variation of larks along an aridity gradient: are desert birds more flexible?. *Ecology*, *84*(7), 1800–1815.

Troscianko, J., Von Bayern, A. M. P., Chappell, J., Rutz, C., & Martin, G. R. (2012). Extreme binocular vision and a straight bill facilitate tool use in New Caledonian crows. *Nature Communications*, *3*(1), 1-7.

van der Meij, M. A. A., & Bout, R. G. (2004). Scaling of jaw muscle size and maximal bite force in finches. *Journal of Experimental Biology*, *207*(16), 2745–2753.

van der Meij, M. A. A., & Bout, R. G. (2006). Seed husking time and maximal bite force in finches. *Journal of Experimental Biology*, *209*(17), 3329–3335.

van der Meij, M. A. A., & Bout, R. G. (2008). The relationship between shape of the skull and bite force in finches. *Journal of Experimental Biology*, *211*(10), 1668–1680.

White, C. R., Blackburn, T. M., Martin, G. R., & Butler, P. J. (2007). Basal metabolic rate of birds is associated with habitat temperature and precipitation, not primary productivity. *Proceedings of the Royal Society B: Biological Sciences*, *274*(1607), 287–293.

Whitfield, M. C., Smit, B., McKechnie, A. E., & Wolf, B. O. (2015). Avian thermoregulation in the heat: scaling of heat tolerance and evaporative cooling capacity in three southern African arid-zone passerines. *Journal of Experimental Biology*, *218*(11), 1705–1714.

Wilkins, M. R., Seddon, N., & Safran, R. J. (2013). Evolutionary divergence in acoustic signals: Causes and consequences. *Trends in Ecology & Evolution*, *28*(3), 156–166.

Wolf, B. O., & Walsberg, G. E. (2000). The role of the plumage in heat transfer processes of birds. *American Zoologist*, *40*(4), 575–584.

3. ADAPTATIVE DIVERGENCE IN BILL MORPHOLOGY AND OTHER THERMOREGULATORY TRAITS IS FACILITATED BY RESTRICTED GENE FLOW IN SONG SPARROWS ON THE CALIFORNIA CHANNEL ISLANDS

Summary

Disentangling the effects of neutral and adaptive processes in maintaining phenotypic variation across environmental gradients is challenging in natural populations. Song sparrows (*Melospiza melodia*) on the California Channel Islands occupy a pronounced west-east climate gradient within a small spatial scale, providing a unique opportunity to examine the interaction of genetic isolation (gene flow) and the environment (selection) in driving variation. We used reduced representation genomic libraries to infer the role of neutral processes (drift and restricted gene flow) and divergent selection in driving variation in thermoregulatory traits with an emphasis on the mechanisms that maintain bill divergence among islands. Analyses of 22,029 neutral SNPs confirm distinct population structure by island with restricted gene flow and relatively large effective population sizes, suggesting bill differences are likely not a product of genetic drift. Instead, we found strong support for local adaptation using 3,294 SNPs in differentiation-based and environmental association analyses coupled with genome-wide association (GWA) tests. Specifically, we identified several putatively adaptive and candidate loci in or near genes involved in bill development pathways (*e.g.*, *BMP*, *CaM*, *Wnt*), confirming the highly complex and polygenic architecture underlying bill morphology. Furthermore, we found divergence in genes associated with other thermoregulatory traits (i.e., feather structure, plumage color, and physiology). Collectively, these results suggest strong divergent selection across an island archipelago results in genomic changes in a suite of traits associated with climate adaptation over small spatial scales. Future research should move beyond the study of

univariate traits to better understand the multidimensional responses to complex environmental conditions.

Introduction

A long-standing goal in evolutionary biology is to understand the mechanisms that generate and maintain adaptive variation across heterogeneous landscapes (Endler, 1986; Fisher, 1930; Reeve & Sherman, 1993). Yet, identifying how microevolutionary processes interact to shape genetic and phenotypic variation is difficult, especially in natural populations where experimental tests are often difficult (Kawecki & Ebert, 2004). Natural populations often exhibit patterns of phenotypic variation correlated with the environment, but this may be a consequence of either divergent selection or adaptive plasticity (Endler, 1986; Ghalambor, McKay, Carroll, & Reznick, 2007; Kawecki & Ebert, 2004; Sultan, 1987). To disentangle the effects of plasticity and evolutionary processes in generating variation, links must be established between individual genotypes and phenotypes and the environmental variables hypothesized to drive adaptive diversity (Barrett & Hoekstra, 2011; Sork et al., 2013). Combining molecular methods with measures of individual phenotypes across different environments can provide key insights into the genetic basis of traits and the factors that maintain adaptive genetic differentiation (J. T. Anderson et al., 2015; Gugger, Fitz-Gibbon, Albarrán-Lara, Wright, & Sork, 2020; Mikles et al., 2020). While this practice has been applied extensively in recent years, the power to detect local adaptation is dramatically reduced for traits controlled by many genes of small effect, especially in organisms with fewer genomic resources (Barrett & Hoekstra, 2011; Yeaman, 2015; Hoban et al., 2016).

These issues are further complicated as the power to detect genomic signals of selection are dependent on demography and the spatial scale at which the environmental agents of selection acts on populations (Bradburd & Ralph, 2019; Tigano & Friesen, 2016). Theoretically, smaller spatial scales result in higher levels of gene flow that counteract the effectiveness of selection to cause local adaptation (Garant, Forde, & Hendry, 2007; Lenormand, 2002; Slatkin, 1987), but numerous empirical studies demonstrate that strong selection may still result in adaptive divergence in the presence of gene flow (Andrew, Ostevik, Ebert, & Rieseberg, 2012; Fitzpatrick, Gerberich, Kronenberger, Angeloni, & Funk, 2015; Sambatti & Rice, 2006). Additionally, whether signatures of selection represent true responses to environmental variation or are spurious associations with neutral genomic divergence (*i.e.,* population structure) may be difficult to infer using either differentiation-based or environmental-association analyses (Ahrens et al., 2018; Lotterhos & Whitlock, 2014; Narum & Hess, 2011). Although commonly used methods to detect selection may control for population structure, thereby reducing the likelihood of false positives (Forester, Jones, Joost, Landguth, & Lasky, 2016; Frichot & Franc, 2015; Frichot, Schoville, Bouchard, & Franc, 2013; Luu, Bazin, & Blum, 2016), using multiple methods to identify congruence is necessary to strengthen inferences regarding adaptation in natural populations.

A well-suited phenotype to investigate the genomic signals of selection is how bill morphology varies in response to climate. Numerous studies have demonstrated that increased bill size is an adaptation to hot, xeric environments (Greenberg et al., 2012; Ryeland et al., 2017; Symonds & Tattersall, 2010; Tattersall et al., 2018). In hotter environments, larger bills are hypothesized to aid in thermoregulation by dissipating more dry heat in response to high ambient temperatures compared to smaller bills (Tattersall et al., 2016). The high heritability of bill

dimensions (Boag, 1983; Grant, 1983; Jensen, Sæther, et al., 2003; Keller et al., 2001; Schluter & Smith, 1986) suggests the bill may readily evolve in response to selection and provides further justification for examining how climate may result in local adaptation in bills. However, changes in the avian bill represent just one of many potential evolutionary mechanisms to cope with thermal stress and climate variation, and selection likely operates on a suite of traits involved in thermoregulation.

Avian populations may exhibit evolutionary responses to climate in many other morphological and physiological traits. For example, avian plumage acts as an insulative layer that buffers birds from ambient temperatures, and modifications to feather structure can buffer individuals from thermal extremes (Wolf & Walsberg, 2000). Climate may also act on plumage coloration, to alter absorption and reflection of solar radiation (Medina et al., 2018; Roulin, 2014; Stuart-Fox, Newton, & Clusella-Trullas, 2017; Walsberg, 1983). Additionally, bird species occupying cooler climates tend to have higher basal metabolic rates compared to species in warmer environments, which may reflect the need for greater metabolic heat production under cooler conditions (Londono, Chappell, Jankowski, & Robinson, 2014; McKechnie, 2008). Yet, while there has been considerable research on how suites of traits affect thermoregulatory ability in birds, few studies have examined how climate acts on genes underlying these traits. If populations are locally adapted to different climatic conditions, putatively adaptive loci should be linked to a diverse array of thermoregulatory traits.

Song sparrows (*Melospiza melodia*) on the California Channel Islands (hereafter, island song sparrows) are an ideal system to examine how interactions among multiple evolutionary processes may yield adaptive divergence in thermoregulatory traits. Song sparrows are distributed across four islands off the coast of southern California and occupy a steep climatic

gradient ranging from cold, wet, and very windy in the west on San Miguel Island to hot, xeric, and less windy in the east on Santa Cruz and Anacapa Islands, with Santa Rosa Island intermediate between San Miguel and Santa Cruz Islands (Fig. 3.1; Schoennerr, Feldmeth, & Emerson, 2003). This temperature gradient has been hypothesized to act as a strong selection pressure on bill morphology to dissipate heat (Greenberg & Danner, 2012). Indeed, recent work found that bill surface area is positively correlated with maximum temperature, but not strongly associated with seed extraction time or bite force (Chapter 1). However, the extent to which this variation is genetically based and the relative roles of restricted gene flow, genetic drift, and selection in generating and maintaining divergence in bills and other traits potentially associated with climate adaptation has yet to be determined.

Here, we use reduced representation genomic libraries to test the relative roles of neutral (restricted gene flow and genetic drift) and adaptive evolutionary processes in shaping thermoregulatory traits. We focus on bill morphology, as it is known to vary among island song sparrow populations, but also consider how genomic divergence could influence other morphological and physiological traits, such as plumage and thermal physiology. First, we compare island and mainland estimates of genetic variation and test for population structure to infer the relative role of neutral evolutionary processes in contributing to bill variation. Second, we focus on the four island populations to test for genomic signatures of selection based on population differentiation (F_{ST} outlier tests) and on the relationship between genomic and environmental variation [genotype-environment association (GEA) analyses]. We search for genes near putatively adaptive loci identified from GEA and F_{ST} outlier tests and determine whether these genes are involved in developmental pathways for climate-related phenotypes (i.e., bill, feather structure, plumage, thermal physiology). Third, we explicitly relate genotypes and

bill phenotypes using genome-wide association (GWA) analyses among island populations. We search for genes near candidate loci identified from GWA to determine whether regions associated with bill divergence in other avian species are similarly responsible for bill variation among island song sparrows. This integrative approach provides a powerful framework for inferring local adaptation in response to climate in a natural populations.

Methods

Genomic and phenotypic sampling

Capture and morphological measurements

We mist-netted song sparrows during the breeding season (February-June 2014-2017) from all four northern California Channel Islands (San Miguel, Santa Rosa, Santa Cruz, and Anacapa Islands) and from coastal regions of mainland California in the Santa Monica National Recreation Area (Fig. 3.1). Sampling during this period ensured all birds were resident breeders and subject to local selection pressures, rather than transient individuals that only use the island during the non-breeding season. We measured bill dimensions (width, W; length, L; and depth, D) from the anterior end of the nostril and calculated total bill surface area assuming a cylindrical cone (Gamboa, Chapter 1; Greenberg & Danner, 2012). Whole blood samples were extracted from the brachial vein and preserved in Queen's lysis buffer (Seutin, White, & Boag, 1991). High-quality genomic DNA was extracted from blood samples (~50µL) with DNeasy Blood and Tissue Extraction kits (Qiagen, Valencia, CA, USA) using the recommended manufacturer's protocol for preserved tissue samples.

RAD-sequencing and genotyping

We prepared libraries for single-end restriction-site associated DNA sequencing (RADseq) using the restriction enzyme SbfI for digestion (Baird et al., 2008; Etter, Bassham, Hohenlohe, Johnson, & Cresko, 2011). The enzyme SbfI is a low-frequency, 8-basepair cutter and produces fewer loci across the entire genome, but greater depth of coverage at each locus, than a high-frequency 6-basepair cutter (Andrews, Good, Miller, & Luikart, 2016). This increases the power to accurately genotype individuals and draw inferences regarding population structure and gene flow (Andrews, Good, Miller, & Luikart, 2016). We selected fragments ranging between 200-600bp. Uniquely barcoded individuals were pooled across six libraries and six lanes and were sent to the University of Oregon Genomics Core Facility for single-end 100bp sequencing and quality control (Appendix 2 Table S2.1).

Analysis of neutral genetic variation to infer the role of genetic drift and gene flow in maintaining divergence

RAD loci assembly and filtering

For analysis of neutral genetic variation, we combined sequencing data from all lanes including individuals from the four northern Channel Islands and from mainland California (Table 3.1). We cleaned, filtered, and assembled RADseq loci *de novo* and called SNPs using STACKS v 2.2 (Catchen, Amores, Hohenlohe, Cresko, & Postlethwait, 2011). Individuals were demultiplexed and read quality (Phred score) was assessed using a sliding window approach. We discarded reads with an uncalled base or with low quality scores (Phred score < 10). We used clean reads to assemble loci *de novo*, call variable SNPs, and create a SNP catalog to map all individuals against for genotyping. We performed the *denovo_map.pl* function using different combinations of filtering parameters and 25 individuals (5 individuals from each population) to

optimize the number of polymorphic loci while minimizing the number of false calls (Paris, Stevens, & Catchen, 2017). Specifically, we tested the effects of varying the minimum number of raw reads necessary to call a putative allele (*m*, *ustacks*, range = 3-7), the number of permitted mismatches between putative alleles to merge alleles into a putative locus (*M*, *ustacks*, range = 2-8), and the number of mismatches permitted between putative loci when constructing a catalog (*n*, *cstacks*, range = M + 1), and then compared output summary statistics (Appendix 2 Table S2.2). We set final parameters to maximize the number of polymorphic sites while accounting for considerations listed in the decision framework by Paris, Stevens, & Catchen (2017).

Estimating neutral genetic variation

We estimated within-population diversity statistics following final filtering of the *de novo* assembly and removal of putatively adaptive loci. To identify and remove putatively adaptive loci that may bias estimates of neutral genetic variation (Luikart, England, Tallmon, Jordan, & Taberlet, 2003), we performed differentiation-based tests and genotype-environmental association analyses (see *Identifying genomic signatures of divergent selection*). We filtered these putatively adaptive loci from the *de novo* SNP matrix using *populations* in STACKS v. 2.2. To compare genetic diversity among regions, we extracted observed heterozygosity (H_o), expected heterozygosity (H_e), and nucleotide diversity (π) from STACKS population summary statistics output. We re-ran *populations* with a minimum allele count of 1 (MAC = 1) and including individuals with 0% missing data to output unbiased estimates of π (Schmidt, Jasper, Weeks, Hoffmann, & Schmidt, 2020). To infer the potential of genetic drift and restricted gene flow to contribute to observed patterns of phenotypic variation, we estimated effective population size (N_e) and pairwise F_{ST}. We calculated effective population size (N_e) using the linkage-disequilibrium method (Waples & Do, 2010) implemented in NeEstimator v. 2 (Do et

al., 2014) assuming random mating. We then estimated the significance of pairwise F_{ST} estimates by performing 1000 bootstrap replicates across all loci using the package *hierfstat* (Goudet, 2005) implemented in R v. 3.6.3 (R Core Team, 2020).

Inferring population genetic structure

We assessed population structure and levels of admixture to determine whether adaptive divergence occurs within the dispersal distance of island song sparrows and to further evaluate the role that gene flow and genetic drift may play in maintaining population divergence. We applied discriminant analysis of principal components (DAPC) using the package *adegenet* (Jombart, 2008) implemented in R v. 3.6.3 (R Core Team, 2020). Briefly, this method reduces genetic variation to principal components using cross-validation analyses and attempts to maximize differences among assigned genetic groups (Jombart, Devillard, & Balloux, 2010). Additionally, we inferred admixture using the program ADMIXTURE v. 1.3 (Alexander, Novembre, & Lange, 2009), which applies the cross-validation method to determine the number of principal components for estimation of the optimal number of genetic clusters (K). We tested values of K ranging from 1-8 to identify the number of genetic clusters and estimate ancestry within the sampled regions (San Miguel, Santa Rosa, Santa Cruz, and Anacapa Islands, and Mainland California).

Identifying genomic signatures of divergent selection

To test for genomic evidence of divergent selection in contemporary island song sparrow populations, we performed population and individual-level analyses using island song sparrow reads aligned to the zebra finch genome. Zebra finches are a model avian organism, and reference genomes and accompanying gene annotations for zebra finches are well-developed. Although song sparrows and zebra finches are distantly related, both species are in the order

Passeriformes, and avian taxa exhibit high synteny across the genome (Ellegren, 2010; Zhang et al., 2014). We assembled RAD loci *de novo* for only island birds following the procedure described for neutral analyses of island and mainland populations. We used BWA-SA implemented in BWA v. 0.7.12 (Li & Durbin, 2010) and *stacks_integrate_align* in STACKS v. 2.2 to align island sparrow reads to the zebra finch reference genome (*Taeniopygia guttata, version 3.2.4*). The chromosomal-level zebra finch genome provides high quality positional and gene annotation information for aligned loci. Gene annotations are highly homologous between the recently developed scaffold-assembly song sparrow reference genome and zebra finch genome (Louha, Ray, Winker, & Glenn, 2020). The high quality chromosomal-level zebra finch reference genome allows us infer locus position across the avian genome with greater confidence compared to the scaffold-assembly song sparrow reference genome. We used the subsequent VCF output from *populations* in STACKS v. 2.2, including individuals with $\leq$20% missing data.

Given the sensitivity of many algorithms for detecting loci under selection and for performing GWA to missing data, we imputed missing genotypes by island using BEAGLE 4.1 (Browning & Browning, 2016). This imputation method uses linear interpolation of known genotypes within samples and a sliding-window approach across markers to infer missing genotypes for individuals within the population (Browning & Browning, 2016). We imputed island VCF files using genotype-likelihoods, 25 phasing iterations (*niterations* = 25) to improve accuracy, and island-specific N_e based on analyses of neutral genetic variation (Pook et al., 2020). We used these final aligned and imputed genotypes to identify putatively adaptive loci with population-level F_{ST} outlier and individual-based GEA analyses below. We subset individuals from this aligned and imputed dataset to also find evidence of a genetic basis to bill

variation using GWA tests (see *Genome-wide associations with body size-corrected bill variation*).

Identification of putatively adaptive loci using differentiation statistics

We identified loci under selection based on population differentiation statistics using the R package PCAdapt (Duforet-frebourg, Luu, Laval, Bazin, & Blum, 2015; Luu et al., 2016). This methodology controls for population structure using principal component analyses and has been found to be effective at identifying loci under selection with relatively low false discovery rates compared to other F_{ST} outlier tests (Luu et al., 2016). We assumed $K = 4$ genetic clusters based on analysis of neutral genetic variation and on visual inspection of a scree plot testing for optimal K between 1-8. We applied the Mahalanobis distance method to rank SNPs using a minor allele frequency (MAF) of 0.05. We corrected for multiple testing using a false discovery rate (FDR) of 0.05 and the Benjamini-Hochberg algorithm, which is more conservative compared to Storey's q-value method (Brinster, Köttgen, Tayo, Schumacher, & Sekula, 2018). We extracted variant names and coordinates for putatively adaptive loci identified based on an adjusted p-value < 0.05.

Identification of putatively adaptive loci using genotype-environment association tests

We further examined adaptive population differentiation by applying individual-based GEA tests using latent-factor mixed modeling (LFMM) implemented in the R package *LEA* (Frichot et al., 2013). This univariate mixed model method performs well at identifying loci under weak selection and low dispersal (Forester et al., 2016; Rellstab, Gugerli, Eckert, Hancock, & Holderegger, 2015; Whitlock & Lotterhos, 2015). LFMM applies a hierarchical Bayesian approach to identify correlations between environmental and genetic variation while controlling for residual population structure using latent factors (Frichot et al., 2013). To

estimate the number of latent factors, we ran 10 iterations of sparse nonnegative matrix factorization (sNMF) testing values of K ranging from 1-8. We selected $K = 4$ after visualization of sNMF results. Maximum temperature data was extracted for each sampling location using 1 km^2 (30s arc) interpolations generated by WorldClim v. 1.4 (Hijmans, Cameron, Parra, Jones, & Jarvis, 2005), which we used as our environmental gradient. We extracted average maximum temperatures for July, the month with the highest average maximum temperature in this region (Western Regional Climate Center, 2017). We performed 10 repetitions of LFMM to test for the association between maximum temperature and genotypes using default parameter settings. We adjusted p-values using the combined z-scores of each repetition and a lambda based on visual inspection of histograms of adjusted p-values. While this method has been shown to be robust at detecting loci under weak selection, simulations also provide evidence for relatively high false positive rates (Forester et al., 2016; Rellstab et al., 2015; Whitlock & Lotterhos, 2015). Consequently, we set the FDR to 0.05 and extracted variant names and coordinates for putatively adaptive loci as identified based on an adjusted p-value < 0.05.

We coupled LFMM GEA analyses with redundancy analyses (RDA) implemented in the R package *vegan* (Oksanen et al., 2013). This individual-based, constrained ordination method has been shown to perform well at identifying true positive loci under weak selection and is appropriate for highly polygenic traits that are likely controlled by many genes of relatively small effect (Forester et al., 2016) and, consequently, is a useful comparison against methods which result in higher false positives. We performed a partial RDA using maximum temperature as a predictor of genetic variation while controlling for geographic distance (i.e., latitude and longitude). We compared results from permutation tests of this partial RDA to models including maximum temperature alone, geographic distance controlling for maximum temperature, and the

combined effects of geographic distance and maximum temperature. We compared model results to estimate the proportion of genetic variance explained by geography alone and by maximum temperature alone. We identified outliers in the partial RDA using maximum temperature conditioned for geography as those loci with an ordination score along the primary axis (maximum temperature) that lie $\pm$ 2.5 standard deviations outside of the mean RDA score.

Functional annotation of putatively adaptive loci

Putatively adaptive loci generated from the three methods were compiled and compared to the zebra finch Ensembl annotation (Yates et al., 2020). We used the default settings in the NCBI Genome Remapping Service to convert coordinates from assembly version 3.2.4 (*Taeniopygia_guttata-3.2.4*; GCF_000151805.1) to coordinates for the most recent annotated genome assembly in Ensembl (*bTaeGut1_v1*; GCF_003957565.1). Visual inspection of linkage disequilibrium (LD) plots using LD calculated within a 1Gb window in PLINK 2.0 (Purcell, 2021; Purcell et al., 2007) suggests high linkage at variant sites within 50kb (Figure S1). Consequently, remapped coordinates were input in BEDOPS v. 2.4.39 (Neph et al., 2012), and all genes within 50kb of variant site coordinates in the zebra finch genome were output for functional annotation. Associated Entrez gene names and common gene symbols were identified for all output genes using the R package *mygene* (Mark, Thompson, Afrasiabi, & Wu, 2020). We used the R Bioconductor package *biomaRt* (Durinck et al., 2005) to output gene ontology names and descriptions for all candidate genes. We searched annotation reports for GO terms related to traits hypothesized to vary with our maximum temperature gradient, specifically bill morphology, plumage and feather morphology, and physiological responses to water and temperature stress (Appendix 2 Table S2.3). Genes with these terms are inferred to be under divergent selection in island populations.

Genome-wide associations with body size-corrected bill variation

Determining SNP-based heritability and inferring underlying genetic architecture

Prior to conducting GWA with body size-corrected bill surface area, we subset our aligned, imputed island song sparrow dataset to include only adult individuals with known phenotypes and inferred the most appropriate GWA model based on the underlying genetic architecture of the trait. Importantly, our objective for these analyses was not to infer all loci underlying bill variation. Rather, we aimed to identify whether there was any genetic basis to bill variation and whether loci associated with bill variation were in or near genes known to affect bill development. We did not include subadults in our analyses, as bill phenotypes may not yet be fully developed. To estimate the proportion of our complex phenotype explained by our RADseq genotypes [SNP-associated heritability (h^2)] and to infer the underlying genetic architecture of our trait, we applied Bayesian sparse linear mixed modeling (BSLMM; Zhou, Carbonetto, & Stephens, 2013) implemented in the program GEMMA (Zhou & Stephens, 2012). Commonly used methods for identifying genes associated with given phenotypes either assume all variants contribute to phenotypic variation (e.g., linear mixed models, LMMs) or assume only a few variants of large effect control phenotypic variation (e.g., Bayesian sparse variable regression, BSVR). BSLMM avoids these simplifying assumptions by modeling both small and large effects to better infer genetic architecture (Zhou, Carbonetto, & Stephens, 2013). We estimated a genetic kinship matrix using GEMMA and used this matrix to include population structure as a random effect when performing BSLMM with size-corrected bill surface area. For modeling of Bayesian modeling of sparse effects, we set burnin to 250,000 and maintained all other default parameters.

We generated descriptive statistics on all output hyperparameters to estimate SNP-associated heritability and to inform GWA modeling. We predicted heritability to be low based on our reduced-representation genomic approach, which does not yield sufficient marker density to identify all loci underlying trait variation (Lowry et al., 2017). Thus, some additive genetic variance in bill variation will remain undetected with our dataset and analyses. We selected univariate and multivariate GWA models based on *rho*, or the approximation to the proportion of genetic variance explained by variants with major effects (Zhou, Carbonetto, & Stephens, 2013). If *rho* was less than 0.5, then we assumed most of the variation in the phenotype was attributed to many loci of small effect and was best modeled using LMMs. However, if *rho* was greater than 0.5, then we assumed much of the variation could be attributed to few loci of large effect and is best modeled using BSVR models.

Genome-wide associations with body size-corrected bill variation

To test for a direct relationship between genotypes and bill surface area corrected for body size, we performed GWA using univariate and multivariate methods. First, we applied univariate LMM implemented in GEMMA, which has more power to detect loci of small effect for polygenic traits compared to BSVR methods (Zhou, Carbonetto, & Stephens, 2013). We accounted for population structure by including the kinship matrix generated in GEMMA, which is modeled as a random effect in the same manner as BSLMM. Output p-values using the Wald frequentist test were based on the null hypothesis that observed phenotypic variation is not related to genotypes at any individual variant site when controlling for population structure and background genetic effects (Zhou & Stephens, 2012). We adjusted p-values using the Benjamini-Hochberg method to correct for multiple testing and called candidates based on an FDR of 0.05 (adjusted p-value < 0.05). Second, we simultaneously modeled the contribution of many variant

sites to body size-corrected bill surface area controlling for geographic distance (i.e., latitude and longitude) using partial RDA. We identified candidate loci in this partial RDA as loci with an ordination score along the primary axis (maximum temperature) that lie $\pm$ 2.5 standard deviations outside of the mean RDA score. These candidate loci were combined with results from LMM. We obtained functional annotations for genes within 50kb of these variant sites following the previously described procedure (see *Functional annotation of putatively adaptive loci*). Similarly, we searched the resulting annotation report for GO terms related to bill morphology to infer a direct relationship between genotype and phenotype (Appendix 2 Table S2.3).

Results

Genomic and phenotypic sampling

We captured, measured, and sampled adult island (n = 461) and mainland (n = 52) song sparrows (Fig. 3.1). Body size-corrected bill surface area varied predictably by island under the hypothesis that bill divergence is related to climate, with birds on colder islands having smaller bills than birds on hotter islands (Gamboa, Chapter 1; Greenberg & Danner, 2012; Table 3.1). We successfully extracted DNA from all individuals and sequenced samples across six lanes (Appendix 2 Table S2.1) to obtain a total of 882,080,645 raw reads (reads per individual, mean = 1,719,455, sd = 1,477,326).

Population structure and effective population size

After excluding individuals with low quality and quantity reads, we included 438 total individuals (coverage mean = 20.22X) in our neutral analyses (Table 3.1). We generated our *de novo* assembly using optimized parameters (m = 3, M = 2, n = 3; Appendix 2 Table S2.2). Following filtering in STACKS, our final *de novo* library included 23,453 SNPs. We visually

inspected a principal components analysis of neutral SNPs to confirm that sequencing lane had little to no effect on population assignments. We excluded 1,424 of these SNPs based on tests for divergent selection, which resulted in 22,029 variant sites for all neutral analyses (Table 3.1).

Analysis of our neutral dataset revealed relatively high genetic diversity despite evidence of restricted gene flow and population structure. Genetic diversity estimates among regions were comparable, with N_e confidence intervals overlapping between mainland and island song sparrows (Table 3.2). We also found isolation-by-distance and moderate population structuring (pairwise F_{ST} range = 0.041 – 0.174; Table 3.3). Admixture analyses provided further evidence for limited dispersal and gene flow among islands and between mainland and island populations (Fig. 3.2A). These results align with DAPC, which identified four main genetic clusters based on discriminant analysis of 45 PCs, which explain 36% of total neutral genetic variation. Specifically, mainland sparrows were consistently separated from island sparrows, and island populations clustered into three groups: (1) San Miguel Island, (2) Santa Rosa Island, (3) Santa Cruz and Anacapa Islands (Fig. 3.2A-B).

Genomic signatures of divergent selection

We aligned reads from 387 island song sparrows (coverage mean = 18.55) to the zebra finch refence genome resulting in 3,294 SNPs (Table 3.1). Differentiation-based (F_{ST} outlier) tests performed in PCAdapt using $K = 4$ recovered 538 outliers (Fig. 3.3A). When comparing these results to GEA tests, LFMM was more liberal, recovering 1,153 putatively adaptive loci (Fig. 3.3B), and partial RDA conditioned on geographic distance (Fig. 3.3C) provided the most conservative estimate across all divergent selection tests with only 64 putatively adaptive loci (Table 3.1). Altogether, F_{ST} outlier and GEA tests identified 1,424 unique, putatively adaptive loci with 343 of these loci occurring in two of the three analyses and one locus occurring across

all three analyses (Table 3.1). We identified 4,011 genes that were either overlapping with putatively adaptive variant sites or were found within 50kb of the variant sites based on the annotated zebra finch genome.

Our GO search revealed several genes associated with pathways known to modify bill morphology, feather development and plumage, and physiological responses to temperature and water stress (Figures S3, S4, and S5; Table S3). Known pathways and genes involved with bill development include calmodulin (e.g., *CASK, CAMSAP2*), epidermal growth factor (e.g., *EGFL7*), fibroblast growth factor (e.g., *FGFR1*, *FGFR2*), bone morphogenetic protein (e.g., *BMP2, BMP4, BMP15*), mitogen-activated protein kinase (e.g., *MAP3K7*, *MAP3K9*, *MAP4K5*), Smad proteins (e.g., *SMAD1*), transforming growth factor beta (e.g., *SMURF1*, *SMURF2*), wingless/integrated (*Wnt*) signaling pathway (e.g., *WNT7A*), and *Notch* signaling pathway (e.g., *JAG2*). Many of these genes also included GO annotations related to feather development and structure (e.g., *PTPRK*, *BMP4*), coloration (e.g., *Mc1r, BCO2, MYRIP, SOX10*), acute heat and cold stress responses (e.g., *HSPA8, HSPD1*), water homeostasis (i.e., *TRPV4, SNN1G*), and temperature homeostasis (i.e., *STAT3*, *FTO*).

Genome-wide analysis of individual variation in body-size corrected bill surface area

We included 306 adult island song sparrows in our GWA analyses (Table 3.1). All analyses performed in GEMMA removed 1,240 loci based on default parameter settings that control for kinship, resulting in 2,054 loci for estimating SNP-based heritability and performing association tests between body size-corrected bill surface area. Based on BSLMM analysis, the retained 2,054 SNPs explained approximately 34% (PVE, or SNP-based h^2, 95% CI = 0.20 – 0.56) of adult bill variation. Of these 2,054 SNPs, 54 SNPs exhibited a large effect, explaining approximately 41% of SNP-based heritability. While these 54 SNPs have a relatively large effect

on the phenotype, the absolute effect sizes of these variants are still relatively small. The BSLMM model parameters *h* and *rho* are informed based on machine-learning, and *rho* of ~45% suggests that bill variation is explained primarily by many genes of relatively small effect, thereby justifying the use of univariate LMMs and RDA for subsequent association tests. Our univariate GWA model, LMM, retained all 2,054 SNPs kept by GEMMA and identified only one candidate gene strongly associated with body size-corrected bill surface area (Fig. 3.3D). Polygenic modeling of all 3,294 variants simultaneously using RDA was less conservative, recovering 21 SNPs strongly associated with body size-corrected bill surface area (Fig. 3.3E). We did not find any overlap between candidate loci identified by the two GWA methods. We identified 42 genes within 50kb of these 21 candidate loci based on the annotated zebra finch genome. Our GO search recovered three genes related to bill morphology including CD2 associated protein (*CD2AP*), fibroblast growth factor receptor 2 (*FGFR2*), and myosin VIIA (*MYO7A*). These three genes together interact with the *BMP* signaling pathway via regulation of transforming growth factor beta production, regulation of the *MAPK* cascade, regulation of the *FGF* signaling pathway, and calmodulin binding (Appendix 2 Table S2.3).

Discussion

The maintenance of phenotypic variation along steep environmental gradients has long served as a model for testing the interplay between selection, gene flow, and drift (Barton, 1999; Endler, 1977; Lenormand, 2002; Savolainen, Lascoux, & Merilä, 2013). Channel Island song sparrows on the northern Channel Islands occupy a steep climatic gradient over a relatively short distance (Fig. 3.1). We used reduced-representation genomic data to infer the roles of different microevolutionary processes in facilitating genomic and phenotypic divergence among

populations on different islands. Analyses of neutral genetic variation revealed that three island populations (San Miguel Island, Santa Rosa Island, and Santa Cruz Island) were moderately genetically differentiated from each other, and highly differentiated from mainland conspecifics. Effective population sizes were relatively large, suggesting a minimal role for genetic drift in driving observed patterns of bill divergence. We found a pattern of isolation-by-distance and restricted gene flow, as well as a strong signature of divergent selection related to climate, among islands. Genome-wide association tests provided further evidence for a genetic basis to observed differences in bill morphology on different islands and suggest relatively high heritability in this polygenic trait. Taken together, our results support the hypothesis that divergent selection caused by the pronounced east-west climatic gradient and restricted gene flow drive adaptive divergence in thermoregulatory traits among Channel Island song sparrow populations. We discuss these results in more detail below.

Neutral processes interact to maintain divergence

Our population structure analyses and estimates of population differentiation suggest restricted gene flow among islands despite their proximity. Reduced gene flow among islands may render selection more effective by decreasing the homogenizing effect of gene flow that otherwise dampens population differences (Garant et al., 2007; Lenormand, 2002). The relatively low levels of gene flow may also increase the efficacy of selection by introducing novel alleles to recipient populations (Garant et al., 2007; Lenormand, 2002). Low levels of admixture were supported among island populations (Fig. 3.2A), and pairwise F_{ST} estimates suggest moderately high genomic differentiation at neutral loci (Table 3.2), despite the proximity of the islands to each other. This is not surprising given that previous work in this system using microsatellites recovered similar patterns of gene flow and population structure (Wilson, Chan, Taylor, &

Arcese, 2015). Furthermore, these findings align with both the ecology of sedentary song sparrow populations, which have relatively low dispersal distances (Arcese, 1989; Arcese et al., 2002) and the trend for island birds to have reduced dispersal capacity compared to mainland conspecifics (Bertrand et al., 2014; Blondel, 2000; Gabrielli, Nabholz, Leroy, Milá, & Thébaud, 2020).

Admixture results confirm population structure with limited gene flow among islands, suggesting the islands are within the dispersal capacity of the sparrows. Wilson *et al.* (2015) hypothesized that dispersal in this system occurs in a stepping stone fashion, consistent with our observation of isolation-by-distance with more geographically separated populations exhibiting higher values of F_{ST} compared to regions that are geographically closer. Assignment plots using ADMIXTURE identified recent migrants to different islands (Figure 3.2A). Increased admixture on eastern islands (Santa Cruz and Anacapa Islands) likely reflects dispersal from populations with higher observed population densities (San Miguel and Santa Rosa Islands) to those with lower densities (Hall, Larramendy, Lee, & Shaskey, 2020; Hall, Larramendy, & Power, 2017, 2018). While song sparrows are generally described as poor flyers (Arcese et al., 2002), strong, daytime westerly-northwesterly winds may aid in the directionality of dispersal to these lower-density eastern regions. Interestingly, assignment plots also identify two recent, adult, male migrants from Santa Cruz Island to San Miguel and Santa Rosa Islands, which are exceptions to the general pattern of west to east movement. This may be evidence of exploratory behavior by non-territorial male floaters, which is more common in years of high population density among song sparrows (Smith & Arcese, 1989). Excluding males likely exhibiting exploratory behavior, our admixture and population structure results suggest similarity in phenotype and genotype

between geographically proximate individuals may be due to an interaction between divergent selection and restricted gene flow (Garant et al., 2007).

Lastly, estimates of effective population size (N_e) and genetic variation were similar in mainland and some island populations, suggesting genetic drift is relatively weak in the island populations and, therefore, unlikely to play an important role in driving bill divergence among islands. Compared to the mainland, effective population sizes were lower on average among island populations, which is consistent with other island-mainland bird comparisons (Leroy et al., 2021). Our estimates of within-population genetic variation were similar to estimates found in other studies of island bird species (Foster, Walker, Rannals, & Sanchez, 2018; Rutledge, Coxon, & White, 2017), yet were reduced in comparison to estimates of N_e in island birds using whole-genome resequencing data (Leroy et al., 2021). However, our N_e estimates were relatively high compared to other species found on the Channels Islands, such as the Channel Islands fox, which inhabits the northern Channel Islands as well (Funk et al., 2016) and island fence lizards (*Sceloporus occidentalis becki*) on Santa Cruz Island (Trumbo, Funk, Pauly, & Robertson, 2021). In summary, our analysis of neutral genetic variation in Channel Islands song sparrows reveals large N_e and substantial genetic differentiation, indicating a limited role of genetic drift, but important role of restricted gene flow, in facilitating observed bill divergence among islands.

Maximum temperature contributes to divergent selection among island populations

Our tests for signatures of selection support the hypothesis that divergent positive selection is likely the most important microevolutionary force driving observed patterns of bill divergence among island populations. Using both differentiation-based tests and GEAs, we found multiple putatively adaptive loci within or near genes associated with bill development. Overall body size-corrected bill surface area is likely controlled by the interaction of multiple

pathways. For example, past work suggests bill length is associated with the calmodulin pathway (Abzhanov et al., 2006; Lundregan et al., 2018), while *BMP* is associated with bill depth in other related sparrows (Walsh et al., 2019) and passerines (Abzhanov, Protas, Grant, Grant, & Tabin, 2004; Lundregan et al., 2018). The interaction of the *BMP* and *Wnt* signaling pathways has been implicated in the diversification of avian bill morphology (Yusuf et al., 2020). Specifically, the interaction of *Wnt* genes with *BMP2* and *FGFR2* is critical for avian and mammalian craniofacial development (Brugmann et al., 2010), and *BMP2* and *FGFR2* were identified in our system as loci under divergent selection, which suggests bill differences arise early in development in island song sparrows. Other signaling pathways and growth factors likely involved in the regulation of *BMP* include *Notch*, *TGF-beta*, *FGF*, *IGF*, *MAPKs*, and *Smads* (Brugmann et al., 2010; Fuentealba et al., 2007; Massagué, 2003; Rahman, Akhtar, Jamil, Banik, & Asaduzzaman, 2015; Sapkota, Alarcón, Spagnoli, Brivanlou, & Massagué, 2007). Many genes in our analyses are important for regulation within these pathways (Appendix 2 Table S2.3), suggesting there are multiple, interacting pathways that shape bill morphology.

Evidence for adaptative divergence in other thermoregulatory traits

While this study was motivated in part because of the observed variation in bill size and its role in thermoregulation, temperature variation should impose direct and indirect selection on other morphological and physiological traits known to affect thermoregulatory ability. For example, many genes associated with bill morphology in this study are also involved in feather development (Schneider, 2005), suggesting potential correlated responses to selection. Indeed, differential expression of *BMP*- and *Wnt*-associated genes are linked to extensive bill and plumage variation in other species (Mason & Taylor, 2015). This is not surprising considering both craniofacial features and feathers arise from the embryonic mesoderm during development

(Schneider, 2005). Indeed, divergence in the density of feather microstructure is also correlated with maximum temperature among islands (in prep.). Such feather modifications affect the insulative capacity of plumage (Wolf & Walsberg, 2000), and this is particularly relevant for birds occupying windier islands with dense marine layers (i.e., San Miguel and Santa Rosa Islands). Although we did not explicitly test for the relationship between wind or fog and genomic divergence, these climatic variables are strongly correlated with maximum temperature. Cold temperatures accompany high humidity, strong winds, and dense fog on San Miguel Island (Schoennerr et al., 2003). The interaction of strong winds and low levels of solar radiation resulting from dense fog may dramatically affect thermal physiology of small passerines (Wolf & Walsberg, 1996; Wolf, Wooden, & Walsberg, 2000). The relationship between absorption of solar radiation and color may explain the inclusion of putatively adaptive loci linked to genes involved in feather color such as BCO2, which is implicated in carotenoid-processing in other passerines (Gazda et al., 2020; Toews et al., 2016), and the well-studied coloration gene, *Mc1r* (Wolf Horrell, Boulanger, & D'Orazio, 2016). Other genes including *MYRIP*, *RAB17*, and *TRPC1*, further modify melanin synthesis, transportation, and deposition (Beaumont et al., 2011; Ivanova & Hemmersbach, 2020; Li et al., 2017; Wasmeier, Hume, Bolasco, & Seabra, 2008). Such results suggest that future studies should examine whether these genetic differences explain variation in plumage and feather traits across the archipelago.

Additional evidence that selection due to climate is driving divergence in traits related to thermal physiology is seen in the list of other putatively adaptive loci. Using maximum temperature as the environmental predictor for our GEAs, we recovered putatively adaptive loci linked to many genes involved in heat stress, including *DNAJB2*, *DNAJB11*, *DNAJC1*, *DNAJC6*, and *HSPBAP1* (Crevel, Bennett, & Cotterill, 2008; Fujikawa, Munakata, Kondo, Satoh, & Wada,

2010; Han, Zhang, & Dong, 2017; Kapila et al., 2016; Sonna, Fujita, Gaffin, & Lilly, 2002; Truttmann et al., 2017; Xu et al., 2018). Notably, we identified several loci in or near genes implicated in other bird species adapted to similar temperature gradients (e.g. *HSPD1*; Andrew, Jensen, Hagen, Lundregan, & Griffith, 2018). We also identified several genes associated with metabolism, including *SLC2A2*, which modulates basal metabolic rate in birds (Xiong & Lei, 2020) and is critical for buffering endotherms from seasonal changes in temperature (Tattersall, Sinclair, Withers, Fields, & Seebacher, 2012). Collectively, these results, combined with our measurements of bill size, suggest this steep climatic gradient imposes strong selection on a suite of morphological and physiological traits associated with climate adaptation.

Genomic analyses provide strong support for a genetic basis to bill variation.

Using association tests which directly model the statistical relationship between genotype and phenotype, we confirm the highly polygenic architecture of bill surface area. Our estimates of SNP-based heritability are relatively high (SNP-based h^2 mean = 0.34) and support the hypothesis that population differences are not strictly a result of plasticity. These estimates are comparable to those in other song sparrow populations (Schluter & Smith, 1986; Smith & Zach, 1979) and to contemporary estimates of bill heritability in other passerines (Jensen, Saether, et al., 2003; Keller et al., 2001; Lundregan et al., 2018). Moreover, given that we certainly missed many loci associated with bill morphology due to a relatively low density of loci genotyped with RADseq, we would expect this estimate of heritability to be biased low. Compared to our population level tests of divergent selection, our association analyses recovered far fewer loci correlated with bill development, perhaps due in part to the low power of GWA tests. Previous work in this system demonstrated a significant difference among island song sparrow populations in body size-corrected bill surface area, but not necessarily in the individual traits

(bill depth, width, and length, tarsometatarsus length, and wing chord) used to quantify body size-corrected bill surface area (Gamboa, Chapter 1). By grouping these variables together, we reduced our ability to identify loci directly correlated with each individual trait that contributes to bill surface area. Still, we identified candidate loci involved in similar bill development pathways including *BMP*, *MAPK*, *FGF*, and calmodulin. This further confirms that bill morphology is a complex trait controlled by many genes of small effect.

RADseq remains a powerful approach for investigating microevolutionary processes

Finally, although the methods used in this study are considered to have reduced resolution for measuring selection compared to whole-genome sequencing, we argue that the surprising number of putatively adaptive genes identified provides robust evidence for divergent selection as a mechanism that facilitates phenotypic divergence. By aligning our reads to the zebra finch reference genome, we greatly reduced the number of variant sites, while increasing our confidence in gene annotations associated with the high quality chromosomal-level zebra finch reference genome. Furthermore, we applied conservative parameter settings for all tests to reduce the number of false positives. These factors would all be expected to reduce the ability to detect evidence for divergent selection associated with bill morphology. Indeed, reduced-representation approaches, such as RADseq, have been criticized as inefficient for detecting signatures of adaptation, due to relatively sparse density of markers across the genome compared to whole-genome sequencing (WGS; Lowry et al., 2017). However, for a given budget, there is a tradeoff between the proportion of the genome sequenced and the number of individuals that can be included in a population genomic analysis (Catchen et al., 2017; McKinney, Larson, Seeb, & Seeb, 2017). Thus, for the loci genotyped, reduced representation approaches can provide greater statistical power than WGS due to larger sample sizes of individuals. While we recognize that

our RADseq dataset almost certainly missed many functional genes involved in local adaptation in Channel Island song sparrows, our goal was not to determine all loci involved in local adaptation to climate variation or the complete genetic basis of bill variation. Rather our goal was to test for *any* evidence of divergent selection in any candidate genes, and to test whether bill variation is at least partly genetically based. Our results confirm that RADseq was an appropriate genomic approach for addressing these questions (Andrews, Good, Miller, & Luikart, 2016).

Conclusions

Understanding how evolutionary processes interact to facilitate adaptive variation across the landscape is challenging in natural populations. We applied multiple genomic approaches to infer local adaptation as it relates to bill morphology in Channel Island song sparrows distributed along a pronounced climatic gradient over small spatial scales. Evidence of relatively high effective population sizes suggest that population differences in bill morphology are likely not a product of genetic drift. Rather, genetically based bill variation is likely maintained by divergent selection in combination with restricted gene flow. The high heritability and polygenic architecture underlying bill variation imply that there are multiple ways that pathways can be altered to achieve different phenotypes. In addition, we find molecular evidence that suggests selection operates not only on bill morphology, but likely also on feather structure, plumage, and other traits influencing thermal physiology, leading to new hypotheses about the suite of traits under selection. An important frontier in the study of climate adaptation will be to better understand how selection acts on suites of traits, and our integrative approach linking genotypes, phenotypes, and the environment provides a framework for exploring these questions in other natural populations.

Tables and Figures

Table 3.1 Island and mainland sample sizes for neutral and adaptive genetic analyses and genome-wide association analyses and regional mean maximum temperatures (Max T) and bill surface areas (Bill SA). Maximum temperature was extracted for individual sampling locations using 1 km^2 interpolations generated by WorldClim for July, the month with the highest average maximum temperature, and included in genotype-environmental association tests. Raw bill surface area (Raw Bill SA) and body-size corrected bill surface area (Size-corrected Bill SA) were calculated following Gamboa (Chapter 1). Genome-wide association analyses were conducted using size-corrected bill surface area as the phenotypic response.

Variable	San Miguel Island	Santa Rosa Island	Santa Cruz Island	Anacapa Islands	Mainland California	Total *n*
I. Neutral analyses – Loci total/neutral analyzed (putatively adaptive removed) = 23,453/22,029 (1,424)						
n	77	94	205	11	51	438
II. Tests for divergent selection – Loci total/putatively adaptive (PCAdapt/LFMM/RDA) = 3,294/1,414 (538/1,153/64)						
n	77	94	205	11	–	387
Max T Mean (95% CI)	20.0°C (18.8 – 20.9)	22.0°C (20.4 – 23.1)	23.0°C (22.2 – 23.6)	20.0°C (19.1 – 20.0)	–	
III. Genome-wide association with body-size corrected bill surface area – Loci total/candidate (LMM/RDA) = 3,294/22 (1/21)						
n	67	79	160	–	–	306
Size-corrected Bill SA Mean (95% CI)	-5.78 (-13.70 – 1.89)	-0.79 (-10.80 – 8.03)	2.35 (-5.91 – 11.7)	–	–	
Raw Bill SA Mean (95% CI)	74.0 mm^2 (65.8 – 81.9)	79.3 mm^2 (70.1 – 88.4)	82.1 mm^2 (73.9 – 92.0)	–	–	

Table 3.2 Diversity statistics for each region using 22,029 neutral loci. Observed heterozygosity (H_o), expected heterozygosity (H_e), and nucleotide diversity (π) were extracted from *populations* in STACKS v. 2.2 (Catchen, Hohenlohe, Bassham, Amores, & Cresko, 2013) summary statistics output. Estimates of π for all variant and fixed sites were based on 170,240 loci after running *populations* (MAC = 1, r = 1). Effective population size (N_e) was calculating using the linkage-disequilibrium method implemented in NeEstimator v. 2 (Do et al., 2014).

Region	*n*	H_o	H_e	π	N_e (95% CI)
San Miguel Island	77	0.09	0.10	0.00129	640 (627 - 653)
Santa Rosa Island	94	0.11	0.12	0.00116	1307 (1273 - 1345)
Santa Cruz Island	220	0.12	0.13	0.00052	488 (486 - 490)
Anacapa Islands	11	0.12	0.13	0.00372	843 (734 - 990)
Mainland California	51	0.12	0.14	0.00339	1306 (1262 - 1349)

Table 3.3 Bootstrapped pairwise F_{ST} mean (above diagonal) and 95% confidence intervals (below diagonal) calculated using 22,029 neutral loci in the R package *hierfstat* (Goudet, 2005).

Region	San Miguel Island	Santa Rosa Island	Santa Cruz Island	Anacapa Islands	Mainland California
San Miguel Island	–	0.066	0.088	0.132	0.174
Santa Rosa Island	0.064 - 0.068	–	0.044	0.069	0.119
Santa Cruz Island	0.085 - 0.090	0.043 - 0.045	–	0.041	0.082
Anacapa Islands	0.130 - 0.136	0.067 - 0.070	0.040 - 0.042	–	0.067
Mainland California	0.171 - 0.178	0.117 - 0.121	0.080 - 0.083	0.064 - 0.069	–

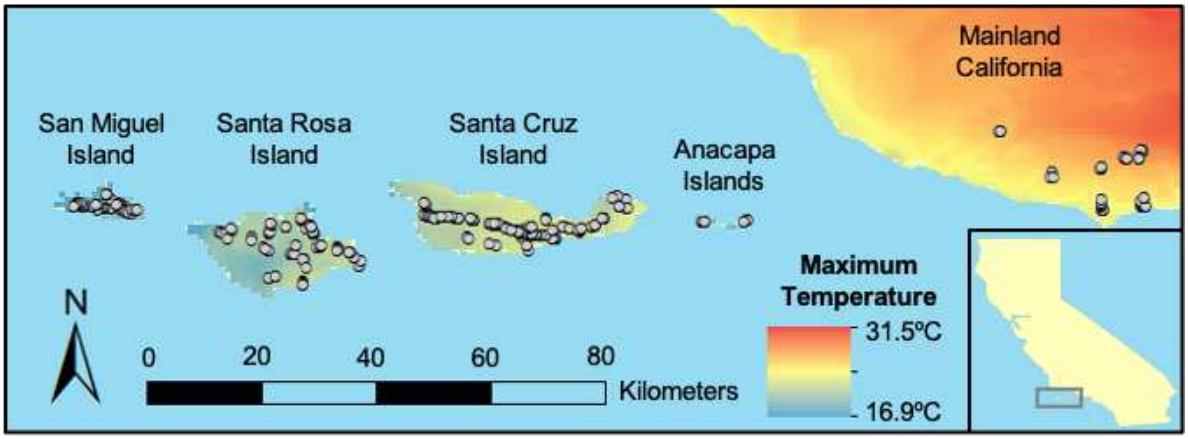

Figure 3.1 Sampling locations of adult song sparrows along the northern Channel Islands archipelago and within mainland California during the breeding season (February-June) from 2014-2017. Color gradient represents WorldClim maximum temperature (range = 16.9°C–31.5°C; Hijmans et al., 2005) data interpolated at a spatial resolution of 1 km^2 (30s arc).

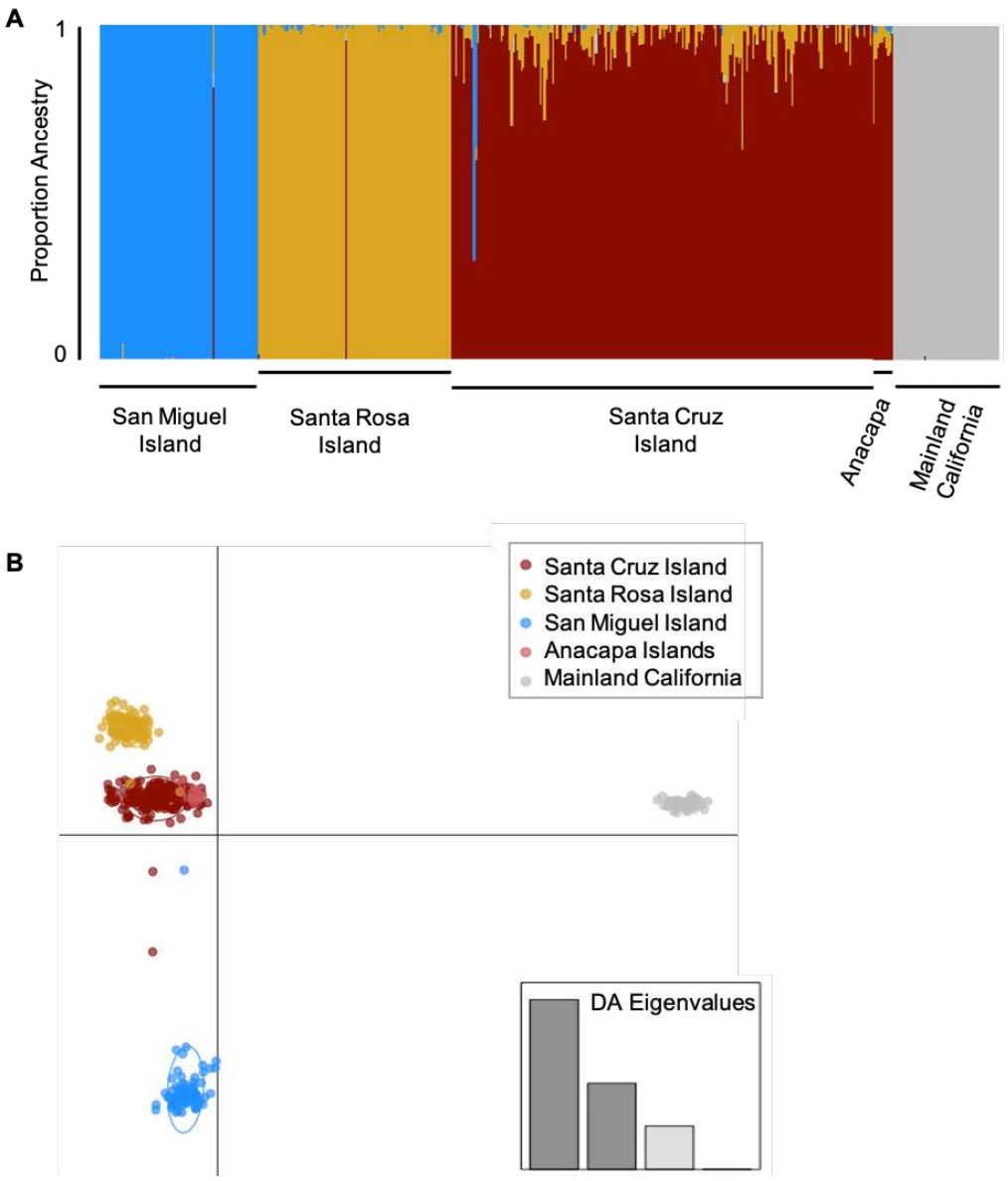

Figure 3.2 Population structure analyses of 22,029 neutral SNPs and 387 island (San Miguel Island, *n* = 77; Santa Rosa Island, *n* = 94; Santa Cruz Island, *n* = 205; Anacapa Island, *n* = 11) and 51 mainland song sparrows using ADMIXTURE (A) and discriminant analysis of principal components (DAPC) in the R package *adegenet* using 45 PCs, which explained 35% of genetic variation (B).

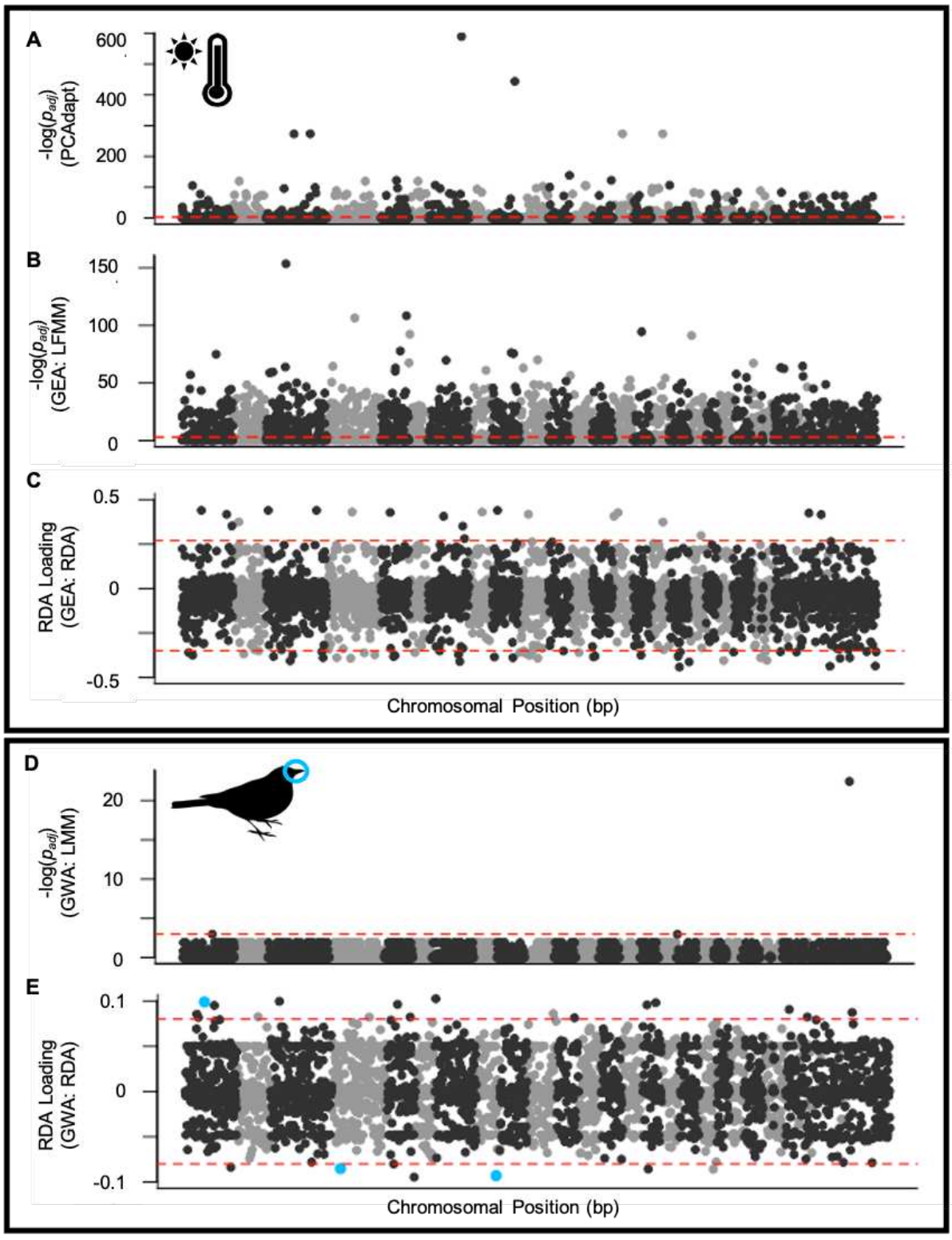

Figure 3.3 Manhattan plots generated using 3,294 SNPs aligned to the zebra finch genome for differentiation-based (F_{ST} outlier) analyses in PCAdapt (A), univariate (LFMM; B), and multivariate (RDA; C) genotype-environment association (GEA) analyses, and univariate (GEMMA LMM; D) and multivariate (RDA; E) genome-wide association (GWA) analyses.

GEA analyses relate maximum temperature and genotypes for 438 island birds (San Miguel, n = 77; Santa Rosa, n = 94; Santa Cruz, n = 205; Anacapa, n = 11). GWA analyses relate body-size corrected bill surface area and genotypes for 306 adult, phenotyped island birds (San Miguel, n = 67; Santa Rosa, n = 79; Santa Cruz, n = 160). Putatively adaptive loci lie above the red dashed line for univariate tests (A,B,D) and above the upper and below the lower red dashed lines for multivariate tests (C,E). Candidate loci located in or within 50kb of genes associated with bill surface area based on GWA analyses are highlighted in blue.

LITERATURE CITED

Abzhanov, A., Kuo, W. P., Hartmann, C., Grant, B. R., Grant, P. R., & Tabin, C. J. (2006). The calmodulin pathway and evolution of elongated beak morphology in Darwin's finches. *Nature*, *442*(7102), 563–567.

Abzhanov, A., Protas, M., Grant, B. R., Grant, P. R., & Tabin, C. J. (2004). Bmp4 and morphological variation of beaks in Darwin's finches. *Science*, *305*(5689), 1462–1465.

Ahrens, C. W., Rymer, P. D., Stow, A., Bragg, J., Dillon, S., Umbers, K. D. L., & Dudaniec, R. Y. (2018). The search for loci under selection: trends, biases and progress. *Molecular Ecology*, *27*(6), 1342–1356.

Alexander, D. H., Novembre, J., & Lange, K. (2009). Fast model-based estimation of ancestry in unrelated individuals. *Genome Research*, *19*(9), 1655–1664.

Anderson, J. T., Perera, N., Chowdhury, B., & Mitchell-Olds, T. (2015). Microgeographic patterns of genetic divergence and adaptation across environmental gradients in Boechera stricta (Brassicaceae). *American Naturalist*, *186*(S1), S60–S73.

Andrew, R. L., Ostevik, K. L., Ebert, D. P., & Rieseberg, L. H. (2012). Adaptation with gene flow across the landscape in a dune sunflower. *Molecular Ecology*, *21*(9), 2078–2091.

Andrew, S. C., Jensen, H., Hagen, I. J., Lundregan, S., & Griffith, S. C. (2018). Signatures of genetic adaptation to extremely varied Australian environments in introduced European house sparrows. *Molecular Ecology*, *27*(22), 4542-4555.

Andrews, K. R., Good, J. M., Miller, M. R., & Luikart, G. (2016). Harnessing the power of RADseq for ecological and evolutionary genomics. *Nature Reviews Genetics*, *17*(2), 81–92.

Barrett, R. D. H., & Hoekstra, H. E. (2011). Molecular spandrels: tests of adaptation at the genetic level. *Nature Review Genetics*, *12*(11), 767–780.

Barton, N. H. (1999). Clines in polygenic traits. *Genetical Research*, *74*(3), 223–236.

Beaumont, K. A., Hamilton, N. A., Moores, M. T., Brown, D. L., Ohbayashi, N., Cairncross, O., … Stow, J. L. (2011). The recycling endosome protein Rab17 regulates melanocytic filopodia formation and melanosome trafficking. *Traffic*, *12*(5), 627–643.

Bertrand, J. A. M., Bourgeois, Y. X. C., Delahaie, B., Duval, T., García-Jiménez, R., Cornuault, J., … Thébaud, C. (2014). Extremely reduced dispersal and gene flow in an island bird. *Heredity*, *112*(2), 190–196.

Blondel, J. (2000). Evolution and ecology of birds on islands: trends and prospects. *Vie et Milieu*, *50*(4), 205–220.

Boag, P. T. (1983). The heritability of external morphology in Darwin's ground finches (Geospiza) on Isla Daphne Major, Galapagos. *Evolution*, *37*(5), 877–894.

Bradburd, G. S., & Ralph, P. L. (2019). Spatial population genetics: it's about time. *Annual Review of Ecology, Evolution, and Systematics*, *50*, 427–449

Catchen, J., Hohenlohe, P. a, Bassham, S., Amores, A., & Cresko, W. a. (2013). Stacks: an analysis tool set for population genomics. *Molecular Ecology*, *22*(11), 3124–3140.

Catchen, J. M., Amores, A., Hohenlohe, P., Cresko, W., & Postlethwait, J. H. (2011). Stacks: building and genotyping loci de novo from short-read sequences. *G3*, *1*(3), 171–182.

Crevel, G., Bennett, D., & Cotterill, S. (2008). The human TPR protein TTC4 is a putative Hsp90 co-chaperone which interacts with CDC6 and shows alterations in transformed cells. *PLoS One*, *3*(3), e0001737.

Do, C., Waples, R. S., Peel, D., Macbeth, G. M., Tillett, B. J., & Ovenden, J. R. (2014). NeEstimator v2: re-implementation of software for the estimation of contemporary effective population size (Ne) from genetic data. *Molecular Ecology Resources*, *14*(1), 209–214.

Endler, J. A. (1977). Geographic variation, speciation, and clines. *Monographs in Population Biology*, *10*, 1–246.

Endler, J. A. (1986). *Natural selection in the wild*. Princeton, New Jersey: Princeton University Press.

Fisher, R. A. (1930). *The genetical theory of natural selection*. Oxford, United Kingdom: The Clarendon Press.

Fitzpatrick, S. W., Gerberich, J. C., Kronenberger, J. A., Angeloni, L. M., & Funk, W. C. (2015). Locally adapted traits maintained in the face of high gene flow. *Ecology Letters*, *18*(1), 37–47.

Forester, B. R., Jones, M. R., Joost, S., Landguth, E. L., & Lasky, J. R. (2016). Detecting spatial genetic signatures of local adaptation in heterogeneous landscapes. *Molecular Ecology*, *25*(1), 104–120.

Frichot, E., & Franc, O. (2015). LEA: an R package for landscape and ecological association studies. *Methods in Ecology and Evolution*, *6*(8), 925–929.

Frichot, E., Schoville, S. D., Bouchard, G., & Franc, O. (2013). Testing for associations between loci and environmental gradients using latent factor mixed models. *Molecular Biology and Evolution, 30*(7), 1687–1699.

Fujikawa, T., Munakata, T., Kondo, S. I., Satoh, N., & Wada, S. (2010). Stress response in the ascidian ciona intestinalis: transcriptional profiling of genes for the heat shock protein 70 chaperone system under heat stress and endoplasmic reticulum stress. *Cell Stress and Chaperones*, *15*(2), 193–204.

Gabrielli, M., Nabholz, B., Leroy, T., Milá, B., & Thébaud, C. (2020). Within-island diversification in a passerine bird. *Proceedings of the Royal Society B: Biological Sciences*, *287*(1923), 20192999.

Garant, D., Forde, S. E., & Hendry, A. P. (2007). The multifarious effects of dispersal and gene flow on contemporary adaptation. *Functional Ecology*, *21*(3), 434–443.

Ghalambor, C. K., McKay, J. K., Carroll, S. P., & Reznick, D. N. (2007). Adaptive versus non-adaptive phenotypic plasticity and the potential for contemporary adaptation in new environments. *Functional Ecology*, *21*(3), 394–407.

Goudet, J. (2005). hierfstat, a package for R to compute and test hierarchical F-statistics. *Molecular Ecology Notes*, *5*(1), 184–186.

Grant, P. R. (1983). Inheritance of size and shape in a population of Darwin's finches, Geospiza conirostris. *Proceedings of the Royal Society B: Biological Sciences*, *220*(1219), 219–236.

Greenberg, R., Cadena, V., Danner, R. M., & Tattersall, G. J. (2012). Heat loss may explain bill size differences between birds occupying different habitats. *PloS One*, *7*(7), e40933.

Greenberg, R., & Danner, R. M. (2012). The influence of the California marine layer on bill size in a generalist songbird. *Evolution*, *66*(12), 3825–3835.

Gugger, P. F., Fitz-Gibbon, S. T., Albarrán-Lara, A., Wright, J. W., & Sork, V. L. (2021). Landscape genomics of Quercus lobata reveals genes involved in local climate adaptation at multiple spatial scales. *Molecular Ecology*, *30*(2), 406–423.

Han, G., Zhang, S., & Dong, Y. (2017). Anaerobic metabolism and thermal tolerance: the importance of opine pathways on survival of a gastropod after cardiac dysfunction. *Integrative Zoology*, *12*(5), 361–370.

Hijmans, R. J., Cameron, S. E., Parra, J. L., Jones, P. G., & Jarvis, A. (2005). Very high resolution interpolated climate surfaces for global land areas. *International Journal of Climatology*, *25*(15), 1965–1978.

Ivanova, K., & Hemmersbach, R. (2020). Guanylyl cyclase-cGMP signaling pathway in melanocytes: differential effects of altered gravity in non-metastatic and metastatic cells. *International Journal of Molecular Sciences*, *21*(3), 1139.

Jensen, H., Sæther, B. E., Ringsby, T. H., Tufto, J., Griffith, S. C., & Ellegren, H. (2003). Sexual variation in heritability and genetic correlations of morphological traits in house sparrow (Passer domesticus). *Journal of Evolutionary Biology*, *16*(6), 1296–1307.

Kapila, N., Sharma, A., Kishore, A., Sodhi, M., Tripathi, P. K., Mohanty, A. K., & Mukesh, M. (2016). Impact of heat stress on cellular and transcriptional adaptation of mammary epithelial cells in riverine buffalo (Bubalus bubalis). *PLoS One*, *11*(9), e0157237.

Kawecki, T. J., & Ebert, D. (2004). Conceptual issues in local adaptation. *Ecology Letters*, *7*(12),

1225–1241.

Keller, L. F., Grant, P. R., Grant, B. R., & Petren, K. (2001). Heritability of morphological traits in Darwin's finches: misidentified paternity and maternal effects. *Heredity*, *87*(3), 325–336.

Lenormand, T. (2002). Gene flow and the limits to natural selection. *Trends in Ecology & Evolution*, *17*(4), 183–189.

Leroy, T., Rousselle, M., Tilak, M. K., Caizergues, A. E., Scornavacca, C., Recuerda, M., … Nabholz, B. (2021). Island songbirds as windows into evolution in small populations. *Current Biology*, *31*(6), 1303-1310.

Li, Y., Geng, X., Bao, L., Elaswad, A., Huggins, K. W., Dunham, R., & Liu, Z. (2017). A deletion in the Hermansky–Pudlak syndrome 4 (Hps4) gene appears to be responsible for albinism in channel catfish. *Molecular Genetics and Genomics*, *292*(3), 663–670.

Londono, G. A., Chappell, M. A., Jankowski, J. E., & Robinson, S. K. (2014). Basal metabolism in tropical birds: latitude, altitude, and the 'pace of life.' *Functional Ecology*, *29*, 338-346.

Lotterhos, K. E., & Whitlock, M. C. (2014). Evaluation of demographic history and neutral parameterization on the performance of Fst outlier tests. *Molecular Ecology*, *23*(9), 2178–2192.

Louha, S., Ray, D. A., Winker, K., & Glenn, T. (2020). A high-quality genome assembly of the North American Song Sparrow, Melospiza melodia. *G3, 10*(4), 1159–1166.

Lowry, D. B., Hoban, S., Kelley, J. L., Lotterhos, K. E., Reed, L. K., Antolin, M. F., & Storfer, A. (2017). Breaking RAD: an evaluation of the utility of restriction site-associated DNA sequencing for genome scans of adaptation. *Molecular Ecology Resources*, *17*(2), 142–152.

Luikart, G., England, P. R., Tallmon, D., Jordan, S., & Taberlet, P. (2003). The power and promise of population genomics: from genotyping to genome typing. *Nature Reviews. Genetics*, *4*(12), 981–994.

Luu, K., Bazin, E., & Blum, M. G. B. (2016). pcadapt: an R package to perform genome scans for selection based on principal component analysis. *Molecular Ecology Resources*, *17*(1), 67–77.

Mason, N. A., & Taylor, S. A. (2015). Differentially expressed genes match bill morphology and plumage despite largely undifferentiated genomes in a Holarctic songbird. *Molecular Ecology*, *24*(12), 3009-3025.

McKechnie, A. E. (2008). Phenotypic flexibility in basal metabolic rate and the changing view of avian physiological diversity: a review. *Journal of Comparative Physiology B, 178*(3), 235–247.

Medina, I., Newton, E., Kearney, M. R., Mulder, R. A., Porter, W. P., & Stuart-Fox, D. (2018). Reflection of near-infrared light confers thermal protection in birds. *Nature Communications*, *9*(1), 3610.

Mikles, C. S., Aguillon, S. M., Chan, Y. L., Arcese, P., Benham, P. M., Lovette, I. J., & Walsh, J. (2020). Genomic differentiation and local adaptation on a microgeographic scale in a resident songbird. *Molecular Ecology*, *29*(22), 4295–4307.

Narum, S. R., & Hess, J. E. (2011). Comparison of Fst outlier tests for SNP loci under selection. *Molecular Ecology Resources*, *11*, 184–194.

Patten, M. A., & Pruett, C. L. (2009). The song sparrow, Melospiza melodia, as a ring species: patterns of geographic variation, a revision of subspecies, and implications for speciation. *Systematics and Biodiversity*, *7*(1), 33–62.

Reeve, H. K., & Sherman, P. W. (1993). Adaptation and the goals of evolutionary research. *The Quarterly Review of Biology*, *68*(1), 1–32.

Roulin, A. (2014). Melanin-based colour polymorphism responding to climate change. *Global Change Biology*, *20*(11), 3344–3350.

Ryeland, J., Weston, M. A., & Symonds, M. R. E. (2017). Bill size mediates behavioural thermoregulation in birds. *Functional Ecology*, *31*(4), 885–893.

Sambatti, J. B. M., & Rice, K. J. (2006). Local adaptation, patterns of selection, and gene flow in the Californian serpentine sunflower (Helianthus exilis). *Evolution*, *60*(4), 696–710.

Savolainen, O., Lascoux, M., & Merilä, J. (2013). Ecological genomics of local adaptation. *Nature*, *14*(11), 807–820.

Schluter, D., & Smith, J. N. M. (1986). Genetic and phenotypic correlations in a natural population of song sparrows. *Biological Journal of the Linnean Society*, *29*(1), 23–36.

Schmidt, T. L., Jasper, M., Weeks, A. R., & Hoffmann, A. A. (2021). Unbiased population heterozygosity estimates from genome-wide sequence data. *Methods in Ecology and Evolution, 00,* 1–11.

Schneider, R. A. (2005). Developmental mechanisms facilitating the evolution of bills and quills. *Journal of Anatomy*, *207*(5), 563–573.

Schoennerr, A. A., Feldmeth, C. R., & Emerson, M. J. (2003). *The Natural History of the Islands of California*. Berkeley, California: University of California Press.

Shuford, W. D., & Gardali, T. (Eds.). (2008). Channel Island song sparrow. In *California bird species of special concern: a ranked assessment of species, subspecies, and distinct populations of birds of immediate conservation concern in California. Studies of Western Birds 1.* Camarillo, CA: Western Field Ornithologists and California Department of Fish and Game.

Slatkin, M. (1987). Gene flow and the geographic structure of natural populations. *Science*,

236(4803), 787–792.

Smith, J. N. M., & Zach, R. (1979). Heritability of some morphological characters in a song sparrow population. *Evolution*, *33*(1), 460-467.

Sonna, L. A., Fujita, J., Gaffin, S. L., & Lilly, C. M. (2002). Invited review: effects of heat and cold stress on mammalian gene expression. *Journal of Applied Physiology*, *92*(50), 1725–1742.

Sork, V. L., Aitken, S. N., Dyer, R. J., Eckert, A. J., Legendre, P., & Neale, D. B. (2013). Putting the landscape into the genomics of trees: approaches for understanding local adaptation and population responses to changing climate. *Tree Genetics and Genomes*, *9*(4), 901–911.

Stuart-Fox, D., Newton, E., & Clusella-Trullas, S. (2017). Thermal consequences of colour and near-infrared reflectance. *Philosophical Transactions of the Royal Society B: Biological Sciences*, *372*(1724), 20160345.

Sultan, S. E. (1987). Evolutionary implications of phenotypic plasticity in plants. In M. K. Hecht, B. Wallace, & G. T. Prance (Eds.), *Evolutionary Biology* (pp. 127-178).

Symonds, M. R. E., & Tattersall, G. J. (2010). Geographical variation in bill size across bird species provides evidence for Allen's rule. *The American Naturalist*, *176*(2), 188–197.

Tattersall, G. J., Chaves, J. A., & Danner, R. M. (2018). Thermoregulatory windows in Darwin's finches. *Functional Ecology*, *32*(2), 358–368.

Tattersall, G. J., Sinclair, B. J., Withers, P. C., Fields, P. A., & Seebacher, F. (2012). Coping with thermal challenges: physiological adaptations to environmental temperatures. *Comprehensive Physiology*, *2*(3), 2151–2202.

Tigano, A., & Friesen, V. L. (2016). Genomics of local adaptation with gene flow. *Molecular Ecology*, *25*(10), 2144–2164.

Trumbo, D. R., Funk, W. C., Pauly, G. B., & Robertson, J. M. (2021). Conservation genetics of an island-endemic lizard: low Ne and the critical role of intermediate temperatures for genetic connectivity. *Conservation Genetics,* 1-15.

Truttmann, M. C., Zheng, X., Hanke, L., Damon, J. R., Grootveld, M., Krakowiak, J., … Ploegh, H. L. (2017). Unrestrained AMPylation targets cytosolic chaperones and activates the heat shock response. *Proceedings of the National Academy of Sciences*, *114*(2), E152–E160.

Walsberg, G. E. (1983). Coat color and solar heat hain in animals. *BioScience*, *33*(2), 88–91.

Wasmeier, C., Hume, A. N., Bolasco, G., & Seabra, M. C. (2008). Melanosomes at a glance. *Journal of Cell Science*, *121*(24), 3995–3999.

Western Regional Climate Center. (2021). Channel Island National Park Stations: RAWS/NDBC Buoy/Manual Ranger Stations. Retrieved from https://wrcc.dri.edu/channel_isl/

Wolf, B. O., & Walsberg, G. E. (2000). The role of the plumage in heat transfer processes of birds. *American Zoologist*, *40*(4), 575–584.

Wolf Horrell, E. M., Boulanger, M. C., & D'Orazio, J. A. (2016). Melanocortin 1 receptor: structure, function, and regulation. *Frontiers in Genetics*, *7*, 95.

Xiong, Y., & Lei, F. (2020). SLC2A12 of SLC2 gene family in bird provides functional compensation for the loss of SLC2A4 gene in other vertebrates. *Molecular Biology and Evolution*, *38*(4), 1276–1291.

Xu, Y., Cui, L., Dibello, A., Wang, L., Lee, J., Saidi, L., … Ye, Y. (2018). DNAJC5 facilitates USP19-dependent unconventional secretion of misfolded cytosolic proteins. *Cell Discovery*, *4*(1), 1-18.

Yates, A. D., Achuthan, P., Akanni, W., Allen, J., Allen, J., Alvarez-Jarreta, J., … Flicek, P. (2020). Ensembl 2020. *Nucleic Acids Research*, *48*(D1), D682–D688.

Zhou, X., Carbonetto, P., & Stephens, M. (2013). Polygenic modeling with Bayesian sparse linear mixed models. *PLoS Genetics*, *9*(2), e1003264.

4. MICROGEOGRAPHIC ADAPTATION IN SONG SPARROWS ALONG A STEEP CLIMATE GRADIENT

Summary

Climate adaptation involves selection on a suite of complex phenotypes among individuals, yet most studies have inferred adaptation to climate based solely on physiological responses to temperature at macroevolutionary scales. To better understand how climate-based selection generates adaptive variation, it is important to evaluate thermal physiology in addition to variation in other correlated traits, including plumage color and feather structure in birds. However, whether avian populations exhibit concerted adaptive responses in thermal physiology and plumage simultaneously and whether any populations differences represent evolutionary responses to temperature remain to be explored. To test the hypothesis that climate drives adaptive divergence in thermal physiology and plumage, we assessed the relationship between environmental temperatures and (i) physiological responses to cold and heat stress, (ii) contour feather microstructure, and (iii) plumage gray intensity in song sparrows occupying a climate gradient on the California Channel Islands and nearby coastal southern California. Additionally, we performed genome-wide association analyses to infer whether morphological variation represents adaptive plasticity or genetically based climate adaptation. We found a significant relationship between maximum temperature and thermal physiology, with birds in colder environments exhibiting higher basal metabolic rates, lower behavioral heat stress temperatures, and lower rates of change in evaporative water loss in response to increasing heat stress. We also found a significant relationship between the pennaceous section of contour feathers and temperature. Birds in colder, windier environments had higher barb and barbule densities and longer total lengths of the pennaceous section, suggesting they have a stronger, overlapping

protective layer to prevent wind and water penetrating to the surface of the skin. On the other hand, several traits (i.e., behavioral cold stress temperatures, characteristics of the plumulaceous section of the feather, and plumage gray intensity) were conserved across our sampling region and did not significantly covary with temperature. Overall, our results suggest that regional climate differences across a small spatial extent can facilitate intraspecific plastic and genetically based adaptive divergence in a suite of thermoregulatory traits. Future studies of climate adaptation should consider multiple physiological and morphological traits to improve our understanding of how climate drives evolution and how populations may respond to future environmental change.

Introduction

Climate adaptation is a multifaceted response to selection operating on a suite of complex phenotypes within individuals (Angilletta Jr, 2009; Scholander et al., 1950). Yet, most of our understanding of climate adaption is derived from comparative studies of species' thermal physiology across broad spatial and latitudinal scales (e.g., Anderson & Jetz, 2005; Buckley & Huey, 2016; Fristoe et al., 2015; Hof et al., 2017; Mitchell et al., 2018; Sunday et al., 2014). Although macrophysiology studies provide evidence for covariation between the environment and some aspects of adaptation, generalizations about interspecific patterns drawn from limited sampling within species may greatly misrepresent climate adaptation across a species' distribution (Chown & Gaston, 2016). First, inferred trends may be misconstrued if we fail to account for intraspecific variation resulting from differential responses at the molecular, cellular, and individual levels (Bozinovic et al., 2020; Burton, Killen, Armstrong, & Metcalfe, 2011; Pörtner et al., 2006). For example, repeated sampling of critical thermal limits in multiple

populations of 15 lizard species on the Iberian Peninsula results in higher variance in heat tolerances when accounting for intraspecific variation, and this runs contrary to inferences drawn from single estimates of thermal limits within species which result in higher variances in cold tolerances (Herrando-Pérez et al., 2020). These incongruent individual and population responses to thermal stress may be fixed and represent evolutionary change (e.g., Dixon et al., 2015; Gamboa et al., *in prep.,* Sørensen, Dahlgaard, & Loeschcke, 2001), or, alternatively, may be plastic and phenotypically flexible (e.g., Campbell-Staton, Bare, Losos, Edwards, & Cheviron, 2018; Cheviron, Whitehead, & Brumfield, 2008; Noh, Everman, Berger, & Morgan, 2017). By examining intraspecific variation in adaptation at finer spatial scales across multiple populations, we improve our understanding of the conditions that facilitate evolutionary responses to climate (Chown & Gaston, 2016). Second, assessing climate adaptation strictly from a macrophysiological perspective assumes adaptation is univariate and ignores the potential of other traits (e.g., morphology) to alter the strength of selection on physiology (Razgour et al., 2019; T. E. Reed, Schindler, & Waples, 2011) Understanding how the dynamic integration of multiple traits and molecular pathways interact to generate adaptive responses to climate remains a long-standing goal in evolutionary physiology (Chown, Gaston, & Robinson, 2004; Chown et al., 2010; Feder, Bennett, & Huey, 2000; Scholander, 1955; Scholander, Flagg, Walters, & Irving, 1953). Despite this central goal and the acknowledgment of coadapted phenotypic responses to thermal environments (Angilletta et al., 2006), far less is known about how multiple traits associated with thermoregulation respond independently or in concert to climate-based divergent selection.

Strong climate-based selection on individuals may result in many different alternate strategies to improve heat retention or dissipation. For example, endotherms maintain high body

temperatures through metabolic processes (Crompton, Taylor, & Jagger, 1978), and a hypothesized evolutionary or plastic response to extreme cold is to increase basal metabolic rate, thereby enhancing thermogenic capacity (Tattersall et al., 2012). Yet, basal metabolic rate and physiological responses to cold stress can remain unchanged in birds and mammals in favor of increased investment in insulation (Scholander et al., 1950). More precisely, avian plumage and mammalian pelage act as insulative layers buffering individuals from thermal heterogeneity and reducing thermal conductance under colder temperatures (Hammel, 1955; Tattersall et al., 2012; Wolf & Walsberg, 2000). In birds, plumage serves important fitness-related functions and readily responds to selection (Price, 2006; Prum & Brush, 1976; Roulin, 2004). Indeed, numerous empirical studies suggest plumage is an important thermoregulatory trait with evidence of covariation between climate and feather density (Osváth et al., 2018) and structure (Barve, Ramesh, Dotterer, & Dove, 2021; Cheek, Alza, & McCracken, 2017; Pap, Osváth, Daubner, Nord, & Vincze, 2020).

Correlations between climate and multiple feather characteristics suggest there are many ways in which plumage may vary with climate to affect solar heat gain or loss (Prum & Dyck, 2003; Schneider, 2005). For example, in an analysis of 50 bird species, barb shape and barbule densities in white contour feathers are significant predictors of near-infrared reflectance, such that higher barbule densities aid in reducing solar heat absorption (Stuart-Fox et al., 2018). Alternatively, in tawny owls, grey morphs have more developed plumulaceous regions of dorsal contour feathers and, consequently, more insulative dorsal plumage compared to brown morphs (Koskenpato, Ahola, Karstinen, & Karell, 2016), and grey morphs are associated with higher fitness and survival in winter months (Brommer, Ahola, & Karstinen, 2005; Karell, Ahola, Karstinen, Valkama, & Brommer, 2011). It is clear plumage and feather divergence among

climatically distinct populations can have important thermal and fitness consequences. Yet, whether intraspecific patterns of feather variation complement or replace adaptive physiological or other morphological responses remains uncertain.

Modifications to the insulative properties of plumage in colder climates may occur independently or in conjunction with increased melanin deposition, which may result in lower reflectance values and greater solar heat gain (Clusella Trullas, van Wyk, & Spotila, 2007; Roulin, 2004, 2014; Stuart-Fox et al., 2017). As with feather structure and density, climate has been shown to covary with overall plumage color (Burtt & Ichida, 2004; Delhey, 2018; Galván, Rodríguez-Martínez, & Carrascal, 2018). For instance, analyses of over 500 bird species in Australia found darker pigmented bird assemblages (lower mean reflectance values) in colder, wetter regions (Delhey, 2018). Similarly, darker birds cluster in colder regions on the Iberian Peninsula and, hence, are hypothesized to have narrower thermal niches than lighter birds that have less overall melanin deposition (Galván et al., 2018). Feather color and microstructure may be more susceptible to climate-based selection than feather density, because feather tracts and buds arise early in development from epithelial and mesenchymal cells such that feather follicles remain fixed over time (Chen et al., 2015; Stettenheim, 2000). On the other hand, final feather coloring and microstructure occurs after feather follicle formation and with each cycle of feather replacement throughout the individual's lifetime (Chen et al., 2015; Stettenheim, 2000). The resulting feather phenotype is determined by genetic and environmental factors (Lin, Jiang, Widelitz, & Chuong, 2006; Ng & Li, 2018; Stettenheim, 2000); multiple studies confirm a genetic basis to individual components of plumage color polymorphism (Bourgeois et al., 2017; Küpper et al., 2016; Poelstra et al., 2014; Uy et al., 2016), while others suggest environmental effects drive and maintain fitness-related plumage variation (Broggi, Gamero, Hohtola, Orell, &

Nilsson, 2011; Hadfield & Owens, 2006; Wylie, Robertson, MacLeod, & Hocking, 2001). Adaptive changes in feather color and structure may buffer populations from climate shifts without generating evolutionary changes (Ghalambor et al., 2007). Thus, change in any one of these feather characteristics can have consequences for the strength of selection on other traits (e.g., thermal physiology). For example, selection for elevated basal metabolic rate may be dampened by adaptive changes in feather structure or color and vice versa. Whether selection on some thermoregulatory traits facilitates or constrains evolution of other traits in response to climate remains uncertain.

Song sparrows (*Melospiza melodia*) on the Channel Islands are distributed along a strong west-east climate gradient and are an ideal system to examine the relationship between climate and variation in thermoregulatory traits. Song sparrows on western islands (San Miguel and Santa Rosa Islands) experience cold, mesic, and windy conditions, while birds on eastern islands (Santa Cruz and Anacapa Islands) inhabit hot, xeric, and less windy conditions (Fig. 4.1; Schoennerr, Feldmeth, & Emerson, 2003). This striking climate gradient is generated by effects of the California Current, which brings cold water from the Gulf of Alaska around the western islands, while the Southern California Counter Current brings warm water from Baja California past the eastern islands (Schoennerr et al., 2003). Previous research has shown restricted gene flow among islands and adaptive bill divergence in contemporary song sparrow populations (Gamboa, Chapter 2). Specifically, bill surface area is positively correlated with maximum temperature and neither significantly predicted by vegetation nor related to foraging traits (e.g., seed extraction time, bite force; Gamboa, Chapter 1). Patterns of bill divergence coupled with genomic analyses provide indirect evidence for local adaptation in bills (Gamboa, Chapter 2), likely as a thermoregulatory tool for dissipating heat (Tattersall et al., 2016). Thermal heat stress

and temperature extremes are likely to shape adaptive phenotypic variation even though song sparrows experience many correlated axes of climate variation (i.e., wind strength and humidity are positive correlated, and both are negatively correlated with temperature) given that maximum temperature significantly predicted bill variation in museum specimens as well (Greenberg & Danner, 2012). Moreover, complementary genotype-environment association (GEA) analyses in island song sparrows reveal maximum temperature is not only correlated with genotypes in bill development genes, but also with other genes that are known to regulate thermal stress responses and plumage (Gamboa, Chapter 2). Nevertheless, it is unknown whether these genetic changes result in measurable phenotypic differences in thermal physiology, plumage color, and feather microstructure.

To further test whether genomic patterns of divergence are associated with traits known to be involved in climate adaptation, we measured thermal physiology and morphology in song sparrows on the California Channel Islands. We compared our results in island populations (San Miguel, Santa Rosa, and Santa Cruz Islands) to the mainland conspecifics to infer whether observed population differences are unique to island song sparrows or represent broader, regional responses to temperature variation. We used flow-through respirometry to estimate basal metabolic rate, evaporative water loss, and thermal stress temperatures (i.e., temperatures that elicit observable behavioral responses to cold stress and to heat stress). We tested the alternative hypotheses that basal metabolic rate is either (1) conserved among populations, as phenotypic flexibility, or reversible observed variation, in this trait across seasons and ontogeny may constrain adaptive evolution (Pettersen, Marshall, & White, 2018; Tattersall et al., 2012), or (2) that colder temperatures favor elevated basal metabolic rate as an adaptive thermogenic response. We also tested whether the climate gradient imposes divergent selection on

temperatures that elicit behavioral responses to cold and heat stress and on rates of change in evaporative water loss in response to increasing heat stress (McKechnie & Wolf, 2019). Specifically, we predict that birds in colder climates should either have higher rates of evaporative water loss to promote cooling in response to increasing temperatures, which is indicative of greater thermal stress. Further, we predict environmental temperatures are positively correlated with behavioral cold and heat stress temperatures (i.e., higher temperatures correlated with behavioral responses to thermal stress in hotter regions and lower temperatures in colder regions). We complement our assessment of thermal physiology with tests to determine whether population plumage characteristics (i.e., contour feather microstructure, plumage gray intensity) covary with temperature. We predict birds in colder, windier environments have more developed contour feathers overall to reduce heat loss and darker plumage to improve solar heat gain. Lastly, we perform genome-wide association analyses to determine whether morphological variation has a genetic basis to infer whether any difference between populations are adaptive evolutionary responses to selection.

Methods

Assessing the relationship between physiological traits and temperature

Capture & acclimation to experimental conditions for estimating physiological traits

We used song playback and mist-nets to capture adult, male song sparrows during the breeding season (March-May 2017, 2019) from the three largest island populations (San Miguel, Santa Rosa, and Santa Cruz Islands) and from coastal regions of mainland California in the Santa Monica National Recreation Area (Fig. 4.1A-C). Given that transient migrants may use the islands as stopovers during the non-breeding season, we sampled during the breeding season to

increase the likelihood that birds were resident breeders and thus subject to environmental selection pressures at the sampling location. All captured individuals were color-banded, weighed, and measured. We specifically targeted male song sparrows, as females have been documented to give biased estimates of basal metabolic rate based on reproductive status (Vezina & Williams, 2002; Vézina & Williams, 2003). Birds included in thermal physiology analyses were captured within three hours of sunset and held overnight in individual cages for subsequent flow-through respirometry experiments. All experimental procedures were conducted with approval by Smithsonian's National Zoological Park IACUC (Proposal Nos. 14-02 and 17-06).

We housed birds in individual cages to minimize stress and ensure a post-absorptive state prior to respirometry experiments. All cages were equipped with two perches at different heights and one water dish. We internally padded cages with ¼ inch (0.635 cm) thick polyvinyl chloride foam to prevent injury and to facilitate ease of cleaning between individuals. We covered cages with blankets to dampen sound and kept cages in a dark, secure location at room temperature (~22-26°C). We withheld food for at least four hours to induce a post-absorptive state (Danner, *pers. comm.*). We performed temperature tolerance experiments on post-absorptive males between the hours of 2100-0400. We continually monitored behavior using infrared cameras. We recorded pre- and post-experiment masses, and, following pre-experiment measurements, we placed the bird in a modified airtight chamber (Snapware Model No. 1098433, Instant Brands Inc.) for acclimation to experimental conditions.

We acclimated birds to experimental chamber conditions for at least 20 minutes prior to the start of experiments. Experimental chambers included a mesh platform to allow for natural perching behavior during sleep and to allow fecal matter to pass through to the chamber floor

where we included a 10mm deep layer of mineral oil to prevent water evaporation (Fig. 4.1G). We used different starting acclimation temperature between cold and heat tolerance experiments (TA_{cold} = 18ºC; TA_{heat} = 25ºC) and assumed both acclimation temperatures were within the thermal neutral zone based on preliminary trials (see *Temperature ramping profile & respirometry system*). Acclimation temperatures were also within or near thermal limits of other passerines of similar mass (Dawson, Buttemer, & Carey, 1985; Hudson & Kimzey, 1966; McKechnie et al., 2017; Eric Krabbe Smith, O'Neill, Gerson, McKechnie, & Wolf, 2017; Tieleman, Williams, & Buschur, 2002; Weathers, 1981). Birds were assigned to either a cold or heat tolerance experiment based on date in the breeding season. Specifically, we performed all cold tolerance experiments early in the breeding season (March-early April) and all heat experiments later in the breeding season (late April-May) to account for seasonal flexibility in metabolic rate (McKechnie, 2008; Swanson, 2010).

Temperature ramping profile & respirometry system

Following acclimation, we adjusted temperatures every 30 minutes and maintained constant test temperatures for at least 10 minutes. We conducted initial trials on live song sparrows to establish acclimation and test temperatures based on behavioral and metabolic responses. Final experimental temperature profiles included one acclimation temperature within the thermoneutral zone (see above), one test temperature within the thermoneutral zone ($T1_{cold}$ = 15ºC; $T1_{heat}$ = 29ºC), and two test temperatures likely to span the lower or upper critical temperatures of the thermoneutral zone ($T2_{cold}$ = 12ºC, $T3_{cold}$ = 9ºC; $T2_{heat}$ = 32ºC, $T3_{heat}$ = 35ºC). We used a Peltier temperature controller (PELT-5, Sable Systems Intl.) to set and maintain temperatures within the incubator (PTC-1, Sable Systems Intl.). Adjustments between test temperatures during experiments were gradual, but ramping rate was dependent on ambient

temperature of incurrent air and could not be directly controlled with our equipment. We inserted thermocouples within the incubator and the test chamber and consistently monitored experimental temperatures using a digital interface (UI-3, Sable Systems, Intl.) in the program ExpeData v. 1.9.2 (Sable Systems, Intl.).

To measure metabolic rate across a range of temperatures, we used push-mode flow-through respirometry (*i.e.,* incurrent air was pushed through the system using a series of pumps and controllers). We used a high-capacity vacuum pump (DAA-V715-EB, Gast Manufacturing, Inc.) to push outdoor air through a series of modified drying columns (Part No., 26800, W. A. Hammond Drierite Co., Ltd.). We scrubbed bulk water vapor by first pushing air through one column of color-indicating silica gel (Part No. 640SGO05, Impak Corporation) and removed the remaining moisture by subsequently pushing air through two drying columns each with 3:1 mixtures of Du-Cal Drierite and indicating Drierite (Part nos. 41050 & 21005, W. A. Hammond Drierite Co., Ltd.). We used a mass flow controller (MC-10LPM, Alicat Scientific) to push the dried air through the Peltier-adjusted incubator at a rate of 2.5 L/min. Incurrent air was passed through a copper McKechnie coil within the incubator to allow for rapid temperature equilibration prior to entering the experimental chamber. Incurrent and excurrent air openings were staggered on opposite sides of the experimental chamber to allow for sufficient gas mixing. We reduced the flow rate of excurrent air to 500 mL/min using a rotameter (RMA-12, Dwyer Instruments) and subsampled this air at a rate of 250 mL/min using the FoxBox field respirometer internal pump (Sable Systems, Intl.). We measured gas concentrations and water vapor pressure in the excurrent air every second with the FoxBox field respirometer and relative humidity meter (RH-300, Sable Systems, Intl.) and recorded readings using a universal interface (UI-3, Sable Systems, Intl.) in the program ExpeData v. 1.9.2 (Sable Systems, Intl.).

To maintain consistency among experiments, we calibrated equipment regularly and replaced spent materials. We replaced all desiccants after every two experiments and recharged used Drierite as needed per manufacturer's instructions. We performed daily calibrations of the FoxBox oxygen sensor using outdoor air and a carbon dioxide sensor using a mixture of 98.999% nitrogen to 1.001% carbon dioxide (X02NI99CP101405, Airgas Inc., analytical uncertainty $\pm$ 2%). We calibrated the RH-300 water vapor pressure sensor every other day using 99.999% nitrogen (NI UHPP10, Airgas Inc., analytical uncertainty $\pm$ 2%) every other day. We allowed all equipment to run for at least 30 minutes before initiating acclimation and visually inspected readings in ExpeData to confirm proper functioning of the respirometry system.

Inferring thermal stress temperatures

To determine thermal stress temperatures, we coupled behavioral observations with measurements of gas and water vapor changes in excurrent air from the experimental chamber. Limitations of our equipment and study system prevented us from exposing birds to extreme hot or cold temperatures outside the hypothesized TNZ, thus limiting our power to accurately estimate thermal limits (i.e., upper and lower critical temperatures) via piecewise regression as in other studies (e.g., McKechnie et al., 2017; Smit et al., 2018). As a proxy for thermal limits, we estimated the temperatures at which birds exhibited behaviors associated with thermal stress (behavioral thermal stress temperatures). Behavioral indicators of heat stress included excessive panting, posture instability, wing-drooping, and frequent eye fluttering (Smit, Harding, Hockey, & E. McKechnie, 2013; Smit et al., 2016; Tattersall et al., 2012). Behavioral indicators of cold stress included persistent ruffling of feathers to increase air trapped near the skin, posture instability, and bill-tucking (Marsh & Dawson, 1989; Tattersall et al., 2016). Multiple simultaneous behavioral indicators were accompanied by a sharp decrease in oxygen

concentrations and a sharp increase in water vapor pressure and carbon dioxide concentrations in excurrent air (Appendix 3 Fig. S3.1). Sudden movements or excessive unrest may result in similar, short-term responses in excurrent air, and these movement responses were excluded from our analyses. We defined the thermal stress temperatures as the temperature above or below which both (1) the bird was visibly thermally stressed based on behavioral observations and (2) the excurrent air concentrations of gas and water vapor exhibited a sharp inflection point and a continuous rate of change for least three minutes (Appendix 3 Fig. S3.1). Following temperature tolerance trials, birds were transferred back to their respective cage, provided food and water, held overnight, and released back to their capture sites within one hour of sunrise.

Calculating metabolic rate and evaporative water loss

We calculated oxygen consumption (VO_2) and water loss (VH_2O) using recorded measurements in ExpeData v. 1.9.2 (Sable Systems, Intl.). We corrected for lag and drift in instrument responses and applied conservative smoothing equations to reduce noise as recommended by the manufacturers (Sable Systems, Intl.). We searched for and extracted data representing the most level readings of oxygen and water vapor pressure over a 200-second period of rest or sleep. Following Lighton (2008), we calculated metabolic rate (VO_2; Equation 10.1) and water loss (VH_2O; Equation 10.9) and converted estimates to watts for metabolic rate and to $g \bullet hr^{-1}$ for evaporative water loss, respectively. We used metabolic rate calculated from the first test temperature in both cold and heat tolerance experiments ($T1_{cold}$ and $T1_{heat}$; neutral temperatures) as a proxy for basal metabolic rate. We were interested in whether regional maximum environmental temperatures affect evaporative water loss and analyzed the rate of change in evaporative water loss following increasing heat exposure. Thus, to quantify the rate of change in evaporative water loss for individuals in heat stress experiments, we calculated the

slope of the line connecting evaporative water loss estimates at heat stress test temperatures ($T2_{heat}$ and $T3_{heat}$).

Estimating environmental temperatures

To estimate environmental temperatures for individual sampling locations, we used temperature data at 1 km^2 (30s) spatial resolution from WorldClim v. 1.4 (Hijmans et al., 2005). We hypothesized that thermal extremes act as a strong selective pressure, because maximum temperature was a significant predictor of bill size in this system (Gamboa, Chapter 1.; Greenberg & Danner, 2012). Thus, we used maximum and minimum environmental temperature rasters for July and January, respectively, to extract temperature data for each sampling location in ArcGIS v. 10.7 (ESRI, 2011).

Statistical analyses of physiological traits with respect to environmental temperature

We performed linear regression models and linear mixed models in R (R Core Team, 2020) to assess the relationship between thermal physiology and environmental temperatures at sampling locations. We used the function *lm* in R to evaluate behavioral thermal stress temperatures and the rate of change in evaporative water loss and the function *lmer* in the R package *lme4* (Bates et al., 2015) to evaluate basal metabolic rate. Linear mixed models were used for basal metabolic rate to control for different acclimation and neutral zone test temperatures by including experiment type (cold or heat) as a random effect. We included physiological trait (behavioral cold and heat stress temperatures, rate of change in evaporative water loss, or basal metabolic rate) as the response for all models. We used maximum environmental temperature as a predictor for models examining behavioral heat stress temperatures, rates of change in evaporative water loss, and basal metabolic rates and minimum environmental temperatures for modeling behavioral cold stress temperatures under the

prediction that cold environmental temperatures are correlated with cold stress responses. We ran null models with no explanatory variables and models including all additive combinations of environmental temperature, mass, and Julian day as predictors, because thermal physiology traits have been known to covary with mass and reproductive state (McKechnie, 2008; Swanson, 2010). We used the *aictab* function in the R package *AICcmodavg* (Mazerolle, 2020) to select the top model based on Akaike information criterion (AIC; Burnham & Anderson 2002).

We generated statistics from the top model for each thermal physiology trait (behavioral cold and heat stress temperatures, rate of change in evaporative water loss, and basal metabolic rate). We output beta estimates and 95% confidence intervals around model parameter estimates using the function *confint* in the *stats* R base package. For the top basal metabolic rate linear mixed model, we estimated the marginal and conditional R^2 values (Nakagawa & Schielzeth, 2013), or the variance explained by maximum temperature only and variance explained by both maximum temperature and experiment type combined, using the *r2_nakagawa* function in the *performance* R package (Lüdecke, Ben-Shachar, Patil, Waggoner, & Makowski, 2021). We applied the function *ggemmeans* in the R package *ggeffects* (Lüdecke, 2018) to output estimated marginal means for behavioral heat stress temperatures, rates of change in evaporative water loss, and basal metabolic rates based on regional mean maximum temperatures and for behavioral cold stress temperatures based on regional mean minimum temperatures.

Assessing the relationship between morphological traits and environmental temperature

Capture & sampling of morphological characters

We used mist-nets and playback experiments to capture and sample adult, male song sparrows during the breeding season (March-June) from 2014-2017 for analysis of morphological traits. We sampled across a broad range of environmental temperatures on the

three largest islands (San Miguel, Santa Rosa, and Santa Cruz Islands) and from coastal regions of mainland California in the Santa Monica National Recreation Area (Fig. 4.1D-E; Table 4.1). All captured individuals were banded, weighed, and measured. Birds were immediately released back to their territory unless they were included in physiological experiments (see *Assessing the relationship between physiological traits and temperature*).

For analysis of feather microstructure, we manually extracted approximately 3-8 breast feathers from the upper right pectoral region of adult males (Fig. 4.1H). The pectoralis muscle is the largest avian skeletal muscle and is a large contributor to metabolic heat production (McNab, 2019; Rowland, Bal, & Periasamy, 2015). Thus, we expect contour feather microstructure in this region to be critical for avian thermoregulation. Song sparrows exhibit complex plumage color patterning, including brown streaking across the breast (Arcese et al. 2002), and we preferentially targeted near-white feathers as differences in melanin-based coloration may result in microstructure variation (Galván, 2011). We preserved samples in individual coin envelopes and stored envelopes in a dark, dry, secure container to prevent feather degradation.

We captured and photographed breeding males sampled on San Miguel, Santa Rosa, and Santa Cruz Islands from 2014-2015 for comparison of plumage gray intensity among islands. We did not include birds from mainland California in this analysis as plumage differences between mainland and island song sparrow populations have been well-described (Patten & Pruett, 2009). We photographed each bird individually in the field against a white, matte paper background in a custom photography box equipped with a ruler and photo calibration grayscale card (QP101, QPCard). To account for normal wear from regular use, we replaced the photography box background and calibration card as needed. All images were taken in manual mode using a digital camera (Canon EOS Rebel T3i) with a 60mm macro lens and an MR-14EX ring flash.

Ring flash power differed between 2014 and 2015 (1/8 and 1/16 power, respectively), and we controlled for differences between years in subsequent analyses. We standardized all other camera and lens settings (ISO 100, F-stop 11, 1/250 sec, lens focal distance 0.44mm). To photograph focal regions, we held the bird in the hand and manipulated the position of the bird such that the focal region (back or crown), ruler, and photo calibration standard were level (Fig. 4.1I-J). We positioned the camera directly over the region of interest and parallel to the photography box. We moved the camera vertically above the bird to ensure the focal region and ruler millimeter markers were in focus. All images were saved as raw files for analysis in image processing software.

Quantification of feather microstructure

We used a compound microscope to analyze breast feather microstructure in ≥20 adult males per sampling region, including 3-5 feathers per male to account for individual variation. We viewed and measured individual feathers with a digital microscope camera (DP71, Olympus Corporation) affixed to a compound light microscope (BX51, Olympus Corporation) and integrated with the program DP2-BSW v. 2.0 (Olympus Corporation). We viewed images under 10X, 40X, and 100X total magnification to estimate feather lengths, number of barbs, and number of barbules, respectively. We divided the contour feather into the distal pennaceous and proximal plumulaceous (downy) sections following Pap et al. (2016). We measured total length and length of both the pennaceous and plumulaceous sections. Within both the pennaceous and plumulaceous sections, we counted the total number of barbs (Fig. 4.2A,C). We counted the total number of barbules within a 1mm section of a barb in the pennaceous and plumulaceous sections (Fig. 4.2B,D) and converted counts to estimates of barb and barbule densities. We observed damage to some of the barbs on the outer regions of both sections, and, consequently, selected

undamaged barbs centered within each section for barbule counts. We began barbule counts along the barb 1mm away from the rachis. All feather measurements were performed by P. Kohlruss-Reuman to ensure consistency and avoid observer bias.

To reduce the complexity of highly-correlated feather microstructure variables, we performed principal component analysis (PCA). We included feather lengths (total, pennaceous, plumulaceous), and barb and barbule densities in both the pennaceous and plumulaceous sections. We applied the R function *prcomp* with centered and scaled data to reduce feather dimensions to ordinal space. We visually inspected and output loadings for the resulting principal components (PCs) using the R package *factoextra* (Kassambara & Mundt, 2020). We extracted PC scores and included the top two PCs in all subsequent analyses of feather microstructure.

Image processing and quantification of plumage gray intensity

To compare plumage darkness among individuals, we filtered and analyzed standardized digital images and quantified gray intensity in heavily melanized plumage regions using image processing software. We uploaded raw back and crown images in the open-source software program RawTherapee v5.8 (RawTherapee, 2020) and screened images with a neutral processing profile to prevent automatic exposure correction. We removed overexposed and underexposed images based on visual inspection of exposure histograms. We imported raw images in ImageJ v.1.53a (C. A. Schneider, Rasband, & Eliceiri, 2012) using DCRaw Reader integrated in the Multispectral Imaging Toolbox Plugin (micaToolbox v. 2.2; Troscianko & Stevens, 2015). We generated comparable multispectral images in the human visible spectrum (32-bit) by calibrating light exposure to the known reflectance of the calibration card. We demarcated boundaries of the focal region and output standard RGB values (range = 0, 255) averaged across all polygon pixels

with the Pattern & Luminance Measurement function in the micaToolbox. We converted standard RGB values to linear values by dividing by 255 and calculated perceived gray values (Y_{linear}, luminosity) weighted by the human visual spectrum based on RGB values following the equation $Y_{linear} = 0.2126R + 0.7152G + 0.0722B$ (IEC, 2003). Data generated from analyses of digital images in the human visual spectrum demonstrate similar patterns in the avian visual spectrum and may be used to assess color variation among populations (Bergeron & Fuller, 2018). Importantly, our goal was not to quantify true plumage color in the avian visual spectrum. Rather, our aim was to output comparable estimates of plumage gray intensity to test whether birds exhibit differences in plumage darkness, which is correlated with solar heat gain potential under certain climate conditions (Wolf & Walsberg, 2000). We performed a nonlinear gamma transformation on Y_{linear} following the equation $Y = 1.055* Y_{linear}^{1/2.4} – 0.055$ (IEC, 2003) and converted gamma-transformed Y values to standard grayscale values by multiplying Y by 255 [range = 0 (black), 255 (white)]. We used standard grayscale values as a proxy for plumage gray intensity and degree of plumage melanization to test for a relationship between color and temperature.

Statistical analyses of feather microstructure and color

We applied linear mixed models to test the relationship between temperature and morphological variation in feather microstructure and plumage gray intensity values. For analysis of each feather microstructure variable (feather PC1 and PC2), we included PC score as a response, maximum temperature as a fixed effect, and individual as a random effect. For analysis of plumage gray intensity in each focal region, we included focal region (back or crown) as a response, maximum temperature as a fixed effect, and year as a random effect to control for different ring flash settings between years. We extracted maximum temperature data, performed

linear mixed modeling, and output regional estimated marginal means for each morphological trait following procedures outlined above (see *Estimating environmental temperatures*).

Genome-wide associations with feather microstructure and plumage gray intensity

To determine whether there is any genetic basis to feather microstructure and plumage color, we performed GWA tests using genomic data and procedures described in Gamboa (Chapter 2). We did not perform GWA tests on thermal physiology traits, because genomic data was generated from individuals sampled from 2014-2017. Consequently, we did not have genotypes for individuals included in respirometry experiments conducted in 2019. Briefly, we cleaned, filtered, and assembled 100-bp single-end RAD-sequencing loci *de novo*, aligned loci to the zebra finch reference genome (*Taeniopygia guttata*, v3.2.4), and imputed missing data, resulting in 3,294 SNPs for GWA tests. We subset this original VCF file using *vcftools* v. 0.1.16 (Danecek et al., 2011) to include only individuals with known feather microstructure phenotypes.

For each feather microstructure trait ($PC1_{feather}$ and $PC2_{feather}$) and plumage gray intensity for each focal region (back and crown), we performed partial redundancy analysis (RDA) and linear mixed modeling (LMM) following Gamboa (Chapter 2). We implemented partial RDA using the function *rda* in the R package *vegan* (Oksanen et al., 2020) and conditioned RDA on latitude and longitude of individual sampling locations to control for previously observed patterns of isolation-by-distance in island song sparrows (Gamboa, Chapter 2). We performed permutation tests (n = 9999) on partial RDA models using the function *anova.cca* to evaluate whether phenotype significantly predicted genotype. We implemented LMM in the program GEMMA, which tests the null hypothesis that observed phenotypic variation is not related to genotypes at any individual variant site when controlling for population structure (Zhou & Stephens, 2012). We adjusted p-values using the Benjamini-Hochberg method to correct for

multiple testing and called candidates based on an FDR of 0.05 (adjusted p-value < 0.05). We obtained functional annotations for genes within 50kb of these variant sites following the procedure described in Gamboa (Chapter 2). To infer a direct relationship between genotype and phenotype, we searched the resulting annotation report for GO terms related to feather development and keratinocyte proliferation.

Results

The relationship between environmental temperatures and physiological traits

We performed flow-through respirometry experiments on 123 male song sparrows during the breeding season in 2017 and 2019. We diagnosed thermal stress responses and estimated behavioral cold and heat stress temperatures in 96 individuals (Table 4.1). After removing individuals with excessive movement during neutral test temperatures ($T1_{cold}$ and $T1_{heat}$), we estimated basal metabolic rate in 91 individuals (Table 4.1). We subset basal metabolic rate experiments to include heat trials only, resulting in 53 individuals used for estimating rates of change in evaporative water loss (Table 4.1).

Following model selection, all top models for evaluating thermal physiology traits included environmental temperature as a predictor (Appendix 3 Table S3.1). Mass was not significantly associated with any thermal physiology responses and was removed from all top models (Appendix 3 Table S3.1). However, we found a significant correlation between Julian day and basal metabolic rate ($\beta = 0.0027$, 95% CI = 0.0005 – 0.0044, $t_{82} = 2.931$, $P < 0.01$) and Julian day and behavioral heat stress temperature ($\beta = 0.09$, 95% CI = 0.04 – 0.14, $t_{2,46} = 3.503$, $P < 0.01$) and, thus, we retained Julian day in top models for assessing the relationship between

maximum environmental temperatures and basal metabolic rates and behavioral heat stress temperatures (Appendix 3 Table S3.1).

Using the top models, we found little variation in behavioral cold stress temperatures and a significant relationship between maximum environmental temperatures and all other physiology traits (behavioral heat stress temperatures, basal metabolic rates, and rates of change in evaporative water loss; Table 4.1, Fig. 4.3A). Although there was a trend for lower behavioral cold stress temperatures in colder regions (Fig. 4.3A), minimum environmental temperature had a weak to negligible effect on behavioral cold stress temperatures ($\beta = 0.40$, 95% CI = -0.13 – 0.93, $t_{1,45} = 1.522$, $p = 0.14$, adjusted $R^2 = 0.028$). As expected, maximum environmental temperatures significantly predicted behavioral heat stress temperatures ($\beta = 0.29$, 95% CI = 0.10 – 0.48, $t_{2,46} = 3.019$, $P < 0.01$, adjusted $R^2 = 0.285$) when including Julian day as a covariate (Table 4.1, Fig. 4.3A). In addition, when including Julian day as a covariate and controlling for experiment type (cold or heat), maximum environmental temperature was significantly negatively correlated with basal metabolic rate ($\beta = -0.02$, 95% CI = -0.03 – -0.01, $t_{90} = -2.354$, $p = 0.021$, marginal $R^2 = 0.05$, conditional $R^2 = 0.175$). Lastly, we observed extensive variation in the rate of change in evaporative water loss within each sampling region (Appendix 3 Fig. S3.2), yet maximum environmental temperatures still significantly predicted rates of change in evaporative water loss, albeit contrary to our predictions ($\beta = 0.008$, 95% CI = 0.005 – 0.010, $t_{1,51} = 6.433$, $P < 0.001$, adjusted $R^2 = 0.437$). These thermal physiology results together suggest birds in colder regions have higher basal metabolic rates, lower behavioral heat stress temperatures, and are less likely to adaptively respond with higher rates of evaporative water loss in response to increases in heat stress (Table 4.1, Fig. 4.3).

The relationship between maximum environmental temperature and morphological traits

Contour feather microstructure

To examine the relationship between feather microstructure and temperature, we analyzed 398 breast contour feathers from 82 adult males (Table 4.1). The first two principal components of a PCA of feather microstructure characteristics explained 60.2% of the variation (PC1 = 37.8%, PC2 = 22.4%; Appendix 3 Table S3.2). PC1 characterized a tradeoff between total length as driven by length of the plumulaceous section and density of barbules in the plumulaceous section (Appendix 3 Fig. S3.3). Positive values for PC1 reflect shorter feathers overall with higher barb densities in the plumulaceous sections, whereas negative values are indicative of lower barb densities in the plumulaceous section and longer total plumulaceous section lengths (Appendix 3 Table S3.2). Traits associated with the pennaceous section loaded most strongly on PC2, with positive values representing longer pennaceous sections with higher densities of both barbs and barbules (Appendix 3 Table S3.2, Appendix 3 Fig. S3.3). Evaluation of regional means suggest birds sampled from colder regions load negatively along PC1 and trend towards greater lengths with lower barb densities in the plumulaceous section (Table 4.1). However, maximum temperature did not significantly predict PC1 ($\beta = 0.10$, 95% CI = -0.02 – 0.23, $t_{80} = 1.699$, $p = 0.093$, marginal $R^2 = 0.02$, conditional $R^2 = 0.51$). In contrast, there was a significant relationship between maximum temperature and PC2 ($\beta = -0.18$, 95% CI = -0.26 – -0.11, $t_{80} = -4.734$, $P < 0.001$, marginal $R^2 = 0.11$, conditional $R^2 = 0.35$). Birds in colder, winder regions (San Miguel and Santa Rosa Islands) have more developed pennaceous sections in breast contour feathers overall (Fig. 4.4).

Crown and back plumage gray intensity

To examine the relationship between plumage darkness and temperature, we analyzed mean back and crown gray intensity values from 154 adult male island song sparrows while controlling for interannual camera adjustments (Table 4.1). Maximum temperature significantly predicted gray values for crown regions (β = -2.59, 95% CI = -4.15 – -0.72, t_{146} = -3.089, P < 0.01, marginal R^2 = 0.016, conditional R^2 = 0.389). Specifically, birds in in colder regions had higher gray values and, thus, lighter crown plumage, contrary to our predictions (Fig. 4.5A). Maximum temperature was not a significant predictor of gray values for back regions (β = -1.49, 95% CI = -3.08 – 0.24, t_{151} = -1.776, p = 0.08, marginal R^2 = 0.016, conditional R^2 = 0.389), and there was little discernable difference in the estimated mean gray values in the human visual spectrum (Fig. 4.5B).

Genome-wide association study of feather microstructure and plumage gray intensity

GWA studies of feather microstructure traits (feather PC1 and PC2) reveal a genetic basis to feather microstructure variation based on 27 phenotyped and genotyped island song sparrows (Table 4.2, Fig. 4.6). Using all 3,294 loci in permutation tests of partial RDA analyses, genotype was not significantly predicted by either $PC1_{feather}$ ($F_{1,23}$ = 1.014, p = 0.358) or $PC2_{feather}$ ($F_{1,23}$ = 0.934, p = 0.497) when controlling for geographic distance. Thus, we did not include partial RDA of feather microstructure traits. LMM removed 1,433 loci based on the inferred kinship matrix in GEMMA, resulting in 1,861 loci for GWA tests with feather microstructure. LMM with feather PC1 identified 263 candidate loci significantly associated with total feather length and barb density and length of the plumulaceous section (Fig. 4.6A). LMM with feather PC2 did not find any loci significantly associated with variation in the development of the pennaceous section (Fig. 4.6B). The 263 candidate loci were found in or within 50kb of 448 genes with 24

unique genes involved in feather development (Table 4.2). Of the 24 candidate genes, six genes directly control keratinocyte development, proliferation, and migration (*CASK*, *PPARD*, *OVOL2*, *BCL11B*, *TP63, EPB41L4B*) and several genes associated with intermediate filaments, including keratin, (*LMNB2*) and pathways known to modify feather development including Wnt (e.g., *WNT7A*, *AXIN1*), Notch (e.g, *GATA2*, *CDKN1B*), BMP (e.g., *SMAD1*), EGF (e.g, *RAB7A*), and TGF-beta receptor (*LOC100224677*).

Moreover, using 97 phenotyped and genotyped island song sparrows, we found support for a genetic basis to pigmentation in both crown and back regions when performing GWA of plumage gray intensity values with partial RDA and LMM (Table 4.3, Fig. 4.7). Permutation tests of partial RDA analyses with 3,294 loci reveal a significant relationship between genotype and both crown ($F_{1,93} = 1.828$, $P < 0.01$) and back plumage ($F_{1,93} = 2.512$, $P < 0.001$) when controlling for geographic distance. Using partial RDA, we identified 55 candidate loci associated with crown gray intensity and 36 candidate loci associated with back gray intensity, resulting in 71 unique candidate loci across both back and crown regions (Fig. 4.7 and Appendix 3 Fig. S3.4). These 71 unique, partial RDA candidate loci were found in or within 50kb of 110 genes, and seven genes were linked with plumage pigmentation pathways (Table 4.3). Although univariate GWA with LMM were more conservative, we found further evidence for a genetic basis to plumage gray intensity variation. LMM removed 1,217 loci based on the inferred kinship matrix in GEMMA, yielding 2,077 loci for GWA tests with plumage gray values. LMM identified 12 candidate loci significantly associated with crown plumage and five candidate loci significantly associated with back plumage, resulting in 15 unique candidate loci across both regions (Fig. 4.7). LMM candidate loci were in or near 17 genes, and two genes were involved in pigmentation pathways (Table 4.3, Fig. 4.7). Plumage results were congruent between GWA

methods; the two LMM candidate genes were also candidate genes in partial RDA. The combined seven unique candidate genes summed across methods and plumage regions likely modify melanin synthesis, transportation, and deposition in plumage by interacting with the melanocyte inducing transcription factor (MITF) gene (*SLC7A5;* Gaudel et al., 2020) and growth factors (*SOX9, FRK, FGFR2*; D'Mello, Finlay, Baguley, & Askarian-Amiri, 2016) and by regulating the protein tyrosine (*RNGTT*, *CD74, NTRK3*), a precursor to melanin synthesis (Chang, 2012; Li et al., 2019; Yu, Wang, Liao, & Tang, 2018).

Discussion

Adaptative evolutionary responses to climate can involve multiple interacting traits, but how these traits covary across populations exposed to different climates remains an open question. We previously found island song sparrow populations occupying different climates differed not only in bill size, but also in several genes associated with thermoregulatory traits. Here, we built upon these results by measuring a suite of physiological and morphological traits to determine whether thermoregulatory traits similarly covary with climate across the Channel Islands and coastal mainland California.

We found a significant relationship between maximum environmental temperature and phenotypic variation in several thermoregulatory traits. Specifically, with increasing maximum temperature there was a significant negative correlation with basal metabolic rate, and significant positive correlation with behavioral heat stress temperatures and the rate of change in evaporative water loss across the climate gradient (Table 4.1 and Appendix 3 Table S3.1, Fig. 4.3A-C). Maximum temperature was also a significant predictor of the development of the pennaceous section in contour feathers (PC2), with birds in colder, windier regions having higher

barb and barbule densities in the longer pennaceous sections of breast contour feathers. Conversely, we observed little variation among populations in behavioral cold stress temperatures and did not find a significant relationship between maximum temperature and the tradeoff between feather length as driven by length of the plumulaceous section and barb density in the plumulaceous section (PC1) (Table 4.1 and Appendix 3 Table S3.1, Figs. 4.3A and 4.4). We observed other patterns contrary to our predictions in plumage gray intensity, with a significant negative correlation between crown gray intensity and maximum temperature and a negative trend between back gray intensity and maximum temperatures (Table 4.1, Fig. 4.5A-B).

GWA analyses did not find a genetic basis to development of the pennaceous section, and observed differences likely represent a plastic response to selection. However, GWA on feather PC1 and on plumage gray intensity confirmed a genetic basis to variation in total length and in plumulaceous section traits of breast contour feathers and pigmentation in back and crown regions (Tables 4.2 and 4.3, Figs. 4.6 and 4.7). When coupled with previous evidence of temperature resulting in divergence in genes associated with feather development and plumage pigmentation (Gamboa, Chapter 2), these results provide strong support for climate driving evolutionary changes in feather microstructure and color. Collectively, these results suggest the climate gradient poses a strong selection pressure on thermal physiology, leading to local adaptation on a microgeographic scale.

Evidence for adaptative divergence in thermal physiology

Many physiological traits, including basal metabolic rate, tend to be conserved seasonally within endothermic species (McKechnie, 2008; McNab, 2002), and it is surprising that we found a significant relationship between climate and basal metabolic rate and behavioral heat stress temperatures given that basal metabolic rate has previously been shown to not vary along similar

environmental gradients (Londono et al., 2014). Rather than exhibiting fixed population differences in basal metabolic rate, avian populations typically demonstrate phenotypic plasticity, largely associated with seasonality, and an ability to rapidly acclimatize to different climate regimes (Cavieres & Sabat, 2008; Cooper & Swanson, 1994; Liknes & Swanson, 1996; McKechnie, 2008; Williams & Tieleman, 2000). In fact, few studies have demonstrated intraspecific divergence in these physiological responses to temperature in birds, and these studies span a broad geographic and environmental range (Tieleman et al., 2003; White et al., 2007).

The pattern of elevated metabolic rates for birds in colder region at this spatial scale is likely a product of multiple axes of environmental variation operating on thermal physiology. We focused our analyses on examining the relationship between temperature, but, importantly, birds in colder regions also experience thermal stress from increased wind speeds and reduced solar radiation owing to the common occurrence of dense fog across the island (Schoennerr et al., 2003). Indeed, high wind speeds and low irradiance are similarly correlated with elevated metabolic rates in other small passerines (Wolf & Walsberg, 1996; Wolf, Wooden, & Walsberg, 2000). The conserved responses in behavioral cold stress temperatures among regions further suggest that increased metabolic rates may be a compensatory mechanism to maintain high body temperatures when thermal limits are evolutionarily constrained.

Although cold tolerances have been shown to have higher variances among and within species and are hypothesized to be more labile than heat tolerances (Araujo et al., 2013; Bennett et al., 2021), our results demonstrate the opposite pattern. We did not observe a significant relationship between minimum environmental temperatures and behavioral cold stress temperatures, but we did find behavioral heat stress temperatures to be correlated with regional

maximum environmental temperatures. The difference between behavioral cold and heat stress temperatures (thermal stress breadth) corresponds with the range of environmental temperatures in our sampling regions (Table 4.1) and may be evidence of thermal niche conservatism (Olalla-Tárraga et al., 2011; Vetaas, Grytnes, Bhatta, & Hawkins, 2018; Wiens & Graham, 2005). Simply, narrow thermal stress breadths and elevated basal metabolic rates in on San Miguel Island may be evolved responses to selection for cold tolerance since colonization as far back as 25 – 39 kya (Guthrie, 1992). Genomic evidence for reduced gene flow and divergence in genes underlying physiology further support the hypothesis that physiological tolerances are adaptive evolutionary responses to regional thermal extremes. Our genomic sampling limited our ability to directly relate physiology phenotypes to genotypes with GWA tests to indirectly infer local adaptation (Barrett & Hoekstra, 2011), and our experimental design precluded individual estimates of the thermal stress breadths. Nevertheless, the clear pattern of covariation between environmental temperatures and physiology highlights differences in thermoregulatory capacity among song sparrow populations at remarkably small spatial scales.

Furthermore, we found substantial variation among estimates of the rate of change in evaporative water loss in island and mainland song sparrows. In general, populations in hotter environments (Santa Cruz Island and mainland California) displayed a greater capacity to lose water via panting with increasing temperatures (Appendix 3 Fig. S3.3). This is contrary to our prediction that birds in colder environments would have elevated rates of evaporative water loss in response to increasing heat as observed in empirical studies of evaporative water loss and metabolic rate in desert-dwelling and heat-adapted bird species (e.g., Marder & Bernstein, 1983; McKechnie et al., 2017; Smit et al., 2018; E. K. Smith, O'Neill, Gerson, & Wolf, 2015; Eric Krabbe Smith, O'Neill, Gerson, McKechnie, & Wolf, 2017; Talbot, Gerson, Smith, McKechnie,

& Wolf, 2018; Whitfield, Smit, McKechnie, & Wolf, 2015). Instead, we did not observe a similar increase in evaporative water loss rates in birds occupying colder environments (San Miguel and Santa Rosa Islands) despite observing behavioral signatures of heat stress at lower temperatures in these populations. Steep increases in evaporative water loss have been observed in other cold-adapted species past the upper critical limit inflection point, but evaporative water loss rates were not effective at dissipating metabolic heat gain at high temperatures in these species (O'Connor et al., 2021). The absence of a strong signature of change in evaporative water loss may be indicative of an inability to adaptively respond to increasing heat stress or novel temperatures, as San Miguel Island birds rarely experience temperatures similar to heat stress experimental temperatures (Western Regional Climate Center, 2021). Notably, we were unable to measure body temperatures continuously throughout the experiments, and, as a result, could not instantaneously assess facultative hyperthermia, which may provide insight into the biological relevance of the rate of change in evaporative water loss at test temperatures. Regardless of the factors that may explain variation in the rate of change in evaporative water loss, our analyses of thermal physiology suggest that climate may drive divergence in usually conserved traits, thereby contributing to climate adaptation among populations.

Evidence for adaptative divergence in feather microstructure and plumage gray intensity

Our results show that feather microstructure is significantly correlated with the steep climate gradient and may contribute to adaptation. Notably, birds in colder, windier, and wetter environments had longer feathers and higher barb and barbule densities in the pennaceous section. Similar patterns have been described among species, with birds in colder environments having longer feathers and higher pennaceous barb densities (Pap et al., 2016). Greater barb and barbule densities and longer feathers provide a more continuous surface that prevents wind and

water from penetrating to the skin (Rijke & Jesser, 2011; Stettenheim, 2000). The protective layer generated from the overlapping pennaceous sections of contour feathers securely traps air near the skin and increases the ability of birds in cold environments to maintain high body temperatures (Stettenheim, 2000). We did not find birds in colder environments to have higher barb or barbule densities in the plumulaceous section of the contour feather, contrary to our predictions and to other studies (Broggi et al., 2011; de Zwaan, Greenwood, & Martin, 2017; Pap et al., 2016). However, we focused only on contour feathers in one region of the body, and cold temperatures have been shown to covary with structural components of contour feathers in other regions and in downy feathers (Cheek et al., 2017; Osváth et al., 2018). These findings indicate that selection operates on multiple components of feather structure across species to aid in climate adaptation, and modifications to the pennaceous section represents just one avenue to improve heat retention in colder environments.

Complementary to observed complexity in thermal physiology responses to environmental temperatures, our analyses of plumage color also suggest multiple environmental axes likely contribute to pigmentation. Under the hypothesis that plumage darkness improves heat absorption in colder environments, we expected to observe darker pigmentation in colder regions to enable greater solar heat absorption. Yet, birds in colder, windier regions had significantly lighter crown plumage and trended towards lighter back plumage compared to birds in hotter regions. This may be additional evidence for selection operating on thermoregulatory ability given that solar heat load gains are dependent on plumage color and feather orientation (Wolf & Walsberg, 2000). Under high wind speed conditions (e.g., San Miguel Island), radiation is more likely to penetrate the surface of lighter plumages and increase solar heat gain compared to darker morphs, which may restrict heat transfer to the surface (Wolf & Walsberg, 2000).

Alternatively, darker gray intensity values corresponding with increased melanin deposition may be adaptive under high solar irradiance conditions in the context of other fitness-related functions. For example, highly melanized feathers have been shown to resist feather-degrading bacilli, and the abundance and virulence of feather-degrading bacilli is significantly correlated with melanism among song sparrow subspecies (Burtt & Ichida, 2004; Luttrell et al., 2015) and between two subspecies in the closely-related swamp sparrow (*Melospiza georgiana*). On the other hand, selection may favor individuals with darker plumage in birds occupying regions of higher solar irradiance (e.g., Santa Cruz Island) may benefit from increased UV protection (Roulin, 2014). Ultimately, solar heat gain from plumage color is likely a product of the combined effect of microstructure, color, environment, and other factors. Nonetheless, previous work which found population differences related to maximum temperature in genes known to modify melanin synthesis, transportation, and deposition including the well-described *Mc1r* gene (Gamboa, Chapter 2) may still be indicative of climate adaptation, and we cannot exclude the possibility that more thorough investigations of plumage color, patterning, and structure across the entire body may have distinct thermoregulatory implications.

Genomic-wide association studies provide support for a genetic basis to morphological variation

We confirmed that some components of variation in feather microstructure and plumage pigmentation have a partial genetic basis. Our GWA results support previous findings in this system that identified genes regulating feather development and pigmentation correlated with maximum temperature (Gamboa, Chapter 2) Similar molecular pathways control both bill and feather development (Schneider, 2005; Wu et al., 2015), and it is not surprising that we observe concerted shifts in feather and bill morphology in our system. For example, GWA with feather microstructure identified the candidate gene *Tp63*, transcription factor p63, which is involved in

odontogenesis, craniofacial development, and keratinocyte differentiation and proliferation (Candi et al., 2006; Soares & Zhou, 2018). Another candidate gene, *Wnt7a*, plays an important role in feather morphogenesis (Lin et al., 2006; Wu et al., 2015), while simultaneously interacting with bone morphogenetic protein (BMP) pathways in the development of avian bills (Wu et al., 2015; Yusuf et al., 2020). Interestingly, our analyses did not find a significant relationship between feather PC2 and genotypes, which suggests adaptive divergence in the pennaceous section of contour feathers is controlled either by regions of the genome not represented by our SNPs, by the environment, or by the interaction of unrepresented genomic regions and the environment. The environment may also regulate expression of pigmentation genes and may explain why plumage divergence did not align with allelic frequency differences in pigmentation genes linked with maximum temperature (Gamboa, Chapter 2). Still, our findings of a partial genetic basis to plumage color and feather structure provide robust, indirect evidence for microgeographic climate adaptation in multiple morphological traits that likely buffer populations when evolution on physiology is constrained.

Conclusions

Integrating knowledge of how physiology and morphology simultaneously relate to ecologically relevant environmental gradients offers a more holistic approach to assess whole-organismal responses to future environmental change. Our combined results demonstrating microgeographic adaptive divergence in thermal physiology and genetically based adaptive variation in feathers and bills allow us to infer that climate adaptation to local environments explain observed patterns of restricted gene flow from hotter to colder islands in island song sparrows (Gamboa, Chapter 2). Further, San Miguel Island birds exhibit genetically based adaptations to cold environments and a reduced capacity to tolerate high temperatures,

potentially rendering them more vulnerable to climate change. Our analyses provide one of the first examples of concerted intraspecific adaptive divergence in endotherm physiology and morphological traits involved in thermoregulation. We highlight the utility of combining genomic, morphological, and physiological data for inferring climate adaptation and understanding population vulnerability, and future studies should consider evaluating adaptation using a suite of traits to infer adaptive capacity to climate.

Tables and Figures

Table 4.1 Song sparrow thermal physiology and morphology by region. Thermal physiology traits include behavioral cold (T_{cs}) and heat (T_{hs}) stress temperatures, basal metabolic rate (BMR) and the rate of change in evaporative water loss (ΔEWL). Feather principal components (PC1 and PC2) are composite scores of microstructure in the pennaceous and plumaceous regions of male breast contour feathers. Estimated marginal means, 95% confidence intervals, and sample sizes using the top model for each response variable are based on mean regional temperatures. Top models were identified using Akaike information criterion (AIC) following Anderson & Burnham (2002) (*see* Table S1). Asterisks denote statistical significance in environmental temperature predicting phenotype in the top model. Estimates for BMR and T_{hs} are adjusted for Julian day value 114 and 124, respectively.

Variable	San Miguel Island (SMI)	Santa Rosa Island (SRI)	Santa Cruz Island (SCI)	Mainland California (MCA)
Regional Temperature Means & 95% CIs				
Maximum Temperature (ºC)	21.39 (21.27 — 21.52)	22.40 (22.36 — 22.44)	23.30 (23.17 — 23.43)	28.31 (28.14 — 28.48)
Minimum Temperature (ºC)	7.80 (7.76 — 7.84)	8.59 (8.57 — 8.62)	8.10 (7.95 — 8.25)	5.78 (5.30 — 6.27)
Thermal Physiology - Regional Estimated Marginal Means & 95% CIs				
T_{hs} (ºC)** Model: T_{hs} ~ Max T + Julian Day	32.85 (32.31 — 33.39)	33.14 (32.70 — 33.58)	33.43 (33.01 — 33.84)	34.83 (33.78 — 35.89)
n	14	11	18	6
T_{cs} (ºC) Model: T_{cs} ~ Min T	15.53 (14.96 — 16.09)	15.84 (15.15 — 16.54)	15.65 (15.15 — 16.54)	14.72 (13.50 — 15.94)
n	6	16	18	14
BMR (W)** Model: BMR ~ Max T + +Julian Day + (1| Experiment)	0.51 (0.35 — 0.69)	0.49 (0.33 — 0.66)	0.48 (0.32 — 0.64)	0.39 (0.22 — 0.55)
n	18	24	33	18

Table 4.1 (*Continued*)

Variable	San Miguel Island (SMI)	Santa Rosa Island (SRI)	Santa Cruz Island (SCI)	Mainland California (MCA)
Thermal Physiology - Regional Estimated Marginal Means & 95% CIs				
ΔEWL* ($g \cdot h^{-1} \cdot C^{-1}$)**	0.00	0.01	0.02	0.06
Model: ΔEWL ~ Max T	(0.00 — 0.01)	(0.00 — 0.02)	(0.01 — 0.03)	(0.05 — 0.07)
n	13	13	15	12
Morphology - Regional Estimated Marginal Means & 95% CIs				
Feather PC1	-0.20	-0.09	0.02	0.53
Model: PC1 ~ Max T + (1| Individual)	(-0.55 — 0.16)	(-0.38 — 0.20)	(-0.26 — 0.29)	(-0.14 — 1.20)
n	20	22	20	20
Feather PC2* **	0.35	0.17	-0.01	-0.90
Model: PC2 ~ Max T + (1| Individual)	(0.13 — 0.57)	(-0.01 — 0.35)	(-0.18 — 0.16)	(-1.31 — -0.49)
n	20	22	20	20
Crown Plumage Gray Intensity*				
Model: Crown Gray Value ~ Max T + (1 | year)	126 (122 — 129)	123 (120 — 126)	120 (117 — 124)	—
N	41	63	50	—
Back Plumage Gray Intensity				
Model: Back Gray Value ~ Max T + (1 | year)	132 (126 — 138)	131 (125 — 137)	129 (123 — 136)	—
n	41	63	50	—

Table 4.2 Candidate genes underlying feather microstructure based on genome-wide association (GWA) analyses of feather PC1 in 27 male, island song sparrows. Linear mixed modeling in GEMMA identified 263 candidate loci when controlling for relatedness among individuals. Zebra finch gene annotations are shown for 24 genes involved in feather development and aligned to or within 50kb of candidate loci. Genomic data and analyses are described in detail in Gamboa (Chapter 2).

GO Report Search Terms: keratin, keratinocyte, feather, integument, epidermal, IGFBP, BMP2, BMP4, BMP, noggin, Notch, TGF-beta, Wnt, map kinase, smad, shh, SMURF1, FGF, epidermal growth factor, hox					
Chr	**Start Position**	**End Position**	**Gene Symbol**	**Gene Name**	**Gene Annotation Pathway or Function**
1	106651639	106838780	CASK	calcium/calmodulin dependent serine protein kinase	negative regulation of keratinocyte proliferation
1A	68533572	68630838	WNK1	WNK lysine deficient protein kinase 1	positive regulation of canonical Wnt signaling pathway
1A	70043940	70047745	CDKN1B	cyclin dependent kinase inhibitor 1B	Notch signaling pathway
2	86103745	86270736	EPB41L4B	erythrocyte membrane protein band 4.1 like 4B	positive regulation of keratinocyte migration
3	80237089	80247395	DLK2	delta like non-canonical Notch ligand 2	negative regulation of Notch signaling pathway
3	90506424	90513899	OVOL2	ovo like zinc finger 2	epidermal cell differentiation, regulation of keratinocyte differentiation and proliferation
4	9170497	9315951	ZFYVE28	zinc finger FYVE-type containing 28	negative regulation of epidermal growth factor receptor signaling pathway
4	57327494	57370096	SMAD1	SMAD family member 1	BMP signaling pathway
5	49149315	49246885	BCL11B	BAF chromatin remodeling complex subunit BCL11B	keratinocyte development, regulation of keratinocyte proliferation
7	3818972	3849643	LOC100224677	TGF-beta receptor type-2-like	transmembrane receptor protein serine/threonine kinase signaling pathway, transforming growth factor beta receptor activity, type II

Table 4.2 (*Continued*)

Chr	Start Position	End Position	Gene Symbol	Gene Name	Gene Annotation Pathway or Function
7	3858270	3891565	SNX4	sorting nexin 4	epidermal growth factor receptor binding
7	10385090	10390478	DES	desmin	intermediate filament including Type II, basic keratins
8	11358247	11576747	RNF220	ring finger protein 220	positive regulation of canonical Wnt signaling pathway
9	14941008	15214563	TP63	tumor protein p63	epidermal cell differentiation, regulation of keratinocyte differentiation and proliferation, regulation of Notch signaling pathway
12	11418047	11499587	GATA2	GATA binding protein 2	negative regulation of Notch signaling pathway
12	11494988	11515510	RAB7A	RAB7A, member RAS oncogene family	epidermal growth factor catabolic process
12	19600230	19633421	WNT7A	Wnt family member 7A	Wnt signaling pathway
14	13843473	13912273	AXIN1	axin 1	Wnt signaling pathway
17	6864385	6940835	ABL1	ABL proto-oncogene 1, non-receptor tyrosine kinase	epidermal growth factor receptor signaling pathway, negative regulation of BMP signaling pathway, positive regulation of Wnt signaling pathway
23	2695374	2743281	HEYL	hes related family bHLH transcription factor with YRPW motif like	Notch signaling pathway
26	1494853	1511857	PPARD	peroxisome proliferator activated receptor delta	keratinocyte proliferation and migration
27	1997150	2005111	LOC115490720	uncharacterized LOC115490720	Notch signaling pathway
28	5480298	5518155	LMNB2	lamin B2	intermediate filament including Type II, basic keratins

Table 4.3 Candidate genes underlying plumage gray intensity in crown and back regions based on genome-wide association (GWA) analyses with 97 male, island song sparrows. Partial redundancy analyses in the R package *vegan* identified 71 candidate loci for both plumage regions. Linear mixed modeling in GEMMA identified 15 candidate loci for both plumage regions when controlling for relatedness among individuals. Zebra finch gene annotations are shown for seven unique genes involved in feather development and aligned to or within 50kb of candidate loci. Genomic data and analyses are described in detail in Gamboa (Chapter 2).

GO Report Search Terms: keratin, keratinocyte, feather, integument, epidermal, IGFBP, BMP2, BMP4, BMP, noggin, Notch, TGF-beta, Wnt, map kinase, smad, shh, SMURF1, FGF, epidermal growth factor, hox						
Chr	**Start Position**	**End Position**	**Gene Symbol**	**Gene Name**	**Gene Annotation Pathway or Function**	**Method**
3	36267216	36438261	RNGTT	RNA guanylyltransferase and 5'-phosphatase	protein tyrosine phosphatase activity	RDA (Back & Crown), LMM (Crown)
3	48307756	48355269	FRK	fyn related Src family tyrosine kinase	protein tyrosine kinase activity, regulation of epidermal growth factor	RDA (Back)
6	30361933	30441611	FGFR2	fibroblast growth factor receptor 2	protein tyrosine kinase activity	RDA (Back & Crown)
10	13898921	14100430	NTRK3	neurotrophic receptor tyrosine kinase 3	activation of MAPK activity, transmembrane receptor protein tyrosine kinase signaling pathway	RDA (Crown)
11	10387876	10431129	SLC7A5	solute carrier family 7 member 5	phenylalanine transport, interaction with MITF	RDA (Crown)
13	11827431	11832061	CD74	CD74 molecule	positive regulation of peptidyl-tyrosine phosphorylation	RDA (Crown)
18	942445	946282	SOX9	SRY-box transcription factor 9	epidermal growth factor receptor signaling pathway	RDA (Back & Crown), LMM (Back & Crown)

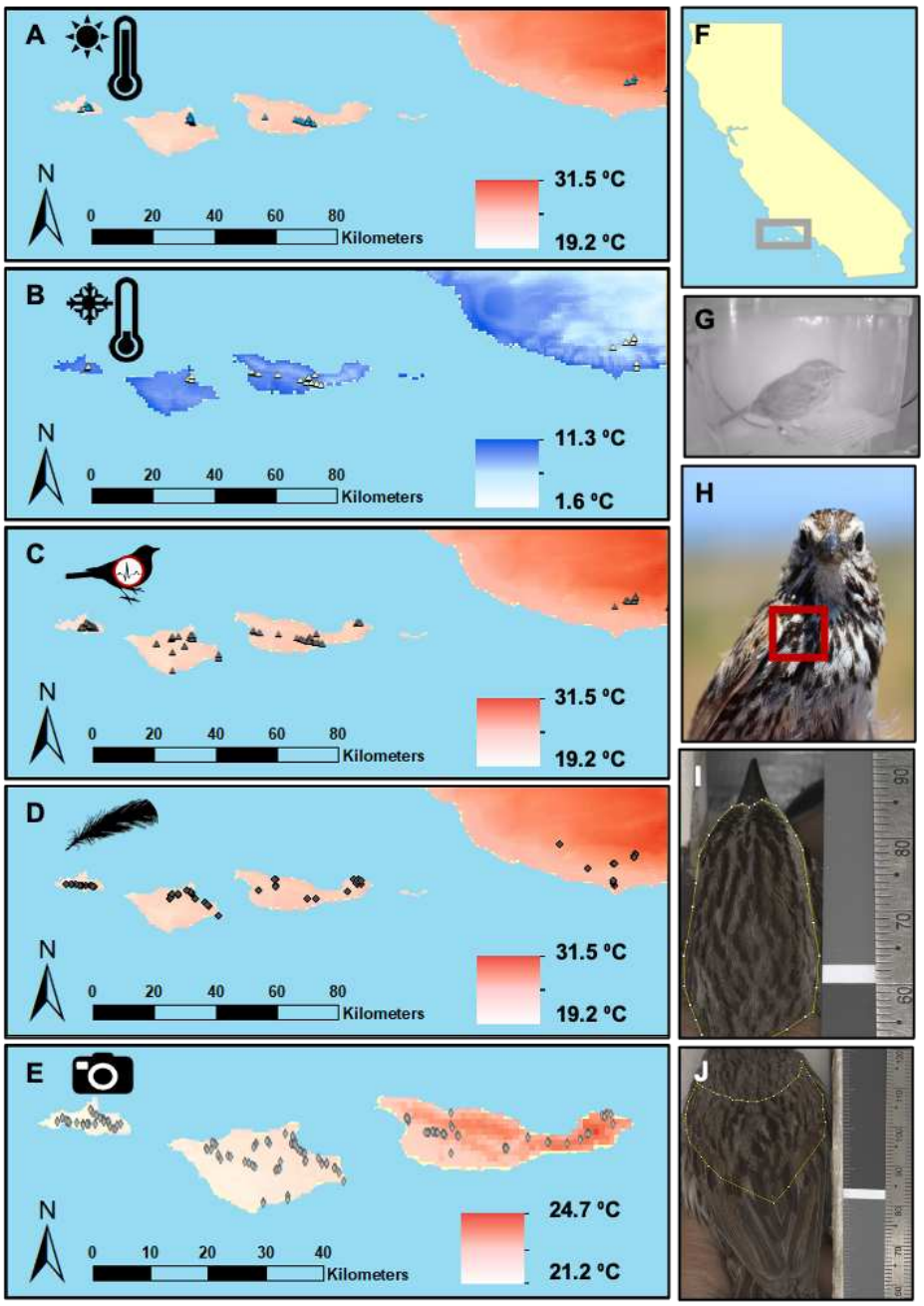

Figure 4.1 Sampling locations for comparison of song sparrow thermal physiology (A-C) and morphology (D-E), maximum (red) and minimum (blue) environmental temperatures, and location of the Channel Islands in California (F). Breeding male song sparrows for estimating ambient temperatures that elicit behavioral responses to heat (A) and cold (B) stress, and basal metabolic rate and evaporative water loss (C) were captured in 2017 and 2019 and held overnight in chambers for flow-through respirometry experiments (G). Feather microstructure analyses (D) were conducted using male breast contour feathers (H) sampled during the breeding season between 2014-2017. Plumage photographs (E) were taken to analyze gray intensity in crowns (I) and backs (J) in breeding males from 2014-2015.

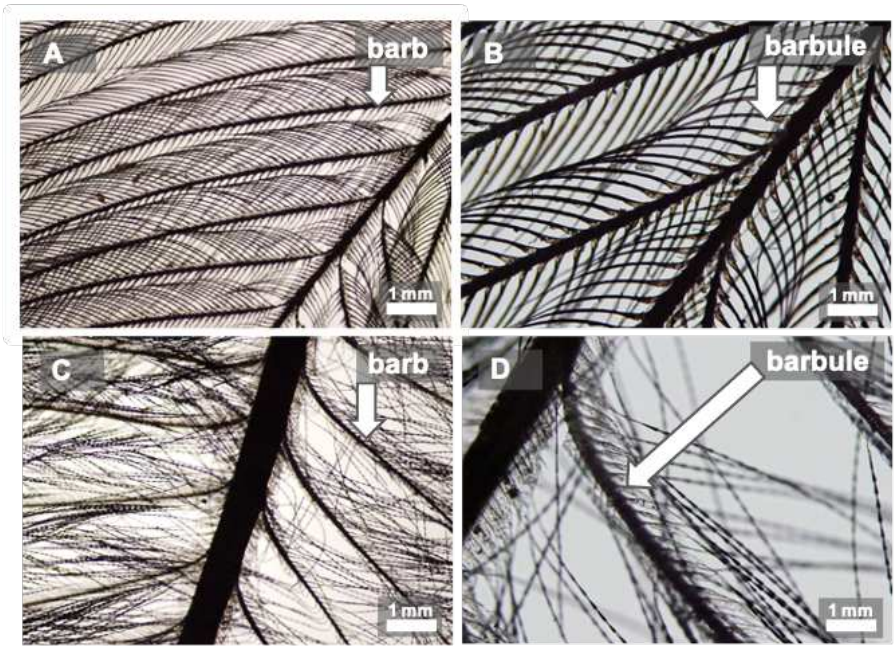

Figure 4.2 Pennaceous section barbs (A) and barbules (B) and plumulaceous section barbs (C) and barbules (D) in breast contour feathers of male song sparrows. Contour feathers were divided into plumulaceous and pennaceous sections following Pap et al. (2016).

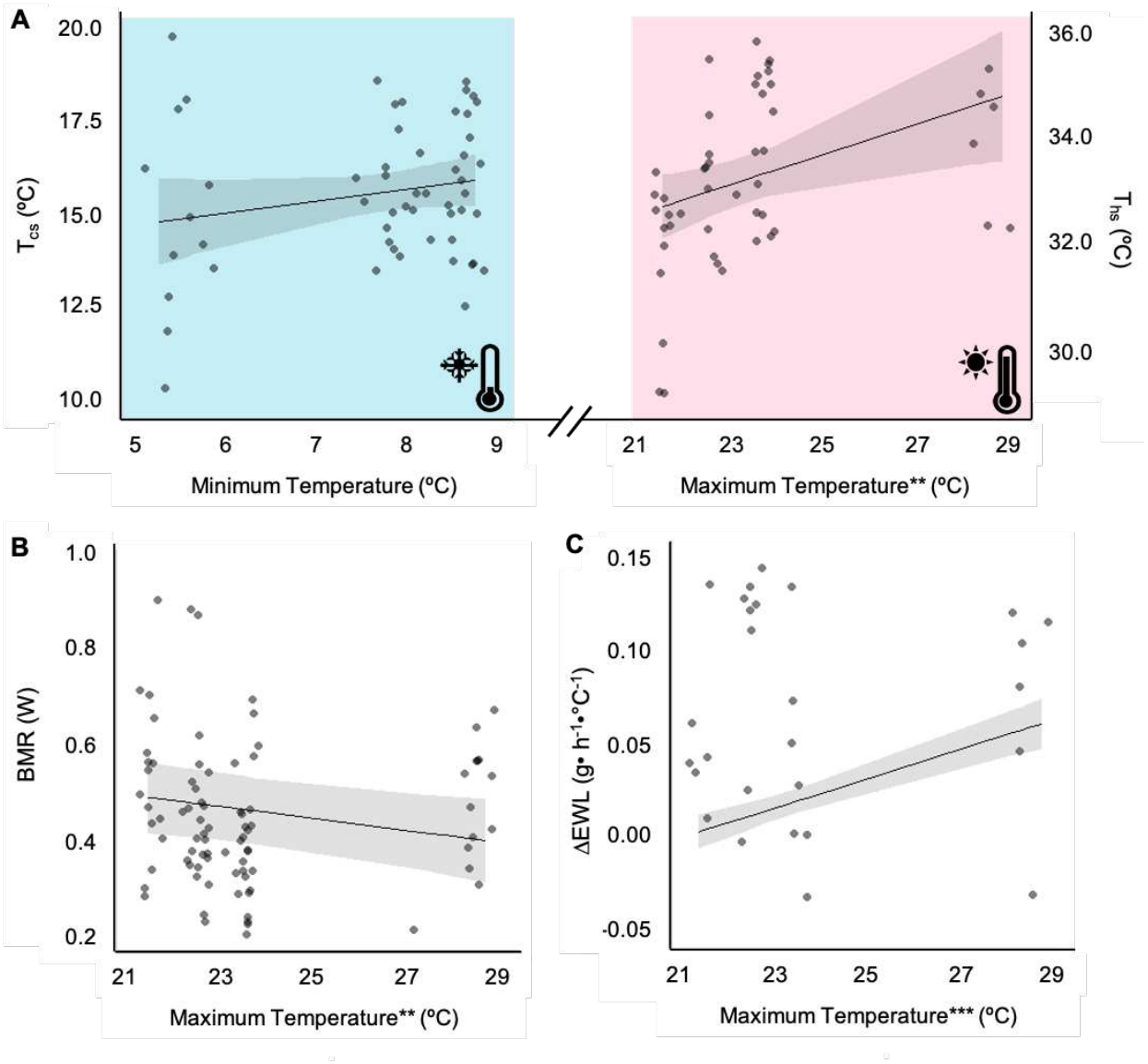

Figure 4.3 Thermal physiology as predicted by environmental temperature in island and mainland song sparrows. Thermal physiology traits include temperatures that elicit behavioral stress responses (A) to cold (T_{cs}) and heat (T_{hs}), basal metabolic rate (BMR; B), and the rate of change in evaporative water loss with respect to increasing temperatures (ΔEWL; C). Asterisks indicate a significant relationship between environmental temperatures and response variables.

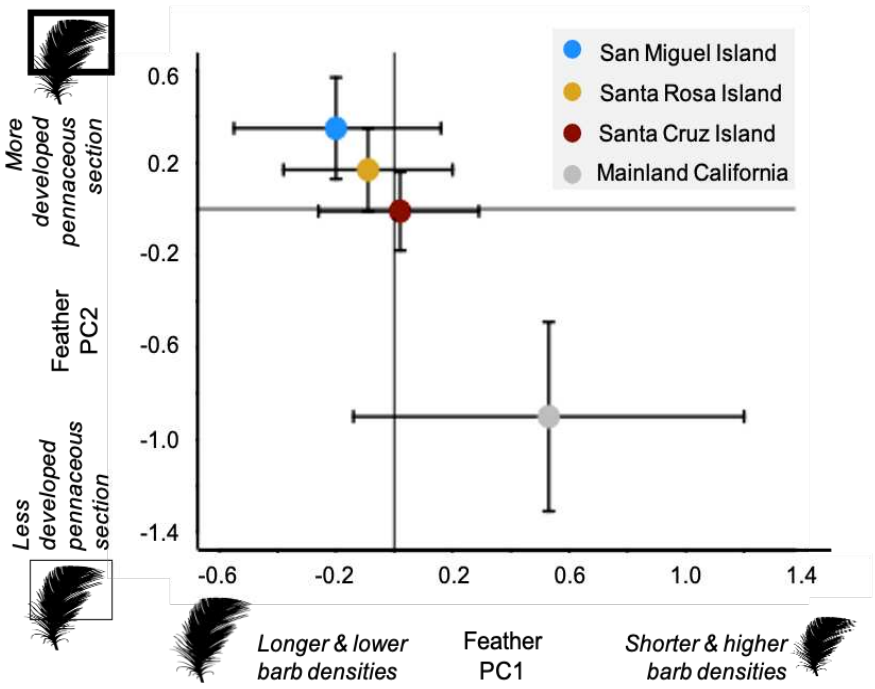

Figure 4.4 Feather PC1 and PC2 (estimated marginal means and 95% confidence intervals) as predicted by regional maximum temperatures in male song sparrows. Maximum temperature is a significant predictor of feather PC2 when controlling for individual effects.

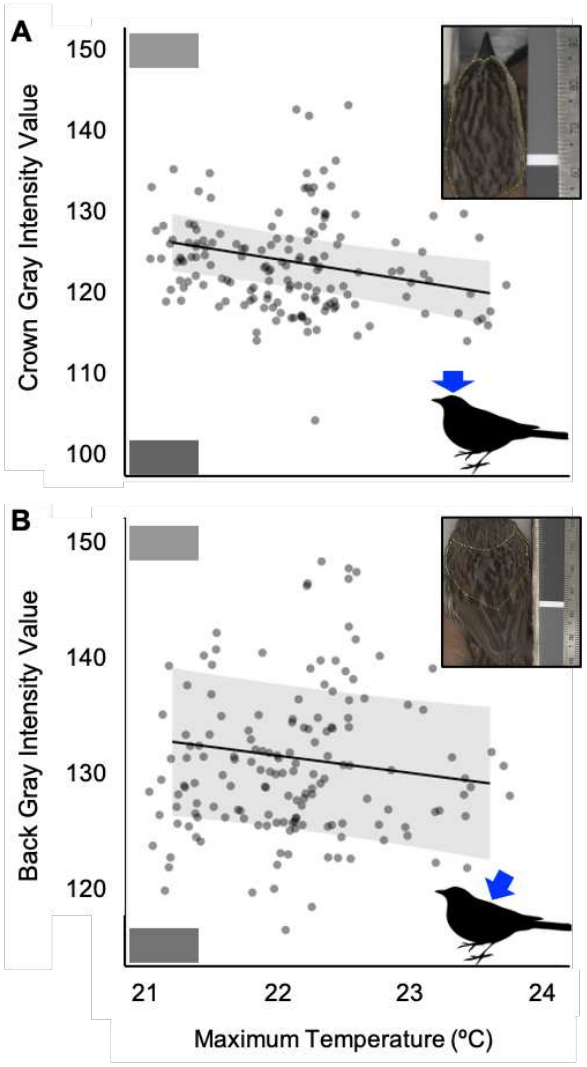

Figure 4.5 Gray intensity values [range = 0 (black), 255 (white)] averaged over male song sparrow crown (A) and back (B) regions. Maximum temperature is a significant predictor of crown gray intensity when controlling for interannual differences in ring flash settings.

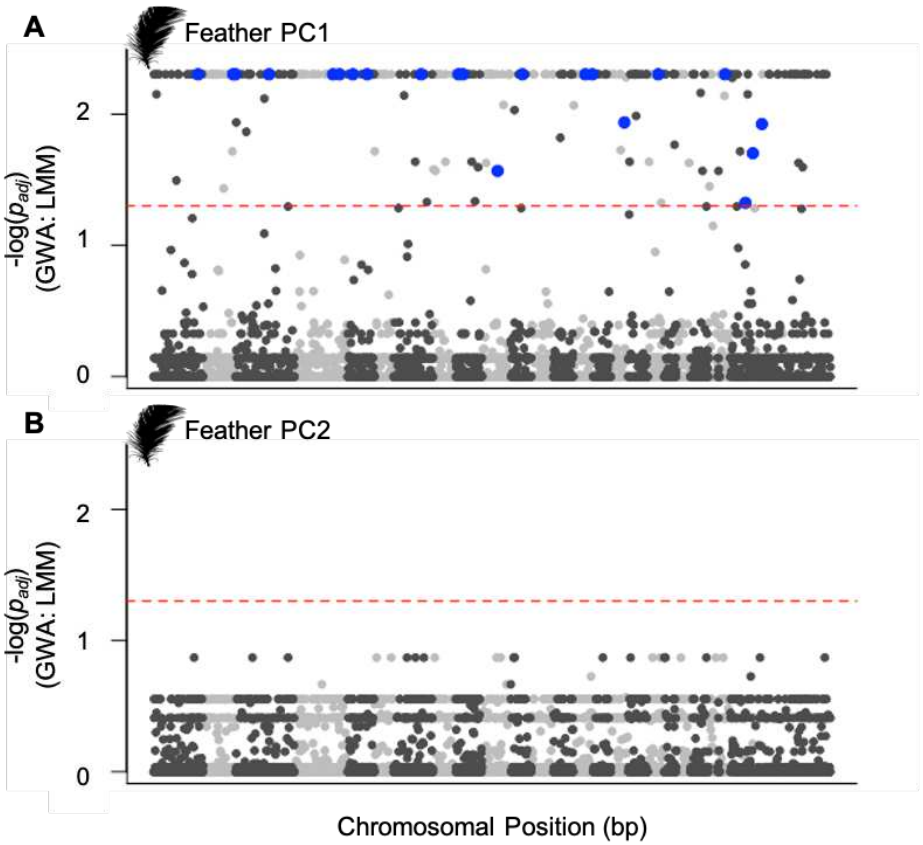

Figure 4.6 Manhattan plots of genome-wide association analyses of feather PC1 (A) and PC2 (B). Linear mixed modeling of phenotypes using 1,861 retained loci in GEMMA identify 263 candidate loci associated with feather PC1 and zero candidate loci associated with feather PC2. All candidate loci lie above the red, dotted significance threshold. Loci in genes or within 50kb of genes involved in feather development pathways are highlighted in blue.

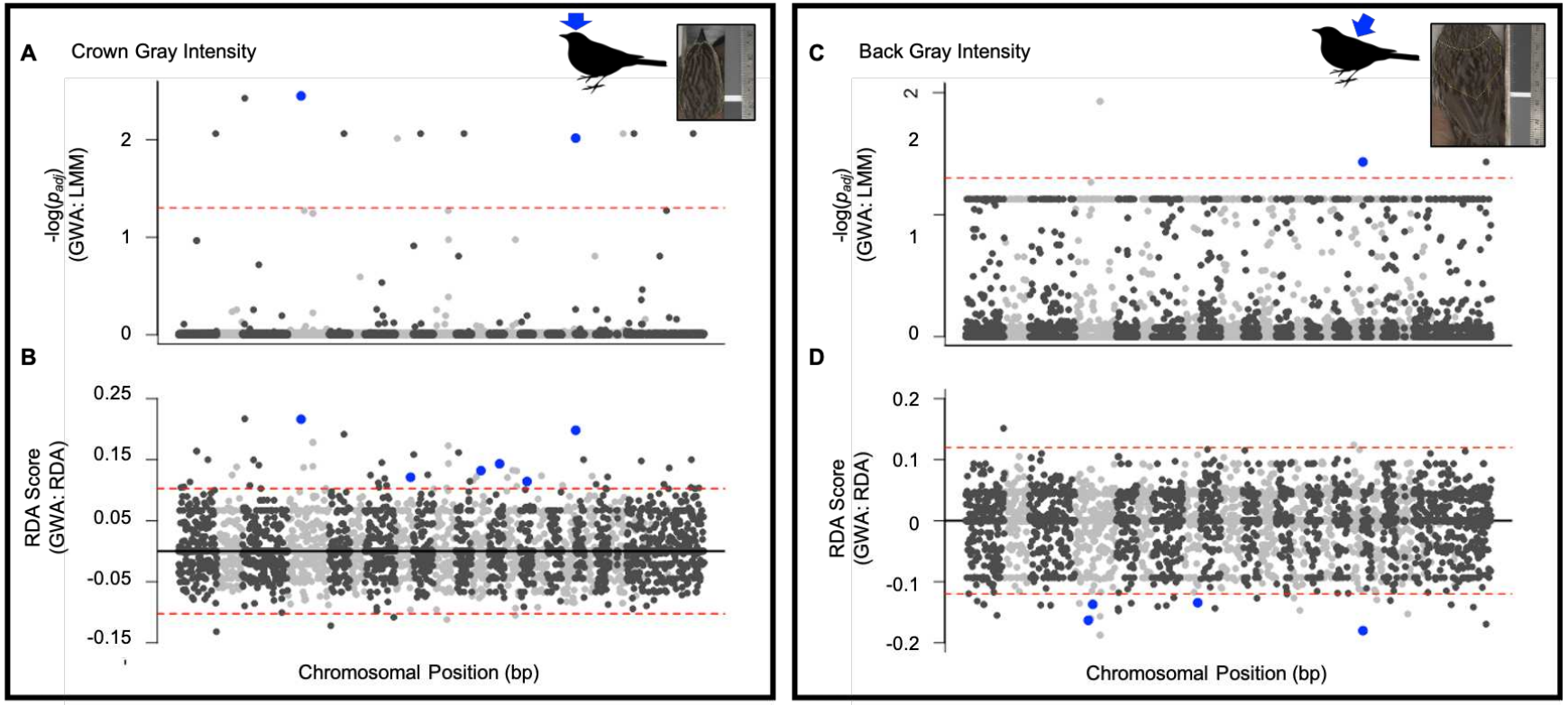

Figure 4.7 Manhattan plots of genome-wide association analyses of plumage gray intensity averaged over the crown (A, B) and back regions (C, D). Linear mixed modeling (LMM) of phenotypes using 2,077 retained loci in GEMMA identify 12 candidate loci associated with crown plumage gray intensity (A) and 5 candidate loci associated with back plumage gray intensity (C). Partial redundancy analyses (RDA) using 3,294 loci in the R package *vegan* and controlling for isolation-by-distance identify 55 candidate loci associated with crown plumage gray intensity (B) and 36 candidate loci associated with back plumage gray intensity (D). Candidate loci for LMM lie above the red, dotted significance threshold. Candidate loci for partial RDA lie above the upper red, dotted significance threshold and below the lower, dotted significance threshold. Loci in genes or within 50kb of genes involved in plumage color and melanin synthesis, transportation, and deposition are highlighted in blue.

LITERATURE CITED

Angilletta, M. J. (2009). *Thermal Adaptation*. Oxford, United Kingdom: Oxford University Press.

Angilletta, M. J., Bennett, A. F., Guderley, H., Navas, C. A., Seebacher, F., & Wilson, R. S. (2006). Coadaptation: a unifying principle in evolutionary thermal biology. *Physiological and Biochemical Zoology*, *79*(2), 282–294.

Araujo, M. B., Ferri-Yanez, F., Bozinovic, F., Marquet, P. A., Valladares, F., & Chown, S. L. (2013). Heat freezes niche evolution. *Ecology Letters*, *16*(9), 1206–1219.

Barrett, R. D. H., & Hoekstra, H. E. (2011). Molecular spandrels: tests of adaptation at the genetic level. *Nature Review Genetics*, *12*(11), 767–780.

Barve, S., Ramesh, V., Dotterer, T. M., & Dove, C. J. (2021). Elevation and body size drive convergent variation in thermo-insulative feather structure of Himalayan birds. *Ecography*, *44*, 1–10.

Bates, D., Mächler, M., Bolker, B. M., & Walker, S. C. (2015). Fitting linear mixed-effects models using lme4. *Journal of Statistical Software*, *67*(1), 1–48.

Bennett, J. M., Sunday, J., Calosi, P., Villalobos, F., Martínez, B., Molina-Venegas, R., … Olalla-Tárraga, M. Á. (2021). The evolution of critical thermal limits of life on Earth. *Nature Communications*, *12*(1), 1–9.

Bergeron, Z. T., & Fuller, R. C. (2018). Using human vision to detect variation in avian coloration: how bad is it? *American Naturalist*, *191*(2), 269–276.

Bourgeois, Y. X. C., Delahaie, B., Gautier, M., Lhuillier, E., Malé, P. G., Bertrand, J. A. M., … Thebaud, C. (2017). A novel locus on chromosome 1 underlies the evolution of a melanic plumage polymorphism in a wild songbird. *Royal Society Open Science*, *4*(160805), 1–14.

Bozinovic, F., Cavieres, G., Martel, S. I., Alruiz, J. M., Molina, A. N., Roschzttardtz, H., & Rezende, E. L. (2020). Thermal effects vary predictably across levels of organization: empirical results and theoretical basis. *Proceedings of the Royal Society B: Biological Sciences*, *287*(1938), 20202508.

Broggi, J., Gamero, A., Hohtola, E., Orell, M., & Nilsson, J. Å. (2011). Interpopulation variation in contour feather structure is environmentally determined in great tits. *PLoS One*, *6*(9), 1–5.

Brommer, J., Ahola, K., & Karstinen, T. (2005). The colour of fitness: plumage coloration and lifetime reproductive success in the tawny owl. *Proceedings of the Royal Society B: Biological Sciences*, *272*(1566), 935–940.

Burnham, K. P., & Anderson, D. R. (2002). *Model selection and multimodel inference: a practice information-theoretic approach* (2nd ed.). New York, New York: Springer Publishing.

Burton, T., Killen, S. S., Armstrong, J. D., & Metcalfe, N. B. (2011). What causes intraspecific variation in resting metabolic rate and what are its ecological consequences?. *Proceedings of the Royal Society B: Biological Sciences*, *278*(1724), 3465–3473.

Burtt, E. H., & Ichida, J. M. (2004). Gloger's rule, feather-degrading bacteria, and color variation among song sparrows. *The Condor*, *106*(3), 681–686.

Campbell-Staton, S. C., Bare, A., Losos, J. B., Edwards, S. V., & Cheviron, Z. A. (2018). Physiological and regulatory underpinnings of geographic variation in reptilian cold tolerance across a latitudinal cline. *Molecular Ecology*, *27*(9), 2243–2255.

Candi, E., Rufini, A., Terrinoni, A., Dinsdale, D., Ranalli, M., Paradisi, A., … Melino, G. (2006). Differential roles of p63 isoforms in epidermal development: selective genetic complementation in p63 null mice. *Cell Death and Differentiation*, *13*(6), 1037–1047.

Cavieres, G., & Sabat, P. (2008). Geographic variation in the response to thermal acclimation in rufous-collared sparrows: are physiological flexibility and environmental heterogeneity correlated? *Functional Ecology*, *22*(3), 509–515.

Chang, T. S. (2012). Natural melanogenesis inhibitors acting through the down-regulation of tyrosinase activity. *Materials*, *5*(9), 1661–1685.

Cheek, R. G., Alza, L., & McCracken, K. G. (2017). Down feather structure varies between low- and high-altitude torrent ducks (Merganetta armata) in the andes. *bioRxiv*, 207555.

Chen, C. F., Foley, J., Tang, P. C., Li, A., Jiang, T. X., Wu, P., … Chuong, C. M. (2015). Development, regeneration, and evolution of feathers. *Annual Review of Animal Biosciences*, *3*(1), 169–195.

Cheviron, Z. A., Whitehead, A., & Brumfield, R. T. (2008). Transcriptomic variation and plasticity in rufous-collared sparrows (Zonotrichia capensis) along an altitudinal gradient. *Molecular Ecology*, *17*(20), 4556–4569.

Chown, S. L., Gaston, K. J., & Robinson, D. (2004). Macrophysiology: large-scale patterns in physiological. *Functional Ecology*, *18*, 159–167.

Chown, S. L., & Gaston, K. J. (2016). Macrophysiology - progress and prospects. *Functional Ecology*, *30*(3), 330–344.

Chown, S. L., Hoffmann, A. A., Kristensen, T. N., Angilletta, M. J., Stenseth, N. C., & Pertoldi, C. (2010). Adapting to climate change: a perspective from evolutionary physiology. *Climate Research*, *43*(1–2), 3–15.

Clusella-Trullas, S., van Wyk, J. H., & Spotila, J. R. (2007). Thermal melanism in ectotherms. *Journal of Thermal Biology*, *32*(5), 235–245.

Cooper, S. J., & Swanson, D. L. (1994). Seasonal acclimatization of thermoregulation in the black-capped chickadee. *The Condor*, *96*(3), 638–646.

Crompton, A. W., Taylor, C. R., & Jagger, J. A. (1978). Evolution of homeothermy in mammals. *Nature*, *272*(5651), 333–336.

D'Mello, S. A. N., Finlay, G. J., Baguley, B. C., & Askarian-Amiri, M. E. (2016). Signaling pathways in melanogenesis. *International Journal of Molecular Sciences*, *17*(7), 1–18.

Danecek, P., Auton, A., Abecasis, G., Albers, C. A., Banks, E., DePristo, M. A., … Durbin, R. (2011). The variant call format and VCFtools. *Bioinformatics*, *27*(15), 2156–2158.

Dawson, W. R., Buttemer, W. A., & Carey, C. (1985). A reexamination of the metabolic response of house fnches to temperature. *The Condor*, *87*(3), 424–427.

de Zwaan, D. R., Greenwood, J. L., & Martin, K. (2017). Feather melanin and microstructure variation in dark-eyed junco Junco hyemalis across an elevational gradient in the Selkirk Mountains. *Journal of Avian Biology*, *48*(4), 552–562.

Delhey, K. (2018). Darker where cold and wet: Australian birds follow their own version of Gloger's rule. *Ecography*, *41*(4), 673–683.

Dixon, G. B., Davies, S. W., Aglyamova, G. V., Meyer, E., Bay, L. K., & Matz, M. V. (2015). Genomic determinants of coral heat tolerance across latitudes. *Science*, *348*(6242), 2014–2016.

ESRI. (2011). *ArcGIS Desktop: Release 10.7*. Redlands, California: Environmental Systems Research Institute.

Feder, M. E., Bennett, A. F., & Huey, R. B. (2000). Evolutionary physiology. *Annual Review of Ecology and Systematics*, *31*(1), 315–341.

Galván, I. (2011). Feather microstructure predicts size and colour intensity of a melanin-based plumage signal. *Journal of Avian Biology*, *42*(6), 473–479.

Galván, I., Rodríguez-Martínez, S., & Carrascal, L. M. (2018). Dark pigmentation limits thermal niche position in birds. *Functional Ecology*, *32*(6), 1531–1540.

Gaudel, C., Soysouvanh, F., Leclerc, J., Bille, K., Husser, C., Montcriol, F., … Ballotti, R. (2020). Regulation of melanogenesis by the amino acid transporter SLC7A5. *Journal of Investigative Dermatology*, *140*(11), 2253-2259.

Ghalambor, C. K., McKay, J. K., Carroll, S. P., & Reznick, D. N. (2007). Adaptive versus non-adaptive phenotypic plasticity and the potential for contemporary adaptation in new environments. *Functional Ecology*, *21*(3), 394–407.

Greenberg, R., & Danner, R. M. (2012). The influence of the California marine layer on bill size in a generalist songbird. *Evolution*, *66*(12), 3825–3835.

Guthrie, D. A. (1992). A late Pleistocene avifauna from San Miguel island, California. *Papers in Avian Paleontology Honoring Pierce Brodkorb. Natural History Museum of Los Angeles County Science Series, 36,* 319-327.

Hadfield, J. D., & Owens, I. P. F. (2006). Strong environmental determination of a carotenoid-based plumage trait is not mediated by carotenoid availability. *Journal of Evolutionary Biology*, *19*(4), 1104–1114.

Hammel, H. T. (1955). Thermal properties of fur. *The American Journal of Physiology*, *182*(2), 369–376.

Herrando-Pérez, S., Monasterio, C., Beukema, W., Gomes, V., Ferri-Yáñez, F., Vieites, D. R., … Araújo, M. B. (2020). Heat tolerance is more variable than cold tolerance across species of Iberian lizards after controlling for intraspecific variation. *Functional Ecology*, *34*(3), 631–645.

Hijmans, R. J., Cameron, S. E., Parra, J. L., Jones, P. G., & Jarvis, A. (2005). Very high resolution interpolated climate surfaces for global land areas. *International Journal of Climatology*, *25*(15), 1965–1978.

Hudson, J. W., & Kimzey, S. L. (1966). Temperature regulation and metabolic rhythms in populations of the house sparrow (Passer domesticus). *Comparative Biochemical Phsiology*, *17*, 203–217.

IEC. (2003). *61966-2-1, Amendment 1*. Geneva, Switzerland.

Karell, P., Ahola, K., Karstinen, T., Valkama, J., & Brommer, J. E. (2011). Climate change drives microevolution in a wild bird. *Nature Communications*, *2*(1), 207–208.

Kassambara, A., & Mundt, F. (2020). *factoextra: Extract and Visualize the Results of Multivariate Data Analyses*. Retrieved from https://cran.r-project.org/package=factoextra

Koskenpato, K., Ahola, K., Karstinen, T., & Karell, P. (2016). Is the denser contour feather structure in pale grey than in pheomelanic brown tawny owls Strix aluco an adaptation to cold environments? *Journal of Avian Biology*, *47*(1), 1–6.

Küpper, C., Stocks, M., Risse, J. E., Remedios, N., Farrell, L. L., Mcrae, B., … Burke, T. (2016). A supergene determines highly divergent male reproductive morphs in the ruff. *Nature Genetics*, *48*(1), 79–83.

Li, D., Wang, X., Fu, Y., Zhang, C., Cao, Y., Wang, J., … Kang, X. (2019). Transcriptome analysis of the breast muscle of Xichuan black-bone chickens under tyrosine supplementation revealed the mechanism of tyrosine-induced melanin deposition. *Frontiers in Genetics*, *10*, 457.

Liknes, E. T., & Swanson, D. L. (1996). Seasonal variation in cold tolerance, basal metabolic rate, and maximal capacity for thermogenesis in White-breasted Nuthatches Sitta carolinensis and Downy Woodpeckers Picoides pubescens, two unrelated arboreal temperate residents. *Journal of Avian Biology*, *27*(4), 279–288.

Lin, C. M., Jiang, T. X., Widelitz, R. B., & Chuong, C. M. (2006). Molecular signaling in feather morphogenesis. *Current Opinion in Cell Biology*, *18*(6), 730–741.

Londono, G. A., Chappell, M. A., Jankowski, J. E., & Robinson, S. K. (2014). Basal metabolism in tropical birds: latitude, altitude, and the 'pace of life.' *Functional Ecology*, 1–9.

Lüdecke, D. (2018). ggeffects: tidy data frames of marginal effects from regression models. *Journal of Open Source Software*, *3*(26), 772.

Lüdecke, D., Ben-Shachar, M. S., Patil, I., Waggoner, P., & Makowski, D. (2021). performance: an R package for assessment, comparison and testing of statistical models. *Journal of Open Source Software*, *6*(60), 3139.

Luttrell, S. A. M., Gonzalez, S. T., Lohr, B., & Greenberg, R. (2015). Digital photography quantifies plumage variation and salt marsh melanism among Song Sparrow (Melospiza melodia) subspecies of the San Francisco Bay. *Auk*, *132*(1), 277–287.

Marder, J., & Bernstein, R. (1983). Heat balance of the partridge Alectoris chukar exposed to moderate, high and extreme thermal stress. *Comparative Biochemistry and Physiology. A, Comparative Physiology*, *74*(1), 149–154.

Marsh, R. L., & Dawson, W. R. (1989). Avian adjustments to cold. In L. C. H. Wang (Ed.), *Animal Adaptation to Cold. Advances in Comparative and Environmental Physiology* (Vol. 4, pp. 206–254).

Mazerolle, M. J. (2020). *Model selection and multimodel inference using the AICcmodavg package.* Retrieved from https://mirror.marwan.ma/cran/web/packages/AICcmodavg/vignettes/

McKechnie, A. E. (2008). Phenotypic flexibility in basal metabolic rate and the changing view of avian physiological diversity: a review. *Journal of Comparative Physiology B, 178*(3), 235–247.

McKechnie, A. E., Gerson, A. R., McWhorter, T. J., Smith, E. K., Talbot, W. A., & Wolf, B. O. (2017). Avian thermoregulation in the heat: evaporative cooling in five Australian passerines reveals within-order biogeographic variation in heat tolerance. *Journal of Experimental Biology*, *220*(13), 2436–2444.

McKechnie, A. E., & Wolf, B. O. (2019). The physiology of heat tolerance in small endotherms. *Physiology*, *34*(5), 302–313.

McNab, B. K. (2002). *The Physiological Ecology of Vertebrates*. Ithaca, New York: Cornell Universty Press.

McNab, B. K. (2019). What determines the basal rate of metabolism?. *Journal of Experimental Biology*, *222*(15), 1–7.

Nakagawa, S., & Schielzeth, H. (2013). A general and simple method for obtaining R2 from generalized linear mixed-effects models. *Methods in Ecology and Evolution*, *4*(2), 133–142.

Ng, C. S., & Li, W. H. (2018). Genetic and molecular basis of feather diversity in birds. *Genome Biology and Evolution*, *10*(10), 2572–2586.

Noh, S., Everman, E. R., Berger, C. M., & Morgan, T. J. (2017). Seasonal variation in basal and plastic cold tolerance: adaptation is influenced by both long- and short-term phenotypic plasticity. *Ecology and Evolution*, *7*(14), 5248-5257.

O'Connor, R. S., Le Pogam, A., Young, K. G., Robitaille, F., Choy, E. S., Love, O. P., … Vézina, F. (2021). Limited heat tolerance in an Arctic passerine: thermoregulatory implications for cold-specialized birds in a rapidly warming world. *Ecology and Evolution*, *11*(4), 1609–1619.

Oksanen, J., Blanchet, F. G., Friendly, M., Kindt, R., Legendre, P., McGlinn, D., … Wagner, H. (2020). *vegan: community ecology package*. Retrieved from https://cran.r-project.org/package=vegan

Olalla-Tárraga, M. Á., Mcinnes, L., Bini, L. M., Diniz-Filho, J. A. F., Fritz, S. A., Hawkins, B. A., … Purvis, A. (2011). Climatic niche conservatism and the evolutionary dynamics in species range boundaries: global congruence across mammals and amphibians. *Journal of Biogeography*, *38*(12), 2237–2247.

Osváth, G., Daubner, T., Dyke, G., Fuisz, T. I., Nord, A., Pénzes, J., … Pap, P. L. (2018). How feathered are birds? Environment predicts both the mass and density of body feathers. *Functional Ecology*, *32*(3), 701–712.

Pap, Péter L., Osváth, G., Daubner, T., Nord, A., & Vincze, O. (2020). Down feather morphology reflects adaptation to habitat and thermal conditions across the avian phylogeny. *Evolution*, *74*(10), 2365–2376.

Pap, Peter L., Vincze, O., Wekerle, B., Daubner, T., Vagasi, C. I., Nudds, R. L., … Osvath, G. (2016). A phylogenetic comparative analysis reveals correlations between body feather structure and habitat. *Functional Ecology, 31*(6), 1241-1251.

Patten, M. A., & Pruett, C. L. (2009). The song sparrow, Melospiza melodia, as a ring species: patterns of geographic variation, a revision of subspecies, and implications for speciation. *Systematics and Biodiversity*, *7*(1), 33–62.

Pettersen, A. K., Marshall, D. J., & White, C. R. (2018). Understanding variation in metabolic rate. *Journal of Experimental Biology*, *221*(1), jeb166876.

Poelstra, J. W., Vijay, N., Bossu, C. M., Lantz, H., Ryll, B., Müller, I., … Wolf, J. B. W. (2014). The genomic landscape underlying phenotypic integrity in the face of gene flow in crows. *Science*, *344*(6190), 1410–1414.

Pörtner, H. O., Bennett, A. F., Bozinovic, F., Clarke, A., Lardies, M. A., Lucassen, M., … Stillman, J. H. (2006). Trade-offs in thermal adaptation: the need for a molecular to ecological integration. *Physiological and Biochemical Zoology*, *79*(2), 295–313.

Price, T. D. (2006). Phenotypic plasticity, sexual selection and the evolution of colour patterns. *Journal of Experimental Biology*, *209*(12), 2368–2376.

Prum, R. O., & Brush, A. H. (1976). The evolutionary origin and diversification of feathers. *The Quarterly Review of Biology*, *51*(2), 211–244.

Prum, R. O., & Dyck, J. (2003). A hierarchical model of plumage: morphology, development, and evolution. *Journal of Experimental Zoology Part B: Molecular and Developmental Evolution*, *298*(1), 73–90.

R Core Team. (2020). *R: A language and environment for statistical computing*. Retrieved from https://www.r-project.org/

RawTherapee. (2020). *RawTherapee*. Retrieved from https://www.rawtherapee.com/

Razgour, O., Forester, B., Taggart, J. B., Bekaert, M., Juste, J., Ibáñez, C., … Manel, S. (2019). Considering adaptive genetic variation in climate change vulnerability assessment reduces species range loss projections. *Proceedings of the National Academy of Sciences*, *116*(21), 10418–10423.

Reed, T. E., Schindler, D. E., & Waples, R. S. (2011). Interacting effects of phenotypic plasticity and evolution on population persistence in a changing climate. *Conservation Biology*, *25*(1), 56–63.

Rijke, A. M., & Jesser, W. A. (2011). The water penetration and repellency of feathers revisited. *Condor*, *113*(2), 245–254.

Roulin, A. (2004). The evolution, maintenance and adaptive function of genetic colour polymorphism in birds. *Biological Reviews of the Cambridge Philosophical Society*, *79*(4), 815–848.

Roulin, A. (2014). Melanin-based colour polymorphism responding to climate change. *Global Change Biology*, *20*(11), 3344–3350.

Rowland, L. A., Bal, N. C., & Periasamy, M. (2015). The role of skeletal-muscle-based thermogenic mechanisms in vertebrate endothermy. *Biological Reviews*, *90*(4), 1279–1297.

Schneider, C. A., Rasband, W. S., & Eliceiri, K. W. (2012). NIH Image to ImageJ: 25 years of image analysis. *Nature Methods*, *9*(7), 671–675.

Schneider, R. A. (2005). Developmental mechanisms facilitating the evolution of bills and quills. *Journal of Anatomy*, *207*(5), 563–573.

Schoennerr, A. A., Feldmeth, C. R., & Emerson, M. J. (2003). *The Natural History of the Islands of California*. Berkeley, California: University of California Press.

Scholander, P. F. (1955). Evolution of climatic adaptation in homeotherms. *Evolution*, *9*(1), 15-26.

Scholander, P. F., Flagg, W., Walters, V., & Irving, L. (1953). Climatic adaptation in arctic and tropical poikilotherms. *Physiological Zoology*, *26*(1), 67–92.

Scholander, P. F., Hock, R., Walters, V., & Irving, L. (1950). Adaptation to cold in Arctic and tropical mammals and birds in relation to body temperature, insulation, and basal metabolic rate. *Biological Bulletin*, *99*(2), 259–271.

Smit, B., Harding, C. T., Hockey, P. A. R., & E. McKechnie, A. (2013). Adaptive thermoregulation during summer in two populations of an arid-zone passerine. *Ecology*, *94*(5), 1142–1154.

Smit, B., Zietsman, G., Martin, R. O., Cunningham, S. J., McKechnie, A. E., & Hockey, P. A. R. (2016). Behavioural responses to heat in desert birds: implications for predicting vulnerability to climate warming. *Climate Change Responses*, *3*(1), 1–14.

Smit, B., Whitfield, M. C., Talbot, W. A., Gerson, A. R., McKechnie, A. E., & Wolf, B. O. (2018). Avian thermoregulation in the heat: phylogenetic variation among avian orders in evaporative cooling capacity and heat tolerance. *Journal of Experimental Biology*, *221*(6), jeb174870.

Smith, E. K., O'Neill, J., Gerson, A. R., & Wolf, B. O. (2015). Avian thermoregulation in the heat: resting metabolism, evaporative cooling and heat tolerance in Sonoran Desert doves and quail. *Journal of Experimental Biology*, *218*(22), 3636–3646.

Smith, Eric Krabbe, O'Neill, J. J., Gerson, A. R., McKechnie, A. E., & Wolf, B. O. (2017). Avian thermoregulation in the heat: Resting metabolism, evaporative cooling and heat tolerance in Sonoran Desert songbirds. *Journal of Experimental Biology*, *220*(18), 3290–3300.

Soares, E., & Zhou, H. (2018). Master regulatory role of p63 in epidermal development and disease. *Cellular and Molecular Life Sciences*, *75*(7), 1179–1190.

Sørensen, J. G., Dahlgaard, J., & Loeschcke, V. (2001). Genetic variation in thermal tolerance among natural populations of Drosophila buzzatii: down regulation of Hsp70 expression and variation in heat stress resistance traits. *Functional Ecology*, *15*(3), 289–296.

Stettenheim, P. R. (2000). The integumentary morphology of modern birds—an overview. *American Zoologist*, *40*(4), 461–477.

Stuart-Fox, D., Newton, E., & Clusella-Trullas, S. (2017). Thermal consequences of colour and near-infrared reflectance. *Philosophical Transactions of the Royal Society B: Biological Sciences*, *372*(1724), 20160345.

Stuart-Fox, D., Newton, E., Mulder, R. A., D'Alba, L., Shawkey, M. D., & Igic, B. (2018). The microstructure of white feathers predicts their visible and near-infrared reflectance properties. *PLoS One*, *13*(7), e0199129.

Swanson, D. L. (2010). Seasonal metabolic variation in birds: functional and mechanistic correlates. In C. F. Thompson (Ed.), *Current Ornithology* (Vol. 17, pp. 75–129).

Talbot, W. A., Gerson, A. R., Smith, E. K., McKechnie, A. E., & Wolf, B. O. (2018). Avian thermoregulation in the heat: metabolism, evaporative cooling and gular flutter in two small owls. *Journal of Experimental Biology*, *221*(12), jeb171108.

Tattersall, G. J., Arnaout, B., & Symonds, M. R. E. (2016). The evolution of the avian bill as a thermoregulatory organ. *Biological Reviews*, *92*(3), 1630-1656.

Tattersall, G. J., Sinclair, B. J., Withers, P. C., Fields, P. A., & Seebacher, F. (2012). Coping with thermal challenges: physiological adaptations to environmental temperatures. *Comprehensive Physiology*, *2*(3), 2151–2202.

Tieleman, B. I., Williams, J. B., & Buschur, M. E. (2002). Physiological adjustments to arid and mesic environments in larks (Alaudidae). *Physiological and Biochemical Zoology*, *75*(3), 305–313.

Tieleman, B. I., Williams, J. B., Buschur, M. E., & Brown, C. R. (2003). Phenotypic variation of larks along an aridity gradient: are desert birds more flexible?. *Ecology*, *84*(7), 1800–1815.

Troscianko, J., & Stevens, M. (2015). Image calibration and analysis toolbox - a free software suite for objectively measuring reflectance, colour and pattern. *Methods in Ecology and Evolution*, *6*(11), 1320–1331.

Uy, J. A. C., Cooper, E. A., Cutie, S., Concannon, R., Poelstra, J. W., Moyle, R. G., & Filardi, C. E. (2016). Mutations in different pigmentation genes are associated with parallel melanism in island flycatchers. *Proceedings of the Royal Society B: Biological Sciences*, *283*(1834), 20160731.

Vetaas, O. R., Grytnes, J. A., Bhatta, K. P., & Hawkins, B. A. (2018). An intercontinental comparison of niche conservatism along a temperature gradient. *Journal of Biogeography*, *45*(5), 1104–1113.

Vezina, F., & Williams, T. D. (2002). Metabolic costs of egg production in the european starling (Sturnus vulgaris). *Physiological and Biochemical Zoology*, *75*(4), 377–385.

Vézina, F., & Williams, T. D. (2003). Plasticity in body composition in breeding birds: what drives the metabolic costs of egg? *Physiological and Biochemical Zoology*, *76*(5), 716–730.

Weathers, W. W. (1981). Physiological thermoregulation in heat-stressed birds: consequences of body size. *Physiological Zoology*, *54*(3), 345–361.

Western Regional Climate Center. (2021). Channel Island National Park Stations: RAWS/NDBC Buoy/Manual Ranger Stations. Retrieved from https://wrcc.dri.edu/channel_isl/

White, C. R., Blackburn, T. M., Martin, G. R., & Butler, P. J. (2007). Basal metabolic rate of birds is associated with habitat temperature and precipitation, not primary productivity. *Proceedings of the Royal Society B: Biological Sciences, 274*(1607), 287–293.

Whitfield, M. C., Smit, B., McKechnie, A. E., & Wolf, B. O. (2015). Avian thermoregulation in the heat: scaling of heat tolerance and evaporative cooling capacity in three southern African arid-zone passerines. *Journal of Experimental Biology*, *218*(11), 1705–1714.

Wiens, J. J., & Graham, C. H. (2005). Niche conservatism: integrating evolution, ecology, and conservation biology. *Annual Review of Ecology, Evolution, and Systematics*, *36*, 519–539.

Williams, J. B., & Tieleman, B. I. (2000). Flexibility in basal metabolic rate and evaporative water loss among hoopoe larks exposed to different environmental temperatures. *Journal of Experimental Biology*, *203*(20), 3153–3159.

Wolf, B. O., & Walsberg, G. E. (1996). Thermal effects of radiation and wind on a small bird and implications for microsite selection. *Ecology*, *77*(7), 2228–2236.

Wolf, B. O., & Walsberg, G. E. (2000). The role of the plumage in heat transfer processes of birds. *American Zoologist*, *40*(4), 575–584.

Wolf, B. O., Wooden, K. M., & Walsberg, G. E. (2000). Effects of complex radiative and convective environments on the thermal biology of the white-crowned sparrow (Zonotrichia leucophrys gambelii). *Journal of Experimental Biology*, *203*(4), 803–811.

Wu, P., Ng, C. S., Yan, J., Lai, Y. C., Chen, C. K., Lai, Y. T., … Chuong, C. M. (2015). Topographical mapping of α-and β-keratins on developing chicken skin integuments: functional interaction and evolutionary perspectives. *Proceedings of the National Academy of Sciences*, *112*(49), E6770–E6779.

Wylie, L. M., Robertson, G. W., MacLeod, M. G., & Hocking, P. M. (2001). Effects of ambient temperature and restricted feeding on the growth of feathers in growing turkeys. *British Poultry Science*, *42*(4), 449–455.

Yu, S., Wang, G., Liao, J., & Tang, M. (2018). Transcriptome profile analysis identifies candidate genes for the melanin pigmentation of breast muscle in Muchuan black-boned chicken. *Poultry Science*, *97*(10), 3446–3455.

Yusuf, L., Heatley, M., Palmer, J. P. G., Barton, H. J., Cooney, C. R., & Gossmann, T. I. (2020). Non-coding rather than coding regions underpin avian bill shape diversification at macroevolutionary scales. *Genome Research*, *30*(4), 553-565.

Zhou, X., & Stephens, M. (2012). Genome-wide efficient mixed-model analysis for association studies. *Nature Genetics*, *44*(7), 821–824.

APPENDIX 1

Table S1.1 Vegetation presence (x) within song sparrow territories on three California Channel Islands [San Miguel Island (n = 58), Santa Rosa Island (n = 112), and Santa Cruz Island (n = 183)].

Scientific name	Common name	San Miguel	Santa Rosa	Santa Cruz
Ferns & Fern Allies				
Equisetaceae sp.	scouring rush		x	x
Unknown	unidentified ferns	x	x	x
Conifers				
Pinus muricata forma muricata	Bishop pine		x	x
Pinus torreyana s. insularis	Santa Rosa Island Torrey Pine		x	
Dicotyledonous Flowering Plants				
Aizoaceae	**Iceplant Family**			
Carpobrotus sp.	pigface	x	x	x
Mesembryanthemum	iceplant	x	x	x
Anacardiaceae	**Sumac Family**			
Rhus integrifolia	lemonade berry	x	x	x
Rhus ovata	sugar bush			x
Toxicodendron diversilobum	Pacific poison oak	x	x	x
Apiaceae	**Celery or Carrot Family**			
Foeniculum vulgare	sweet fennel		x	x
Daucus pusillus	rattlesnake weed	x	x	x
Asteraceae	**Sunflower Family**			
Achillea millefolium	common yarrow	x	x	x
Artemisia californica	coastal sagebrush	x	x	x
Aster sp.	aster		x	x
Baccharis pilularis s. consanguinea	coyote brush	x	x	x
Baccharis salicifolia	mulefat	x	x	x

Table S1.1 (*Continued*)

Scientific name	Common name	San Miguel	Santa Rosa	Santa Cruz
Dicotyledonous Flowering Plants				
Cirsium sp.	thistle	x	x	x
Coreopsis gigantean	giant coreopsis	x	x	x
Eriophyllum confertiflorum v. *confertiflorum*	golden yarrow	x	x	x
Isocoma sp.	coastal goldenbush	x	x	x
Malacothrix sp.	dandelions	x	x	x
Brassicaceae	**Mustard Family**			
Brassica rapa	field mustard	x	x	x
Cactaceae	**Cactus Family**			
Opuntia sp.	prickly pear	x	x	x
Caryophyllaceae	**Pink Family**			
Silene sp.	pink	x	x	x
Chenopodiaceae	**Goosefoot Family**			
Atriplex sp.	saltbush	x	x	x
Chenopodium	goosefoot	x	x	x
Convolvulaceae	**Morning Glory Family**			
Calystegia macrostegia	Northern island	x	x	x
s. *macrostegia*	morning glory			
Crassulaceae	**Stonecrop Family**			
Dudleya sp.	dudleya	x	x	x
Fabaceae	**Pea Family**			
Astragalus sp.	locoweed	x	x	x
Lathyrus vestitus v. *vestitus*	wild sweet pea		x	x
Lotus sp.	deerweed, lotus	x	x	x
Lupinus sp.	lupine	x	x	x
Trifolium sp.	clover	x	x	x
Vicia sp.	vetch	x	x	x

Table S1.1 (*Continued*)

Scientific name	Common name	San Miguel	Santa Rosa	Santa Cruz
Dicotyledonous Flowering Plants				
Fagaceae	**Oak Family**			
Quercus sp.	oak			x
Myrtaceae	**Myrtle Family**			
Eucalyptus sp.	gum			x
Nyctaginaceae	**Four-o'-clock Family**			
Abronia sp.	sand-verbena	x	x	x
Onagraceae	**Evening Primrose Family**			
Camissonia sp.	primrose	x	x	x
Clarkia sp.	misc. flowering plants	x	x	x
Epilobium sp.	fuchsia	x	x	x
Papaveraceae	**Poppy Family**			
Eschscholzia californica	California poppy	x	x	x
Unknown	unidentified poppies	x	x	x
Polygonaceae	**Buckwheat Family**			
Eriogonum sp.	buckwheat	x	x	x
Rumex sp.	dock	x	x	x
Portulacaceae	**Purslane Family**			
Calandrinia sp.	misc. flowering plants	x	x	x
Claytonia sp.	Miner's lettuce	x	x	x
Primulaceae	**Primrose Family**			
Dodecatheon clevelandii	shooting star	x		
Ranunculaceae	**Buttercup Family**			
Ranunculus californicus	California buttercup	x	x	x
Rhamnaceae	**Buckthorn Family**			
Ceanothus arboreus	island ceanothus		x	x
Ceanothus megacarpus	big-pod ceanothus		x	x
Rhamnus californica	coffee berry			

Table S1.1 (*Continued*)

Scientific name	Common name	San Miguel	Santa Rosa	Santa Cruz
Dicotyledonous Flowering Plants				
Rhamnaceae (*continued*)	**Buckthorn Family** (*continued*)			
Rhamnus pirifolia	island redberry			x
Rosaceae	**Rose Family**			
Adenostoma fasciculatum	chamise		x	x
Heteromeles arbutifolia	toyon	x	x	x
Prunus ilicifolia s. lyonii	island cherry		x	x
Rosa californica	California wild rose			x
Salicaeae	**Willow Family**			
Populus sp.	cottonwood		x	x
Salix sp.	willow	x	x	x
Scrophulariaceae	**Figwort Family**			
Castilleja sp.	paintbrush	x	x	x
Castilleja sp.	clover	x	x	x
Mimulus sp.	monkeyflower		x	x
Solanaceae	**Nightshade Family**			
Lycium sp.	boxthorn	x	x	x
Verbenaceae	**Vervain Family**			
Verbena lasiostachys	verbena	x	x	x
Monocotyledonous Flowering Plants				
Alliaceae	**Onion Family**			
Allium praecox	early onion	x	x	x
Dichelostemma capitatum	blue dicks	x	x	x
Cyperaceae	**Sedge Family**			
Carex sp.	sedge		x	x
Iridaceae	**Iris Family**			
Sisyrinchium bellum	blue-eyed grass	x	x	x

Table S1.1 (*Continued*)

Scientific name	Common name	San Miguel	Santa Rosa	Santa Cruz
Monocotyledonous Flowering Plants				
Juncaceae	**Rush Family**			
Juncus sp.	rush	x	x	x
Liliaceae	**Lily Family**			
Calochortus albus	fairy lanterns		x	x
Zigadenus fremontii	death-camas	x	x	x
Poaceae	**Grass Family**			
Achnatherum diegonense	San Diego needlegrass	x	x	x
Avena sp.	oats	x	x	x
Bromus sp.	brome	x	x	x
Hordeum sp.	barley	x	x	x
Hordeum murinum	foxtail	x	x	x
Nassella pulchra	purple needlegrass	x	x	x
Polypogon monspeliensis	rabbitsfoot grass	x	x	x
Vulpia sp.	fescue	x	x	x
Typhaceae	**Cattail Family**			
Typha sp.	cattail		x	x

Figure S1.1. Experimental chambers for in-situ foraging efficiency trials conducted on song sparrows from San Miguel and Santa Cruz Islands during the breeding season (Feb-June) in 2014. Trial cages (44.5 cm x 22.2 cm x 26.7 cm) were equipped with two perches at different heights and absorbent material to collect excess fecal matter and minimize stress. We provided a plastic, visual block on one of the four sides of each cage to protect subjects from potential predators and extreme weather conditions which may influence stress and willingness to forage (Clinchy, Sheriff, & Zanette, 2013; Lima & Dill, 1990). We secured a translucent cloth on three of the remaining four sides to allow for light to enter thereby stimulating activity. The plastic shield contained a hole fitted to the lens of high definition Sanyo Dual Camera Xacti WH1 camcorders (Sanyo Model VPC-WH1YL), which were mounted on the outer side of the shield on flexible tripods.

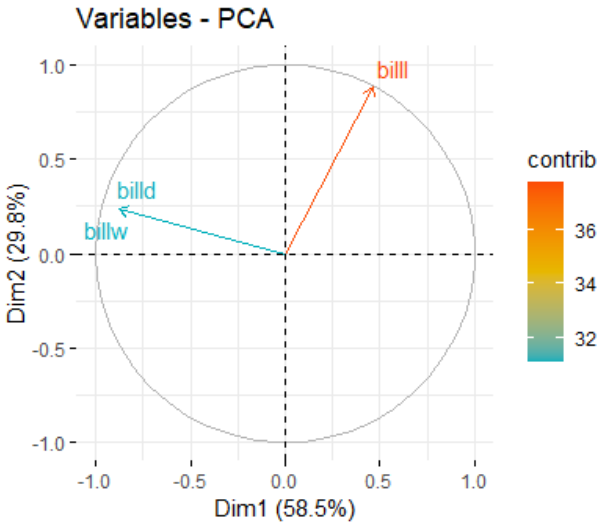

Figure S1.2. Variable loadings of principal component analyses (PCA) of bill dimensions [depth (billd), length (billl), and width (billw)] for analyses of foraging efficiency. PCA was conducted on bill dimensions in 33 individuals (San Miguel Island, $n = 10$; Santa Cruz Island, $n = 23$) to generate a composite score of overall bill morphology. Bill depth and width loaded equally (44%), and bill length did not strongly load on PC1 (12%).

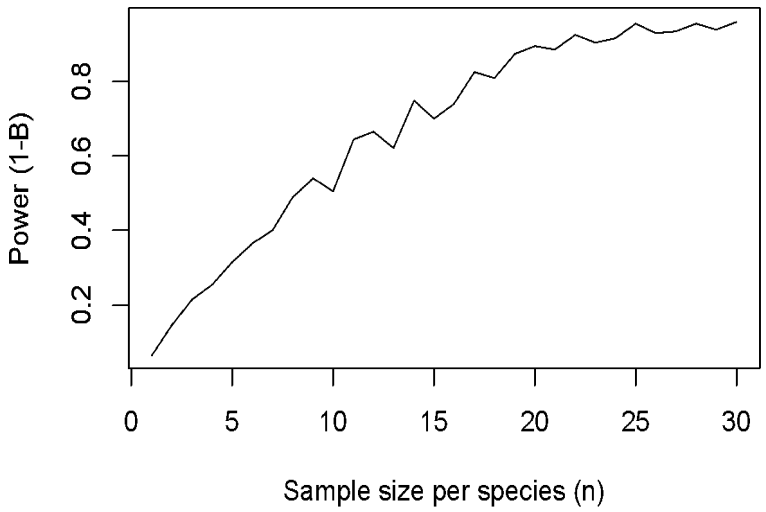

Figure S1.3. Results from power analyses for bite force. We performed power analyses to test if sample sizes were sufficient to detect biologically relevant differences between paired populations. We predicted biologically relevant differences in bite force would be 1.5 Newtons. We simulated data based on our means and variances measured in this study and then compared the model fit following Bolker (2009).

APPENDIX 2

Table S2.1 We submitted 6 lanes of 534 total individuals from 2015-2018 to the University of Oregon Genomics & Cell Characterization Core Facility for single-end 100bp RAD sequencing.

			Individuals by Population					
Submission No.	Year Sequenced	Total Individuals	San Miguel Island	Santa Rosa Island	Santa Cruz Island	Anacapa Islands	Mainland California	Illumina Platform
1	2015	96	22	24	49	0	0	HiSeq 2500
2	2015	95	3	12	80	0	0	HiSeq 2500
3	2015	94	0	0	94	0	0	HiSeq 2500
4	2016	93	62	31	0	0	0	HiSeq 2500
5	2016	92	0	65	27	0	0	HiSeq 2500
6	2018	65	0	0	0	11	54	HiSeq 4000

Table S2.2 We submitted 6 lanes of 534 total individuals from 2015-2018 to the University of Oregon Genomics & Cell Characterization Core Facility for single-end 100bp RAD sequencing.

PARAMETER TEST	PARAMETER SETTINGS				LOCI	
	m	*M*	*n* calculation	*n*	Identified	Polymorphic
m	3	2	M-1	1	115605	84995
	4	2	M-1	1	110886	80996
	5	2	M-1	1	106529	77138
	6	2	M-1	1	102461	73367
	7	2	M-1	1	98507	69606
M & *n*	3	2	M	2	275419	86000
	3	3	M	3	260804	85821
	3	4	M	4	252691	85591
	3	5	M	5	247453	85294
	3	6	M	6	243519	85094
	3	7	M	7	240587	84909
	3	8	M	8	238313	84800
	3	2	M-1	1	293318	84995
	3	3	M-1	2	268750	85552
	3	4	M-1	3	257591	85440
	3	5	M-1	4	250689	85274
	3	6	M-1	5	246101	85056
	3	7	M-1	6	242561	84923
	3	8	M-1	7	240106	84785
	3	2	M+1	3	263754	86404
	3	3	M+1	4	254553	85943
	3	4	M+1	5	248664	85610
	3	5	M+1	6	244248	85323
	3	6	M+1	7	241178	85082
	3	7	M+1	8	238406	84908
	3	8	M+1	9	236439	84783

Table S2.3 We submitted 6 lanes of 534 total individuals from 2015-2018 to the University of Oregon Genomics & Cell Characterization Core Facility for single-end 100bp RAD sequencing.

Chr	Start Position	End Position	Gene Symbol	Gene Name	Pathway or Function	Method
Genes inferred to bill morphology (GO terms: calmodulin, BMP, FGF, Wnt, transforming growth factor beta, MAP kinase, odontogenesis, neural crest, mesoderm, Notch, epidermal growth factor, SMAD, face morphogenesis)						
1	19181675	19220708	C2CD3	C2 domain containing 3 centriole elongation regulator	neural tube development	LFMM
1	24343584	24395367	FSTL1	follistatin like 1	endothelial cell differentiation	LFMM
1	28919801	28998098	MYO7A	myosin VIIA	calmodulin binding	RDA.BILL
1	36667352	36878619	MAML2	mastermind like transcriptional coactivator 2	Notch signaling pathway	LFMM
1	90906381	90925298	MXRA5	matrix remodeling associated 5	response to TGF-beta	PCAdapt, LFMM
1	106142036	106201259	BCOR	BCL6 corepressor	odontogenesis	RDA.MAXT
1	106651639	106838780	CASK	calcium/calmodulin dependent serine protein kinase	protein kinase activity	PCAdapt, LFMM
1A	7417734	7581993	SEMA3A	semaphorin 3A	neural crest formation; neural crest cell development	RDA.MAXT
1A	12898301	12940494	LAMB1	laminin subunit beta 1	odontogenesis	PCAdapt, LFMM
1A	48103977	48126457	PDGFB	platelet derived growth factor subunit B	MAPK cascade	LFMM
1A	48500857	48511352	SOX10	SRY-box transcription factor 10	Wnt signaling pathway; neural crest cell migration	LFMM
1A	48574516	48575280	LOC100217677	noggin-like	BMP signaling pathway	LFMM
1A	66674234	66896528	CALD1	caldesmon 1	calmodulin binding	LFMM
1A	68533572	68630838	WNK1	WNK lysine deficient protein kinase 1	Wnt signaling pathway	PCAdapt

Table S2.3 (*Continued*)

Chr	Start Position	End Position	Gene Symbol	Gene Name	Pathway or Function	Method
1A	70043940	70047745	CDKN1B	cyclin dependent kinase inhibitor 1B	Notch signaling pathway	LFMM
2	15686987	15747799	JCAD	junctional cadherin 5 associated	MAPK cascade	PCAdapt, LFMM
2	62418377	62522689	DUSP22	dual specificity phosphatase 22	response to EGF	RDA.MAXT
2	91035172	91122420	INVS	inversin	Wnt signaling pathway	LFMM
2	98805073	98831919	PTPN2	protein tyrosine phosphatase non-receptor type 2	epidermal growth factor receptor signaling pathway	PCAdapt
2	146942242	147130977	PTK2	protein tyrosine kinase 2	TGF-beta signaling pathway	PCAdapt, RDA.MAXT
2	149825825	150085622	ZC3H3	zinc finger CCCH-type containing 3	SMAD binding	LFMM
3	4051431	4079620	GATA4	GATA binding protein 4	SMAD binding	LFMM
3	5015010	5047670	TFAP2B	transcription factor AP-2 beta	BMP signaling pathway; SMAD binding and protein signal transduction	LFMM
3	37144546	37192208	MAP3K7	mitogen-activated protein kinase kinase kinase 7	regulation of MAPK activity	PCAdapt, LFMM
3	46361137	45076609	FYN	FYN proto-oncogene, Src family tyrosine kinase	cellular response to TGF-beta stimulus	PCAdapt
3	53328140	53703123	PTPRK	protein tyrosine phosphatase receptor type K	TGF-beta receptor signaling pathway	PCAdapt, LFMM
3	80237089	80247395	DLK2	delta like non-canonical Notch ligand 2	Notch signaling pathway	PCAdapt, LFMM
3	85382230	85389608	BCL2L11	BCL2 like 11	odontogenesis of dentin-containing tooth	PCAdapt
3	85590929	85731127	SPTBN1	spectrin beta, non-erythrocytic 1	regulation of SMAD protein signal transduction	PCAdapt, LFMM
3	85931008	85996239	CCDC88A	coiled-coil domain containing 88A	epidermal growth factor receptor binding and signaling pathway	PCAdapt, LFMM

Table S2.3 (*Continued*)

Chr	Start Position	End Position	Gene Symbol	Gene Name	Pathway or Function	Method
3	86062569	86127974	EFEMP1	EGF containing fibulin extracellular matrix protein 1	epidermal growth factor receptor signaling pathway	PCAdapt, LFMM
3	88314656	88320170	BMP2	bone morphogenetic protein 2	BMP signaling pathway; odontogenesis of dentin-containing tooth; SMAD binding and signal transduction; MAPK cascade; Wnt signaling pathway	LFMM
3	90506424	90513899	OVOL2	ovo like zinc finger 2	regulation of SMAD protein signal transduction; neural crest cell migration; cellular response to TGF-beta stimulus	PCAdapt, LFMM
3	95141087	95205172	ITPKB	inositol-trisphosphate 3-kinase B	MAPK cascade	LFMM
3	97175747	97391280	CAMKMT	calmodulin-lysine N-methyltransferase	calmodulin-lysine N-methyltransferase activity	LFMM
4	9170497	9315951	ZFYVE28	zinc finger FYVE-type containing 28	regulation of epidermal growth factor-activated receptor activity	PCAdapt, LFMM
4	24009987	24012064	PHOX2B	paired like homeobox 2B	cellular response to BMP stimulus; neural crest cell migration	PCAdapt, LFMM
4	27459806	27536638	KDR	kinase insert domain receptor	MAPK cascade	LFMM
4	44071739	44107306	MFHAS1	malignant fibrous histiocytoma amplified sequence 1	MAPK cascade	LFMM
4	46270879	46327565	EGF	epidermal growth factor	epidermal growth factor receptor signaling pathway; regulation of MAPK activity	PCAdapt
4	47091043	47161993	LEF1	lymphoid enhancer binding factor 1	BMP signaling pathway; odontogenesis of dentin-containing tooth; osteoblast differentiation; somitogenesis; Wnt signaling pathway	PCAdapt
4	48870820	48931614	NFKB1	nuclear factor kappa B subunit 1	Wnt signaling pathway	PCAdapt, LFMM

Table S2.3 (*Continued*)

Chr	Start Position	End Position	Gene Symbol	Gene Name	Pathway or Function	Method
4	51157212	51384631	BMPR1B	bone morphogenetic protein receptor type 1B	BMP signaling pathway; bone mineralization; cartilage development; osteoblast differentiation; SMAD binding	PCAdapt
4	57327494	57370096	SMAD1	SMAD family member 1	BMP signaling pathway; cellular response to BMP stimulus; mesodermal cell fate commitment; SMAD protein signal transduction; MAPK cascade; TGF-beta receptor signaling pathway	LFMM
4	63658072	63679397	SPRY1	sprouty RTK signaling antagonist 1	regulation of MAPK activity; TGF-beta receptor signaling pathway	PCAdapt, LFMM
4	64653816	64759480	PDE5A	phosphodiesterase 5A	MAPK cascade	PCAdapt, LFMM
4A	805522	817000	NOX1	NADPH oxidase 1	MAPK cascade	LFMM
4A	5983924	6016384	AR	androgen receptor	MAPK cascade	LFMM
4A	6781008	6937448	GPC3	glypican 3	BMP signaling pathway; Wnt signaling pathway	PCAdapt
4A	11567014	11802890	LOC100220716	serine/threonine-protein kinase PAK 3	regulation of MAPK activity	LFMM
4A	14595197	14649158	BMP15	bone morphogenetic protein 15	growth factor activity	LFMM
4A	19020519	19056612	MED12	mediator complex subunit 12	Wnt signaling pathway	LFMM
5	8313026	8344073	DDB1	damage specific DNA binding protein 1	Wnt signaling pathway	PCAdapt
5	14569348	14900711	KCNQ1	potassium voltage-gated channel subfamily Q member 1	calmodulin binding	LFMM
5	15582936	15622934	DUSP8	dual specificity phosphatase 8	regulation of MAPK activity	LFMM
5	22838419	22907171	MADD	MAPK activating death domain	activation of MAPK activity	PCAdapt, LFMM

Table S2.3 (*Continued*)

Chr	Start Position	End Position	Gene Symbol	Gene Name	Pathway or Function	Method
5	23101135	23182801	LRP4	LDL receptor related protein 4	odontogenesis of dentin-containing tooth; Wnt signaling pathway	PCAdapt
5	23540183	23585123	CREB3L1	cAMP responsive element binding protein 3 like 1	SMAD binding	PCAdapt
5	27442130	27504499	MAP3K9	mitogen-activated protein kinase kinase kinase 9	MAPK cascade	LFMM
5	28613950	28673031	ZFP36L1	ZFP36 ring finger protein like 1	MAPK cascade; EGF response; TGF-beta response	LFMM
5	29288772	29344139	MPP5	membrane palmitoylated protein 5	TGF-beta receptor signaling pathway	LFMM
5	34930638	34988808	STRN3	striatin 3	calmodulin binding	LFMM
5	49149315	49246885	BCL11B	BAF chromatin remodeling complex subunit BCL11B	odontogenesis of dentin-containing tooth	PCAdapt, LFMM
5	53805128	53873461	JAG2	jagged canonical Notch ligand 2	odontogenesis of dentin-containing tooth; Notch signaling pathway	LFMM
5	56212732	56223979	SIX4	SIX homeobox 4	pharyngeal system development	LFMM, RDA.MAXT
5	56244927	56248145	SIX1	SIX homeobox 1	pharyngeal system development	LFMM, RDA.MAXT
5	58778196	58799663	BMP4	bone morphogenetic protein 4	BMP signaling pathway; odontogenesis of dentin-containing tooth; osteoblast differentiation; SMAD binding and protein signal transduction; MAPK kinase activity	LFMM
5	60092964	60153511	MAP4K5	mitogen-activated protein kinase kinase kinase kinase 5	regulation of MAPK activity	PCAdapt, LFMM
6	2508740	2616545	SGPL1	sphingosine-1-phosphate lyase 1	face morphogenesis	PCAdapt, LFMM
6	4120893	4123781	DKK1	dickkopf WNT signaling pathway inhibitor 1	BMP signaling pathway; Wnt signaling pathway; face morphogenesis	PCAdapt

Table S2.3 (*Continued*)

Chr	Start Position	End Position	Gene Symbol	Gene Name	Pathway or Function	Method
6	11364203	11696974	ZMIZ1	zinc finger MIZ-type containing 1	SMAD binding; Notch signaling pathway; TGF-beta receptor signaling pathway	LFMM
6	21011812	21013865	NKX2-3	NK2 homeobox 3	odontogenesis of dentin-containing tooth	LFMM
6	21246388	21250509	SFRP5	secreted frizzled related protein 5	BMP signaling pathway, Wnt signaling pathway	PCAdapt, LFMM
6	22263502	22267426	LZTS2	leucine zipper tumor suppressor 2	Wnt signaling pathway	RDA.MAXT
6	22957894	23101198	NEURL1	neuralized E3 ubiquitin protein ligase 1	Notch signaling pathway; TGF-beta receptor signaling pathway	LFMM
6	26420220	26592627	TCF7L2	transcription factor 7 like 2	Wnt signaling pathway	LFMM
6	30361933	30441611	FGFR2	fibroblast growth factor receptor 2	MAPK cascade, FGF signaling pathway	LFMM, RDA.BILL
7	599993	645792	VWC2L	von Willebrand factor C domain containing 2 like	BMP signaling pathway	LFMM
7	3818972	3849643	LOC100224677	TGF-beta receptor type-2-like	TGF-beta receptor activity, type II	PCAdapt, LFMM
7	3858270	3891565	SNX4	sorting nexin 4	epidermal growth factor receptor binding	PCAdapt, LFMM
7	5854006	5991958	IQCB1	IQ motif containing B1	calmodulin binding	PCAdapt
7	20003349	20092303	NRP2	neuropilin 2	neural crest cell migration	LFMM
7	21742353	21961311	SATB2	SATB homeobox 2	osteoblast development	LFMM
7	25279000	25376878	COL5A2	collagen type V alpha 2 chain	SMAD binding	LFMM
7	25386148	25435585	COL3A1	collagen type III alpha 1 chain	SMAD binding; TGF-beta receptor signaling pathway	LFMM
7	35845201	35896409	ACVR2A	activin A receptor type 2A	BMP signaling pathway	LFMM
8	987161	1013521	LOC100225657	Wnt ligand secretion mediator	Wnt signaling pathway	RDA.MAXT

Table S2.3 (*Continued*)

Chr	Start Position	End Position	Gene Symbol	Gene Name	Pathway or Function	Method
8	6420770	6475284	SSBP3	single stranded DNA binding protein 3	mesendoderm development	RDA.MAXT
8	11358247	11576747	RNF220	ring finger protein 220	Wnt signaling pathway	PCAdapt, LFMM
8	16028626	16031269	CCN1	cellular communication network factor 1	BMP signaling pathway; osteoblast differentiation (neural crest or mesoderm that gives rise to bone)	LFMM
8	22659578	22740585	CAMSAP2	calmodulin regulated spectrin associated protein family member 2	calmodulin binding	PCAdapt, LFMM
9	3922828	3925341	NRROS	negative regulator of reactive oxygen species	TGF-beta receptor signaling pathway	LFMM
9	5775123	5846572	MAP3K13	mitogen-activated protein kinase kinase kinase 13	regulation of MAPK activity	PCAdapt
9	14941008	15214563	TP63	tumor protein p63	Notch signaling pathway; odontogenesis of dentin-containing tooth; mesoderm development	PCAdapt, LFMM
9	22465421	22479913	PDCD10	programmed cell death 10	Notch signaling pathway, regulation of MAPK activity	PCAdapt, LFMM
10	1654620	1667525	CSPG4	chondroitin sulfate proteoglycan 4	regulation of MAPK activity	LFMM
10	4113667	4131709	SNX1	sorting nexin 1	epidermal growth factor receptor binding	PCAdapt, LFMM
10	4138234	4233202	CSNK1G1	casein kinase 1 gamma 1	Wnt signaling pathway	PCAdapt, LFMM
10	5805275	5806237	FOXB1	forkhead box B1	somitogenesis	PCAdapt
10	7875275	8064943	TCF12	transcription factor 12	SMAD binding	LFMM
10	13898921	14100430	NTRK3	neurotrophic receptor tyrosine kinase 3	regulation of MAPK activity	LFMM
10	14670968	14874022	AKAP13	A-kinase anchoring protein 13	MAPK scaffold activity	LFMM

Table S2.3 (*Continued*)

Chr	Start Position	End Position	Gene Symbol	Gene Name	Pathway or Function	Method
10	18355374	18425629	LRRK1	leucine rich repeat kinase 1	Wnt signaling pathway	PCAdapt
10	18710976	18722468	CILP	cartilage intermediate layer protein	regulation of SMAD protein signal transduction; cellular response to TGF-beta stimulus	LFMM
11	259649	277436	SALL1	spalt like transcription factor 1	Wnt signaling pathway	LFMM
11	3926412	4049082	NUP93	nucleoporin 93	SMAD protein signal transduction	LFMM
11	7970193	8424152	CDH13	cadherin 13	epidermal growth factor receptor signaling pathway	PCAdapt, LFMM
11	9160202	9191314	CRISPLD2	cysteine rich secretory protein LCCL domain containing 2	face morphogenesis	LFMM
11	11295398	11298664	CDK10	cyclin dependent kinase 10	regulation of MAPK activity	PCAdapt
12	606274	609917	CAV3	caveolin 3	MAPK cascade; TGF-beta receptor signaling pathway	LFMM
12	1223860	1383618	ITPR1	inositol 1,4,5-trisphosphate receptor type 1	calcineurin complex interacting with calmodulin	RDA.MAXT
12	8783383	8840893	QARS1	glutaminyl-tRNA synthetase 1	MAPK cascade	PCAdapt
12	9328273	9463829	GRIP2	glutamate receptor interacting protein 2	Notch signaling pathway	PCAdapt, LFMM
12	11418047	11499587	GATA2	GATA binding protein 2	Notch signaling pathway	PCAdapt
12	11494988	11515510	RAB7A	RAB7A, member RAS oncogene family	epidermal growth factor catabolic process	PCAdapt, LFMM
12	14418745	14426762	DUSP7	dual specificity phosphatase 7	regulation of MAPK activity	LFMM
12	15869649	15877801	MST1R	macrophage stimulating 1 receptor	regulation of MAPK activity	LFMM
12	19600230	19633421	WNT7A	Wnt family member 7A	WNT signaling pathway; cellular response to TGF-beta stimulus	PCAdapt

Table S2.3 (*Continued*)

Chr	Start Position	End Position	Gene Symbol	Gene Name	Pathway or Function	Method
13	5084765	5150477	WWC1	WW and C2 domain containing 1	MAPK cascade	PCAdapt
13	7496538	7507553	RELL2	RELT like 2	MAPK cascade	PCAdapt
13	11522490	11580350	FLT4	fms related tyrosine kinase 4	MAPK cascade	LFMM
14	993310	1052096	EEF2K	eukaryotic elongation factor 2 kinase	calmodulin binding	PCAdapt, LFMM
14	2170397	2226850	FAM20C	FAM20C golgi associated secretory pathway kinase	odontoblast differentiation	PCAdapt
14	5076798	5122137	SMURF1	SMAD specific E3 ubiquitin protein ligase 1	BMP signaling pathway; BMP signaling pathway; SMAD binding; TGF-beta receptor signaling pathway	LFMM
14	5342843	5373132	MAP2K3	mitogen-activated protein kinase kinase 3	regulation of MAPK activity	PCAdapt
14	5618384	5629987	FLCN	folliculin	TGF-beta receptor signaling pathway	LFMM
14	6133147	6177086	EPN2	epsin 2	Notch signaling pathway	PCAdapt, LFMM
14	7532729	7561668	TRAF7	TNF receptor associated factor 7	regulation of MAPK activity	LFMM
14	13843473	13912273	AXIN1	axin 1	Wnt signaling pathway; SMAD binding	PCAdapt, LFMM
15	1808341	1855451	NF2	neurofibromin 2	MAPK cascade; odontogenesis of dentin-containing tooth; mesoderm formation	PCAdapt, LFMM
15	2201427	2257025	NOS1	nitric oxide synthase 1	calmodulin binding	LFMM
15	4365007	4458655	TAOK3	TAO kinase 3	MAPK cascade	PCAdapt, LFMM
15	6240162	6265653	PPM1F	protein phosphatase, Mg2+/Mn2+ dependent 1F	calmodulin-dependent protein phosphatase activity	PCAdapt, LFMM
15	9963080	9973700	TRPV4	transient receptor potential cation channel subfamily V member 4	calmodulin binding	LFMM

Table S2.3 (*Continued*)

Chr	Start Position	End Position	Gene Symbol	Gene Name	Pathway or Function	Method
17	6864385	6940835	ABL1	ABL proto-oncogene 1, non-receptor tyrosine kinase	BMP signaling pathway; Wnt signaling pathway, planar cell polarity pathway; epidermal growth factor receptor signaling pathway	PCAdapt, LFMM
17	8062252	8179507	VAV2	vav guanine nucleotide exchange factor 2	epidermal growth factor receptor binding	LFMM
17	8971005	8987616	EGFL7	EGF like domain multiple 7	Notch signaling pathway	LFMM
18	3681264	3740822	SMURF2	SMAD specific E3 ubiquitin protein ligase 2	SMAD binding; TGF-beta receptor signaling pathway	PCAdapt, LFMM
19	3056287	3102349	NXN	nucleoredoxin	Wnt signaling pathway	LFMM, RDA.MAXT
19	3314296	3335312	TRPV1	transient receptor potential cation channel subfamily V member 1	calmodulin binding	LFMM
19	4780625	4787990	SERPINF2	serpin family F member 2	regulation of TGF-beta production	PCAdapt, LFMM
19	6979854	6990125	DHX33	DEAH-box helicase 33	regulation of MAPK activity	PCAdapt
19	7004084	7097933	CAMKK1	calcium/calmodulin dependent protein kinase kinase 1	protein kinase activity	PCAdapt, LFMM
20	5426625	5467243	PLCG1	phospholipase C gamma 1	epidermal growth factor receptor signaling pathway; cellular response to epidermal growth factor stimulus	LFMM
20	5830044	5876387	STK4	serine/threonine kinase 4	Wnt signaling pathway	LFMM
20	7459764	7465267	POFUT1	protein O-fucosyltransferase 1	Notch signaling pathway	LFMM
20	9877765	9890068	GATA5	GATA binding protein 5	BMP signaling pathway	LFMM
20	11668449	11686824	APCDD1L	APC down-regulated 1 like	Wnt signaling pathway	LFMM
21	2216802	2315004	SKI	SKI proto-oncogene	BMP signaling pathway; TGF-beta receptor signaling pathway; SMAD binding; SMAD protein signal transduction	LFMM

Table S2.3 (*Continued*)

Chr	Start Position	End Position	Gene Symbol	Gene Name	Pathway or Function	Method
21	7797633	7812161	NBL1	NBL1, DAN family BMP antagonist	BMP signaling pathway	LFMM
21	8202356	8329160	EPHB2	EPH receptor B2	inactivation of MAPKK activity	PCAdapt, LFMM, RDA.MAXT
21	8415439	8468478	EPHA8	EPH receptor A8	MAPK cascade	LFMM
22	509491	539844	FGFR1	fibroblast growth factor receptor 1	MAPK cascade	PCAdapt
23	1005978	1027132	STK40	serine/threonine kinase 40	MAPK cascade	PCAdapt, RDA.MAXT
23	2051285	2055747	PEF1	penta-EF-hand domain containing 1	neural crest formation; neural crest cell development	RDA.MAXT
23	2238486	2240198	MARCKSL1	MARCKS like 1	calmodulin binding	PCAdapt, LFMM
23	2242983	2259691	HDAC1	histone deacetylase 1	odontogenesis of dentin-containing tooth; Wnt signaling pathway	PCAdapt
23	2695374	2743281	HEYL	hes related family bHLH transcription factor with YRPW motif like	Notch signaling pathway	PCAdapt, LFMM
24	6094242	6123089	DIXDC1	DIX domain containing 1	Wnt signaling pathway	LFMM
25	153090	173650	KCNN3	potassium calcium-activated channel subfamily N member 3	calmodulin binding	LFMM
25	184196	196278	ADAR	adenosine deaminase RNA specific	osteoblast differentiation (neural crest or mesoderm that gives rise to bone)	PCAdapt, LFMM
25	459369	461443	LAMTOR2	late endosomal/lysosomal adaptor, MAPK and MTOR activator 2	activation of MAPK activity	LFMM
25	489404	506420	IQGAP3	IQ motif containing GTPase activating protein 3	calmodulin binding; activation of MAPK activity	LFMM

Table S2.3 (*Continued*)

Chr	Start Position	End Position	Gene Symbol	Gene Name	Pathway or Function	Method
25	531772	612244	MEF2D	myocyte enhancer factor 2D	osteoblast differentiation (neural crest or mesoderm that gives rise to bone)	LFMM
26	5680478	5760407	KLHL12	kelch like family member 12	Wnt signaling pathway; neural crest cell development	LFMM
27	1916828	1980192	NBR1	NBR1 autophagy cargo receptor	MAPK cascade	LFMM
27	1997150	2005111	LOC115490720	uncharacterized LOC115490720	Notch signaling pathway	LFMM
27	2199562	2233080	STAT3	signal transducer and activator of transcription 3	Notch signaling pathway	LFMM
27	2731452	2738410	IGFBP4	insulin like growth factor binding protein 4	MAPK cascade	LFMM
28	1061207	1067397	DAPK3	death associated protein kinase 3	Wnt signaling pathway	LFMM
28	1105955	1112365	ZBTB7A	zinc finger and BTB domain containing 7A	SMAD binding; Notch signaling pathway; TGF-beta receptor signaling pathway	LFMM
28	5617079	5676280	RANBP3	RAN binding protein 3	SMAD binding	LFMM
Z	5389306	5470857	TRABD2A	TraB domain containing 2A	Wnt signaling pathway	PCAdapt
Z	35025066	35094130	LPAR1	lysophosphatidic acid receptor 1	regulation of MAPK activity	LFMM
Z	67444113	67571305	KANK1	KN motif and ankyrin repeat domains 1	Wnt signaling pathway	LFMM
Z	74995256	75116589	MLLT3	MLLT3 super elongation complex subunit	Wnt signaling pathway	LFMM
Genes inferred to plumage and feather development (GO terms: ASIP, MC1R, MITF, agouti, melanin, keratin, carotenoid, melanosome, melanocyte)						
1	106651639	106838780	CASK	calcium/calmodulin dependent serine protein kinase	regulation of keratinocyte proliferation	PCAdapt
1A	48500857	48511352	SOX10	SRY-box transcription factor 10	melanocyte differentiation	LFMM

Table S2.3 (*Continued*)

Chr	Start Position	End Position	Gene Symbol	Gene Name	Pathway or Function	Method
2	33972781	33976125	HOXA7	homeobox A7	negative regulation of keratinocyte differentiation	LFMM
2	44153548	44173849	BFSP2	beaded filament structural protein 2	intermediate filament (keratins)	LFMM
2	44467336	44825182	MYRIP	myosin VIIA and Rab interacting protein	melanosome	LFMM
2	67635334	67701873	DTNBP1	dystrobrevin binding protein 1	BLOC-1 complex	PCAdapt, LFMM
2	86103745	86270736	EPB41L4B	erythrocyte membrane protein band 4.1 like 4B	positive regulation of keratinocyte migration	LFMM
3	53328140	53703123	PTPRK	protein tyrosine phosphatase receptor type K	regulation of keratinocyte proliferation	LFMM
3	90506424	90513899	OVOL2	ovo like zinc finger 2	regulation of keratinocyte proliferation	PCAdapt
4A	17306906	17333475	ATP7A	ATPase copper transporting alpha	regulation of melanin biosynthetic process	PCAdapt
5	28613950	28673031	ZFP36L1	ZFP36 ring finger protein like 1	regulation of keratinocyte differentiation & proliferation	LFMM
5	34478826	34593252	PRKD1	protein kinase D1	regulation of keratinocyte proliferation	LFMM
5	49149315	49246885	BCL11B	BAF chromatin remodeling complex subunit BCL11B	regulation of keratinocyte differentiation & proliferation	LFMM
6	30361933	30441611	FGFR2	fibroblast growth factor receptor 2	negative regulation of keratinocyte proliferation	LFMM
7	3202968	3209818	RAB17	RAB17, member RAS oncogene family	melanosome	RDA.MAXT
7	10385090	10390478	DES	desmin	intermediate filament	PCAdapt, LFMM
9	11123568	11140877	TRPC1	transient receptor potential cation channel subfamily C member 1	melanin biosynthesis process	LFMM

Table S2.3 (*Continued*)

Chr	Start Position	End Position	Gene Symbol	Gene Name	Pathway or Function	Method
9	14941008	15214563	TP63	tumor protein p63	keratinocyte differentiation	PCAdapt, LFMM
10	19111218	19128458	RAB11A	RAB11A, member RAS oncogene family	melanosome transport	LFMM
11	7970193	8424152	CDH13	cadherin 13	keratinocyte proliferation	PCAdapt, LFMM
11	11375885	11376829	MC1R	melanocortin 1 receptor	melanocortin receptor activity; pigmentation	PCAdapt
12	459048	462127	VHL	von Hippel-Lindau tumor suppressor	melanin metabolic process	LFMM
15	3063387	3177508	BCR	BCR activator of RhoGEF and GTPase	keratinocyte differentiation	PCAdapt
18	8548212	8555492	LOC100232344	melanin-concentrating hormone receptor 1-like	melanin-concentrating hormone receptor activity	LFMM
20	5830044	5876387	STK4	serine/threonine kinase 4	keratinocyte differentiation	LFMM
23	3060915	3088875	CLIC4	chloride intracellular channel 4	keratinocyte differentiation	LFMM
24	3620266	3651481	JAM3	junctional adhesion molecule 3	desmosome	LFMM, RDA.MAXT
24	6159090	6174551	BCO2	beta-carotene oxygenase 2	carotenoid metabolic process	LFMM
26	1494853	1511857	PPARD	peroxisome proliferator activated receptor delta	keratinocyte proliferation	LFMM
26	6252515	6301023	PKP1	plakophilin 1	desmosome	LFMM
28	1078101	1095811	PIAS4	protein inhibitor of activated STAT 4	positive regulation of keratinocyte apoptotic process	LFMM
28	5480298	5518155	LMNB2	lamin B2	intermediate filament (keratins)	LFMM
Z	39688891	39716655	B4GALT1	beta-1,4-galactosyltransferase 1	desmosome	LFMM
Z	63460918	63629394	AP3B1	adaptor related protein complex 3 subunit beta 1	melanosome organization	LFMM

Table S2.3 (*Continued*)

Chr	Start Position	End Position	Gene Symbol	Gene Name	Pathway or Function	Method
Genes inferred to metabolism and physiological responses to temperature (GO terms: AQP, SLC2A2, PRKCH, HSP, PKC, heat shock, renal, glomerular, angiotensin, vasopressin, water homeostasis, temperature homeostasis)						
1	4149885	4155811	PHOX2A	paired like homeobox 2A	noradrenergic neuron differentiation	PCAdapt
1	56582503	56627018	AKAP11	A-kinase anchoring protein 11	renal water homeostasis	PCAdapt
1	106142036	106201259	BCOR	BCL6 corepressor	heat shock protein binding	RDA.MAXT
1A	1124365	1592306	PLXNA4	plexin A4	sympathetic nervous system development	PCAdapt, LFMM
1A	11028606	11044892	DNAJC2	DnaJ heat shock protein family (Hsp40) member C2	heat shock (Hsp70) protein binding	PCAdapt
1A	36615622	36944738	SYT1	synaptotagmin 1	chromaffin granule membrane (metabolism)	PCAdapt
1A	48103977	48126457	PDGFB	platelet derived growth factor subunit B	positive regulation of glomerular mesangial cell proliferation	LFMM
2	18808363	18915566	DNAJC1	DnaJ heat shock protein family (Hsp40) member C1	heat shock (Hsp40) chaperone binding	PCAdapt, LFMM
3	5015010	5047670	TFAP2B	transcription factor AP-2 beta	renal water homeostasis	LFMM
3	97175747	97391280	CAMKMT	calmodulin-lysine N-methyltransferase	heat shock protein binding	LFMM
4	24009987	24012064	PHOX2B	paired like homeobox 2B	noradrenergic neuron differentiation	PCAdapt
4	25823641	25929908	CORIN	corin, serine peptidase	regulation of renal sodium excretion	PCAdapt
4	40927744	40942078	PPID	peptidylprolyl isomerase D	heat shock (Hsp90) protein binding	LFMM
4	48870820	48931614	NFKB1	nuclear factor kappa B subunit 1	cellular response to angiotensin	PCAdapt
4	53351577	53463073	SNCA	synuclein alpha	heat shock (Hsp70) protein binding	PCAdapt
4	67313744	67318861	JCHAIN	joining chain of multimeric IgA and IgM	glomerular filtration	PCAdapt
4A	805522	817000	NOX1	NADPH oxidase 1	regulation of systemic arterial blood pressure by renin-angiotensin	LFMM

Table S2.3 (*Continued*)

Chr	Start Position	End Position	Gene Symbol	Gene Name	Pathway or Function	Method
5	2649595	2688799	DNAJC24	DnaJ heat shock protein family (Hsp40) member C24	heat shock (Hsp40) chaperone binding	PCAdapt
5	14569348	14900711	KCNQ1	potassium voltage-gated channel subfamily Q member 1	renal absorption	LFMM
5	46056193	46089188	LGMN	legumain	renal system process	PCAdapt
5	58778196	58799663	BMP4	bone morphogenetic protein 4	renal system process	LFMM
6	2935895	3011176	DNAJB12	DnaJ heat shock protein family (Hsp40) member B12	integral component of membrane	LFMM
6	18278386	18288919	ACTA2	actin alpha 2, smooth muscle	glomerular mesangial cell development	PCAdapt
7	5668353	5706880	HSPBAP1	HSPB1 associated protein 1	heat shock protein binding	PCAdapt
7	10355111	10360462	DNAJB2	DnaJ heat shock protein family (Hsp40) member B2	Hsp70 protein binding	PCAdapt
7	10661391	10839308	PLA2R1	phospholipase A2 receptor 1	positive regulation of glomerular visceral epithelial cell apoptotic process	LFMM
7	20003349	20092303	NRP2	neuropilin 2	ventral trunk neural crest cell migration	LFMM
7	22532108	22542284	HSPD1	heat shock protein family D (Hsp60) member 1	response to cold	LFMM
8	1490581	1532287	DNAJC6	DnaJ heat shock protein family (Hsp40) member C6	heat shock (Hsp40) chaperone binding	LFMM
8	6380254	6392477	TTC4	tetratricopeptide repeat domain 4	Hsp90 protein binding	RDA.MAXT
8	30318266	30446111	PBX1	PBX homeobox 1	adrenal gland development	PCAdapt
9	4893009	4904976	DNAJB11	DnaJ heat shock protein family (Hsp40) member B11	signaling receptor binding	LFMM
9	14941008	15214563	TP63	tumor protein p63	sympathetic nervous system development	PCAdapt, LFMM
9	21437105	21445610	SLC2A2	solute carrier family 2 member 2	glucose transmembrane transport	LFMM

Table S2.3 (*Continued*)

Chr	Start Position	End Position	Gene Symbol	Gene Name	Pathway or Function	Method
11	259649	277436	SALL1	spalt like transcription factor 1	adrenal gland development	LFMM
11	1315348	1543119	FTO	FTO alpha-ketoglutarate dependent dioxygenase	temperature homeostasis	LFMM
11	3477623	3519232	HSF4	heat shock transcription factor 4	regulation of transcription, DNA-templated	LFMM
13	13708321	13758743	CYFIP2	cytoplasmic FMR1 interacting protein 2	SCAR complex	PCAdapt
14	8105846	8118554	SCNN1G	sodium channel epithelial 1 gamma subunit	multicellular organismal water homeostasis	LFMM
15	3063387	3177508	BCR	BCR activator of RhoGEF and GTPase	renal system process	PCAdapt, LFMM
15	9963080	9973700	TRPV4	transient receptor potential cation channel subfamily V member 4	multicellular organismal water homeostasis	LFMM
17	6943829	6947095	QRFP	pyroglutamylated RFamide peptide	neuropeptide hormone activity	PCAdapt, LFMM
17	7670067	7725734	TSC1	TSC complex subunit 1	heat shock (Hsp70, Hsp90) protein binding	RDA.MAXT
19	1427623	1433515	LHX1	LIM homeobox 1	renal vesicle morphogenesis	PCAdapt, LFMM
19	3314296	3335312	TRPV1	transient receptor potential cation channel subfamily V member 1	temperature homeostasis	LFMM
19	4330603	4332859	SDF2	stromal cell derived factor 2	chaperone complex	PCAdapt
19	4780625	4787990	SERPINF2	serpin family F member 2	regulation of blood vessel diameter by renin-angiotensin	PCAdapt, LFMM
19	5772043	5784127	UNC45B	unc-45 myosin chaperone B	heat shock (Hsp90) protein binding	LFMM
20	7428245	7446132	ASXL1	ASXL transcriptional regulator 1	glomerular visceral epithelial cell development	LFMM

Table S2.3 (*Continued*)

Chr	Start Position	End Position	Gene Symbol	Gene Name	Pathway or Function	Method
21	3530126	3534657	RNF207	ring finger protein 207	Hsp70 protein binding	LFMM
23	3809134	3841900	WASF2	WASP family member 2	SCAR complex	PCAdapt
24	4366826	4438718	HSPA8	heat shock protein family A (Hsp70) member 8	heat shock protein family A (Hsp70) chaperone complex	LFMM
25	217543	221607	IL6R	interleukin 6 receptor	positive regulation of glomerular mesangial cell proliferation	PCAdapt, LFMM
26	1398371	1417348	FKBP5	FKBP prolyl isomerase 5	heat shock protein binding	LFMM
27	2199562	2233080	STAT3	signal transducer and activator of transcription 3	temperature homeostasis	LFMM
Z	67444113	67571305	KANK1	KN motif and ankyrin repeat domains 1	glomerular visceral epithelial cell migration	LFMM

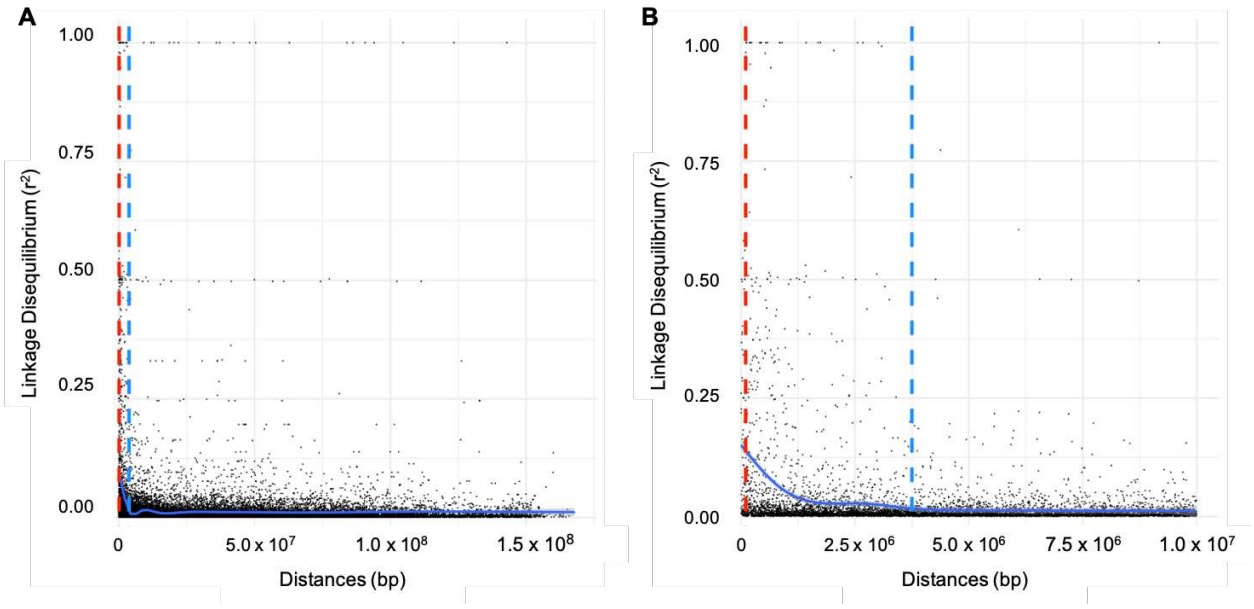

Figure S2.1 Linkage disequilibrium as a function of distance for Santa Cruz Island calculated using a 1Gb maximum window in vcftools v. 0.1.16 (Auton & Marcketta, 2009) as shown across all distances (A) and zoomed in across a subset of distances (B). Vertical red and blue dashed lines display 50kb and 3.75Mb, respectively.

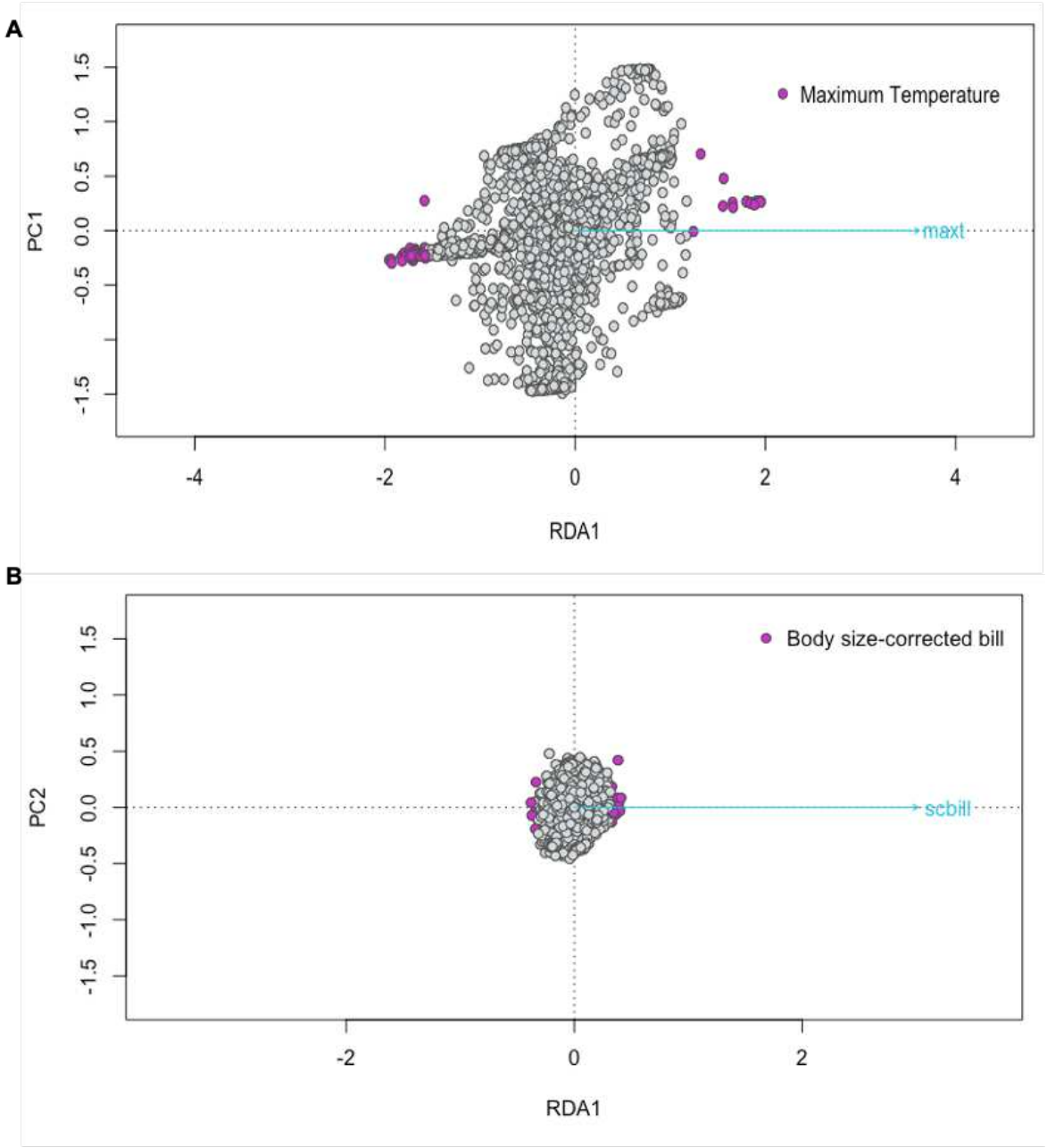

Figure S2.2 Partial redundancy analysis controlling for latitude and longitude with putatively adaptive and candidate loci are highlighted. We modeled the relationship between genotype and environment using 3,294 SNPs as the response [387 island song sparrows (San Miguel Island, n = 77 Santa Rosa Island, n = 94; Santa Cruz Island, n = 205; Anacapa Island, n = 11)] and maximum temperature as the predictor (A). Maximum temperature is the maximum temperature over 1 km^2 at the sampling location based on WorldClim interpolations for July, the hottest month experienced by island sparrows. We also performed a genome-wide association (GWA) test using 3,294 SNPs as the response [306 phenotyped island song sparrows (San Miguel Island, n = 67; Santa Rosa Island, n = 79; Santa Cruz Island, n = 106)] and body size-corrected bill surface area as the predictor (B). Anacapa was excluded from GWA due to the low sample size.

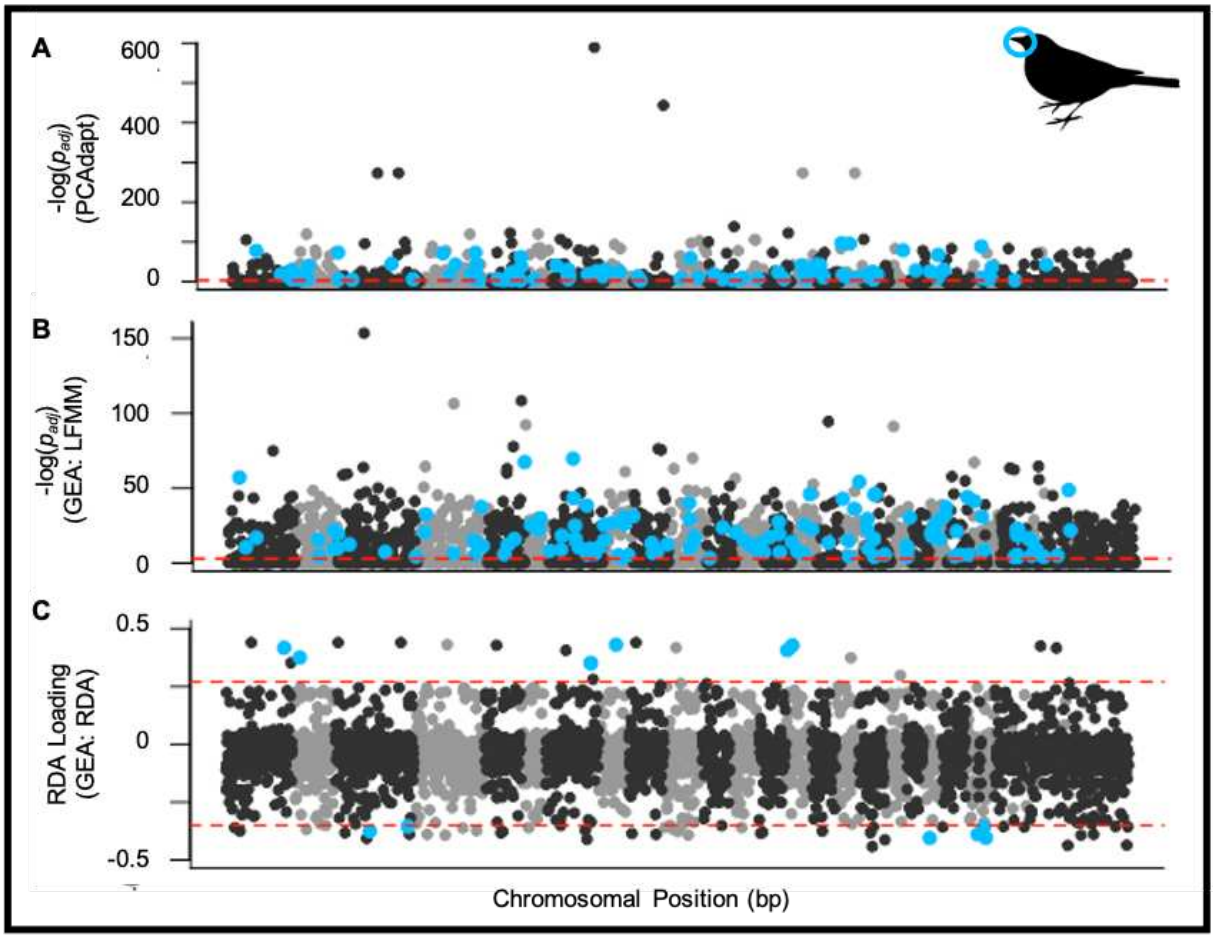

Figure S2.3 Putatively adaptive loci are found in or within 50kb of 176 unique genes associated with bill and craniofacial development in birds. Genes are linked to 138 putatively adaptive loci (blue circles) based on 3,294 SNPs aligned to the zebra finch genome and identified using differentiation-based (F_{ST} outlier) analyses in PCAdapt (n = 26 loci; A) and genotype-environmental association analyses [LFMM (n = 35 loci), B; RDA, (n = 4 loci), C]. GEA analyses relate maximum temperature and genotypes for 438 island birds (San Miguel, n = 77; Santa Rosa, n = 94; Santa Cruz, n = 205; Anacapa, n = 11).

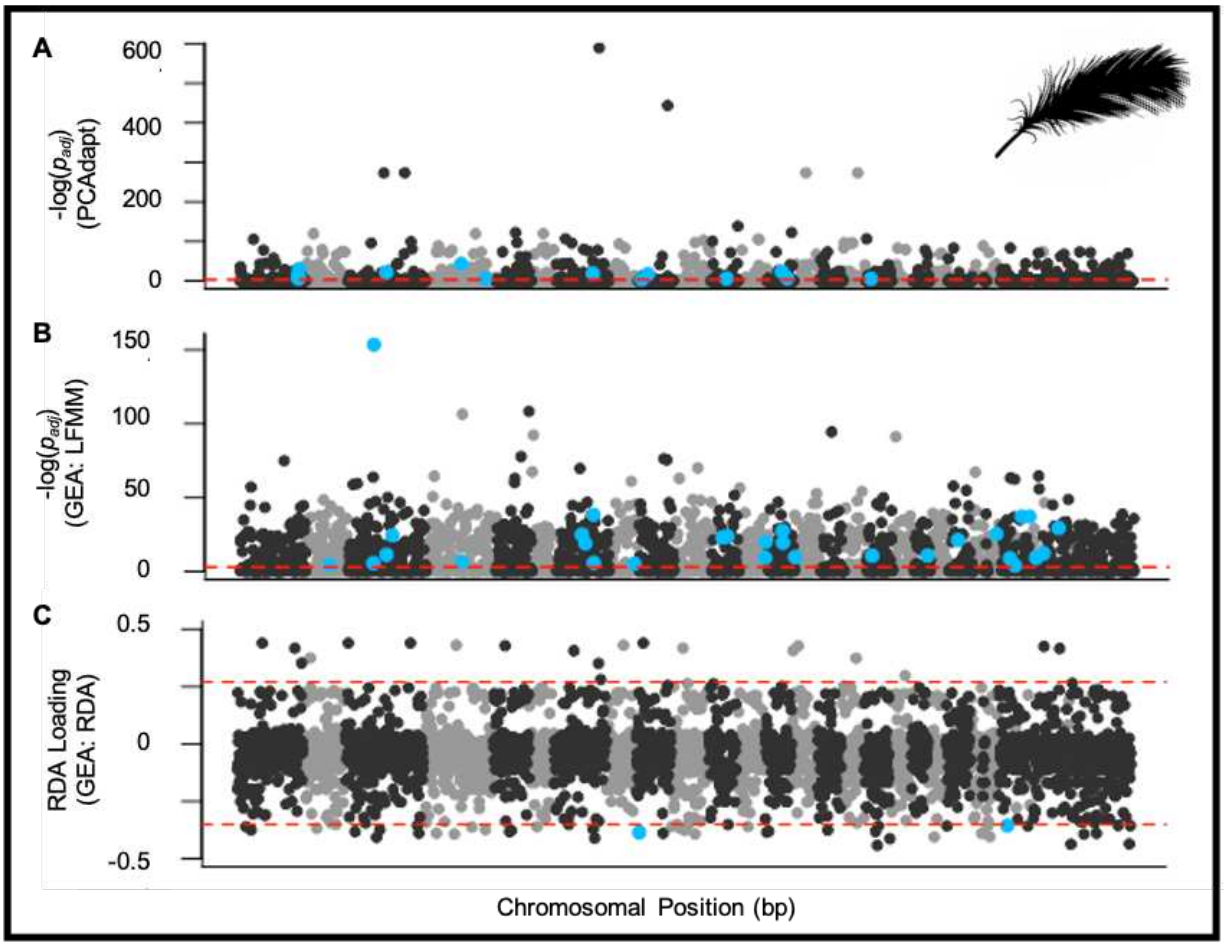

Figure S2.4 Putatively adaptive loci are found in or within 50kb of 34 unique genes associated with feather development and melanin synthesis, transportation, and deposition. Genes are linked to 40 putatively adaptive loci (blue circles) based on 3,294 SNPs aligned to the zebra finch genome and identified using differentiation-based (FST outlier) analyses in PCAdapt (n = 12 loci; A) and genotype-environmental association analyses [LFMM (n = 26 loci), B; RDA, (n = 2 loci), C]. GEA analyses relate maximum temperature and genotypes for 438 island birds (San Miguel, n = 77; Santa Rosa, n = 94; Santa Cruz, n = 205; Anacapa, n = 11).

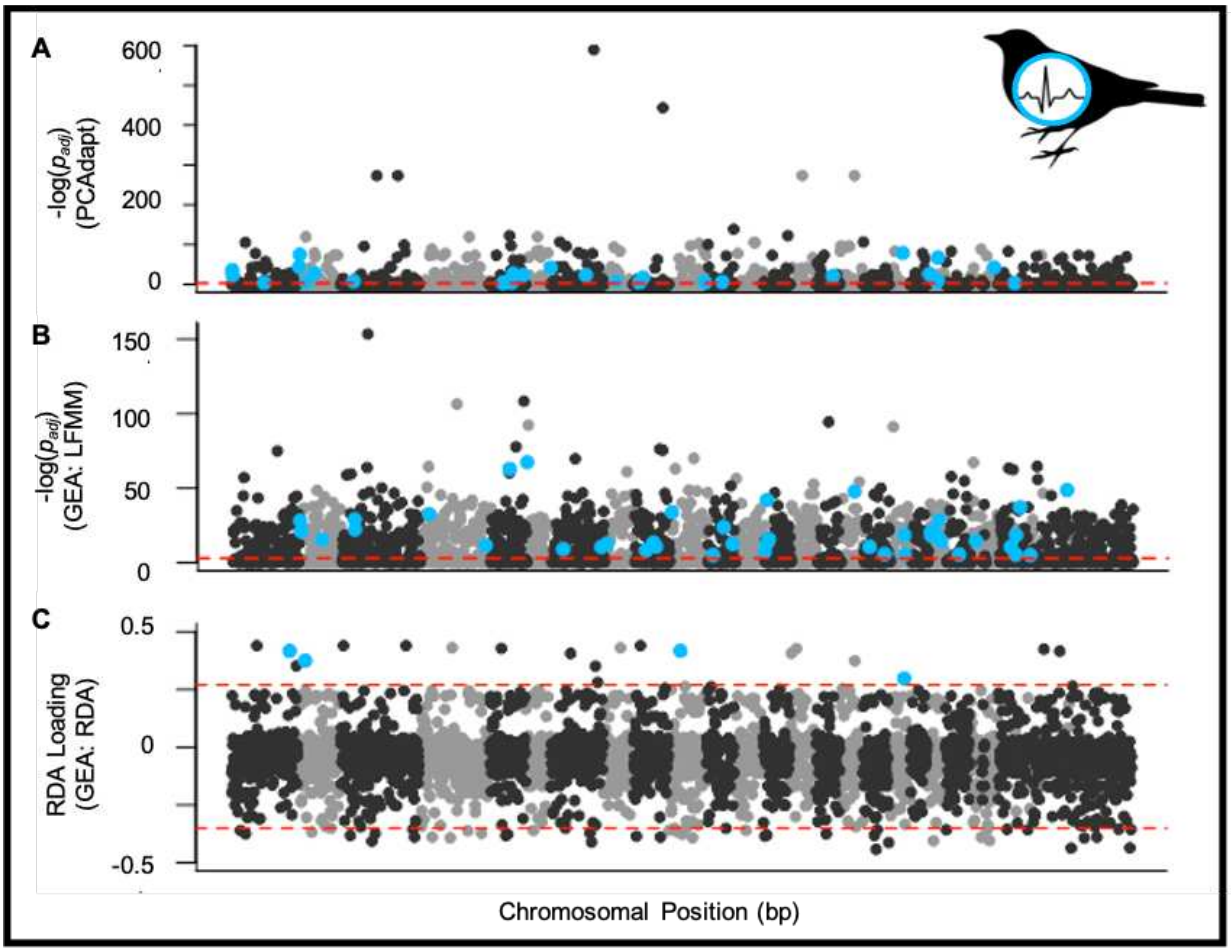

Figure S2.5 Putatively adaptive loci are found in or within 50kb of 56 unique genes associated with physiological responses to climate variation. Genes are linked to 65 putatively adaptive loci (blue circles) based on 3,294 SNPs aligned to the zebra finch genome and identified using differentiation-based (F_{ST} outlier) analyses in PCAdapt (n = 26 loci; A) and genotype-environmental association analyses [LFMM (n = 35 loci), B; RDA, (n = 4 loci), C]. GEA analyses relate maximum temperature and genotypes for 438 island birds (San Miguel, n = 77; Santa Rosa, n = 94; Santa Cruz, n = 205; Anacapa, n = 11).

APPENDIX 3

Table S3.1 Model selection results for analyses of the relationship between thermal physiology and environmental temperatures in song sparrows on the California Channel Islands and coastal mainland California. Thermal physiology response variables include thermal stress temperatures (T_{hs}, T_{cs}), basal metabolic rate (BMR), and rate of change in evaporative water loss in response to increasing heat stress (ΔEWL). Predictors included mean maximum environmental temperatures in June (max T) or mean minimum temperatures in January (min T) extracted from WorldClim v. 1.4 (Hijmans et al., 2005), body mass, and Julian day (Julian). Julian day is a proxy for reproductive status and seasonality. Random effects in linear mixed models are shown in parentheses. Variables displayed include additive model description with physiology response and covariates, number of parameters estimated (*K*), the difference in second-order Akaike information criteria corrected for small sample size (ΔAIC_c), and corresponding AIC_c weights (w_i). Top models for all response variables are shown in bold, and asterisks denote statistical significance in environmental temperature predicting response.

Model Description	K	ΔAIC_c	w_i
T_{hs} ~ max T + mass + Julian	5	2.37	0.22
T_{hs} ~ max T + mass	4	11.21	0.00
T_{hs} ~ max T + Julian **	**4**	**0.00**	**0.74**
T_{hs} ~ max T	3	9.21	0.01
T_{hs} ~ mass	3	15.49	0.00
T_{hs} ~ Julian	3	6.48	0.03
T_{hs} ~ 1 (null model)	2	13.87	0.00
T_{cs} ~ min T + mass + Julian	5	4.33	0.03
T_{cs} ~ min T + mass	4	2.18	0.10
T_{cs} ~ min T + Julian	4	2.10	0.10
T_{cs} ~ min T	**3**	**0.00**	**0.29**
T_{cs} ~ mass	3	1.92	0.11
T_{cs} ~ Julian	3	2.28	0.09
T_{cs} ~ 1 (null model)	2	0.07	0.28
BMR ~ max T + mass + Julian + (1 | experiment type)	6	1.74	0.24
BMR ~ max T + mass + (1 | experiment type)	5	5.31	0.04
BMR ~ max T + Julian + (1 | experiment type) **	**5**	**0.00**	**0.56**
BMR ~ max T + (1 | experiment type)	4	3.35	0.04
BMR ~ mass + (1 | experiment type)	4	5.80	0.03
BMR ~ Julian + (1 | experiment type)	4	7.57	0.01
BMR ~ 1 + (1 | experiment type) (null model)	3	6.93	0.02

Table S3.1 (*Continued*)

Model Description	**K**	**ΔAIC_c**	w_i
ΔEWL ~ max T + mass + Julian	5	3.52	0.08
ΔEWL ~ max T + mass	4	1.42	0.24
ΔEWL ~ max T + Julian	4	2.00	0.18
ΔEWL ~ max T ***	**3**	**0.00**	**0.49**
ΔEWL ~ mass	3	25.79	0.00
ΔEWL ~ Julian	3	22.45	0.00
ΔEWL ~ 1 (null model)	2	29.24	0.00

Table S3.2 Loadings from principal component analysis of feather microstructure variables including total length, length of the pennaceous section, length of the plumulaceous section, and barb and barbule densities in both pennaceous and plumulaceous sections.

Variable	PC1	PC2	PC3	PC4
Total Length	**-0.56**	0.29	-0.08	0.04
Length (Pennaceous)	-0.28	**0.44**	**-0.50**	**0.45**
Length (Plumulaceous)	**-0.53**	0.06	0.27	-0.28
Barb Density (Pennaceous)	0.32	**0.47**	0.18	-0.36
Barb Density (Plumulaceous)	**0.46**	0.21	-0.23	0.33
Barbule Density (Pennaceous)	0.11	**0.66**	0.15	-0.26
Barbule Density (Plumulaceous)	-0.01	0.13	**0.75**	**0.64**
Variation Explained	37.8	22.4	14.9	13.3
Cumulative Variation Explained	37.8	60.2	75.1	88.4

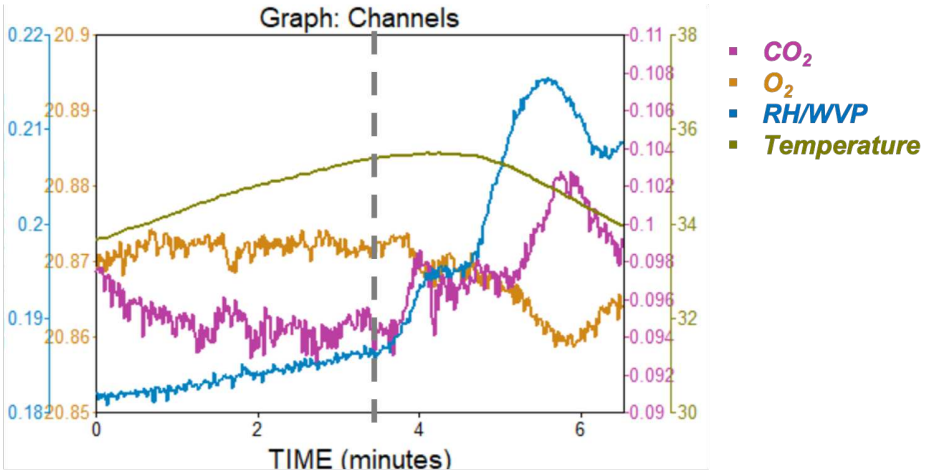

Figure S3.1 Expedata v. 1.9.2 (Sable Systems Intl.) readings of oxygen and carbon dioxide concentrations and water vapor pressure following thermal stress during flow-through respirometry experiments. Heat stress results in increased water vapor pressures, increased carbon dioxide concentrations, and decreased oxygen concentrations.

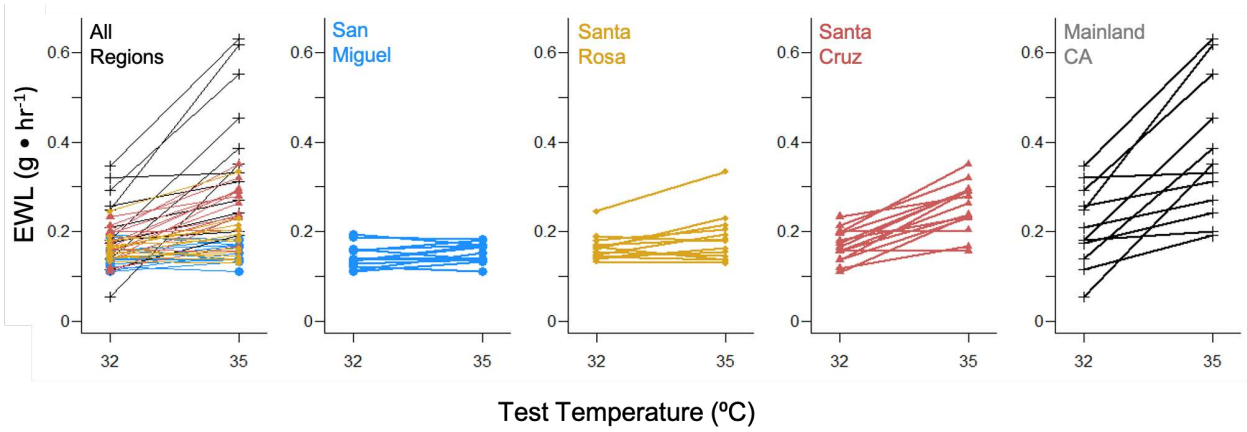

Figure S3.2 Evaporative water loss (EWL) in individual male song sparrows at heat stress temperatures.

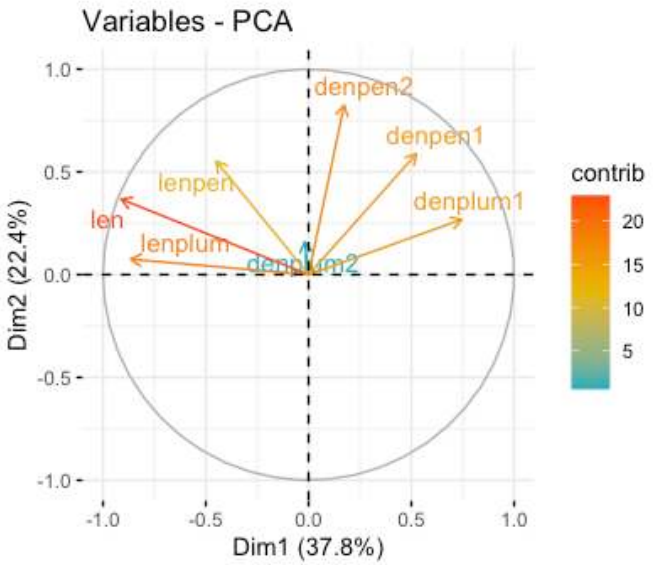

Figure S3.3 Loadings plot for PC1 and PC2 from principal component analysis of feather microstructure variables including total length, length of the pennaceous section, length of the plumulaceous section, and barb and barbule densities in both pennaceous and plumulaceous sections.